UNIVERSITÄTSKLINIKUM HAMBURG-EPPENDORF

Center for Molecular Neurobiology Hamburg (ZMNH),
Prof. Dr. Matthias Kneussel

The functional role of the cell adhesion molecule L1: characterization of L1/687 and L1/858-863 transgenic mice

Dissertation

with the aim of achieving a PhD
at the Medical Faculty of the University of Hamburg

submitted by:
Viviana Granato/ Avellino, Italy

Hamburg 2022

(wird von der Medizinischen Fakultät ausgefüllt)

**Angenommen von der
Medizinischen Fakultät der Universität Hamburg am:** _13.02.2023_

**Veröffentlicht mit Genehmigung der
Medizinischen Fakultät der Universität Hamburg.**

Prüfungsausschuss, der/die Vorsitzende: _Prof. Dr. Dr. Melitta Schachner_

Prüfungsausschuss, zweite/r Gutachter/in: _PD Dr. Uwe Borgmeyer_

Prüfungsausschuss, dritte/r Gutachter/in: _____

Contents

C H A P T E R 1

INTRODUCTION

1.1   Cell adhesion molecules

Cell adhesion molecules (CAMs) are a group of surface glycoproteins involved in a range of cellular functions such as proliferation, differentiation, apoptosis, gene expression and, in particular, adhesion and migration [1]. CAMs mediate cell-cell adhesion through homophilic or heterophilic interactions, binding to other neural cell adhesion molecules on the same cell (cis interaction) or to other neuronal cell adhesion molecules on adjacent cells or to extracellular matrix proteins (trans interactions) [2]. Adhesion molecules are generally divided into different groups: selectins, integrins, cadherins, members of the immunoglobulin superfamily (IgCAMs), nectins and mucins [3], C- type lectin-like domain proteins (CTLDs) and the CD44 family [1] (Figure 1.1). While IgCAMs, cadherins and integrins are involved in neural processes, CTLDs have mostly immunological functions.

In the first stages of the development of the nervous system, neurons have to migrate to the target areas elongating their axons. Cell migration, axon extension and dendrite arborization are key steps for the growth and the maturation of complex neural architecture of the developing brain. In these first phases, CAMs are responsible for the initial contacts of axons and neurites, through homophilic and heterophilic interactions and play a role in axon-guidance and target recognition, synapse formation and regulation of synaptic structures as well as in astrocyte-synapse contacts [4]. Moreover, CAMs are involved in highly coordinated brain functions, such as memory and learning [5].
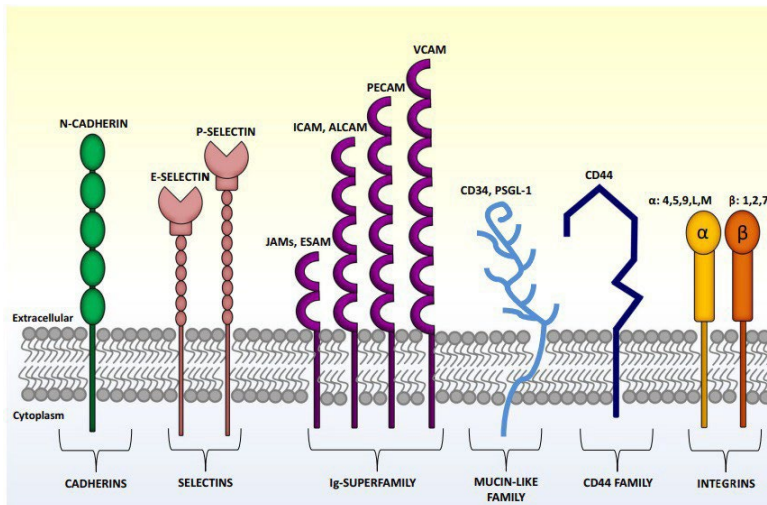
Figure 1.1: Representative figure of the CAM family proteins. CAMs are divided into selectins, integrins, cadherins, IgCAMs, mucins and CD44 family proteins. Cadherins are homodimers with five extracellular cadherin repeats with Ca^{2+} binding sites; selectins consist of a lectin domain at the C-terminus followed by an EGF (epidermal growth factor) like domain and a variable number of short consensus repeat (SCR) domains; Ig-superfamily proteins contain Ig-like domains and a transmembrane region and can additionally exhibit fibronectin-type III repeats and an intracellular domain; mucin-like family proteins are composed of a sequence of repeated amino acids rich in serine and/or threonine; CD44 family proteins are single-chain molecules with an extracellular domain containing the ligand-binding sites, a standard stem region, a transmembrane domain and a cytoplasmic tail; integrins are heterodimers composed of *alpha* and *beta* subunits forming an extracellular ligand-binding site. Image from [6].

The IgCAM family includes the L1 subfamily, which comprises L1, the close homolog of L1 (CHL1), NgCAM-related cell adhesion molecule (NrCAM) and neurofascin [7]. The L1 family molecules play a key role in the regulation of neuronal development [8]. Defects in the L1 subfamily members are implicated in multiple neurological diseases, as X-linked mental retardation, low IQ syndrome, schizophrenia and development delay [9]. In addition, knock-out mice of L1 subfamily proteins, display migration errors in corticospinal axons, olfactory neurons, retinal axons and in the hippocampal CA3 area [2].

1.1.1   The cell adhesion molecule L1

The cell adhesion molecule L1 is a 200-220 kDa glycoprotein, containing an extracellular region of 6 Ig-like domains (Ig1-Ig6) at the N-terminus, five fibronectin-type-III domains (FNI-FN5), a single transmembrane region and a highly conserved intracellular domain at the C-terminus (Figure 1.2) [2].
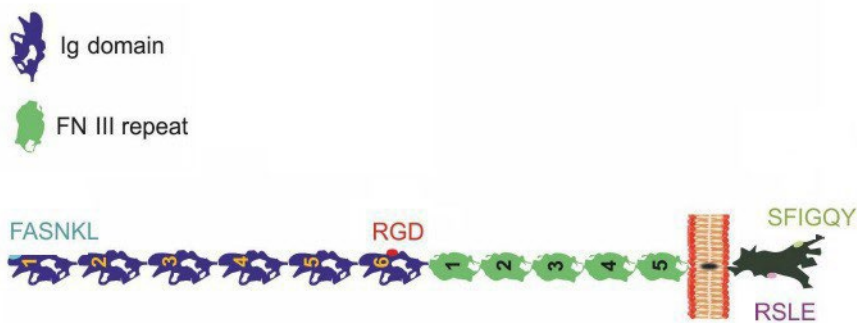
Figure 1.2: L1 structure. L1 is a 200-220 kDa glycoprotein formed of six Ig-like domains at the amino-terminal end, followed by five fibronectin type III homologous repeats, a single transmembrane region and an intracellular tail at the C-terminal end. L1 presents different sequences for homophilic or heterophilic interactions located at the Ig-like domains for the interaction with other CAM proteins (FASNKL) and integrins (RGD) or located on the intracellular domain and responsible for the interaction with ankyrins (SFIGQY) and the link between L1 and actin (RSLE). Image modified from [10].

The L1CAM gene is located on the X chromosome and the protein is expressed in different tissues, as brain, urinary and reproductive tracts and endothelium [10]. In the nervous system L1 is expressed in the developing peripheral nervous system on neurons and non-myelinating Schwann cells and, in the central nervous system, on non-myelinated axons and growth cones of differentiating neurons [11]. L1 can bind homophilically to other L1 proteins, with the Ig-like domains having a major role in this type of interactions between adjacent cells, or heterophilically to other CAMs including Ig superfamily proteins NCAM [10], CD24

[12] and neurophilin through the FASNKL sequence located in the Ig1 domain, [13] that binds also with a component of the semaphorin 3A (Sema3A) complex and neuropilin-1 (NP-1), affecting the growth cone [14]. The Ig6-domain contains an Arg-Gly-Asp sequence (RGD-motif) responsible for cis binding to integrins [15]. The Ig-like domains also potentially bind heterophilically with extracellular matrix proteins as laminin [2] and the receptor tyrosine kinases like the epidermal growth factor receptor (EGFR), which interacts with L1 during the development of the nervous system [16]. Moreover, L1 can homophilically bind in trans to other L1 fragments, or full-length L1, affecting different processes as axon fasciculation and guidance [17]. The FN-type-III domains are also involved in heterophilic interactions, in particular binding to the Ig domains of fibroblast growth factor receptor 1 (FGFR1) playing a key role in neuronal differentiation [18]. The intracellular domain of L1 (L1-ICD) is responsible for the interaction between L1 and the cytoskeleton and ankyrins are the main binding partners of the L1-ICD. These interactions are highly controlled and determine different downstream processes for L1 [19]. The binding between L1 and ankyrins is mediated by a 30 amino acid sequence in the L1-ICD, containing the motif FIGQ/AY, and connecting L1 through ankyrins [20] with other cytoskeleton proteins, such as spectrin [21]. Mutations in this sequence are involved in the Gareis-Mason syndrome, characterized by neurological disorders and mental retardation [22]. In addition, a neuronal form of L1 contains the RSLE motif [23], which binds to the adaptor protein 2 (AP-2) and connects L1

with ezrin-radixin-moesin (ERM), and hence links L1 with actin [20]. The molecular mass of L1 can be different between cell types according to the glycosylation state of L1. The Ig1-4 domains contain four glycosylation sites, Ig5-6 contain five and FN1-FN5 have twelve sites [24], and glycosylations can affect interactions of L1 [24]. Besides glycosylation, L1 can undergo other post translational modifications that can affect L1's function. These modifications include *SUMOylation*, required for proteolytic processes events. L1 contains two different sumoylation sites, a canonical sumoylation type I site, Met-Lys-Asp-Glu (MKDE) [25], and a non-canonical type II Gly-Lys-Lys-Glu (GKKE) site [26]. Other modifications are *ubiquitination*, involved in neurite outgrowth and cell adhesion, influencing the lysosomal degradation and controlling the re-appearance of L1 at the plasma membrane [27], and *phosphorylation*, e.g. of a tyrosine residue upstream of the RSLE motif, preventing the binding between L1 and AP-2 and the clathrin-mediated internalization of L1 and inhibiting L1-mediated neurite outgrowth [28], or of the tyrosine residue of the FIGQY motif in the cytoplasmatic domain that mediates ankyrin binding and regulates neuronal growth [29].

As most of neuron-specific genes, the expression of the L1 gene is highly regulated on the transcriptional level: L1 transcription is controlled by the transcription factor REST (RE1-Silencing Tran-scription factor) [30] and nuclear factor 1-A (NF-1A) [31] which act as repressors, and Slug which acts as positive regulator factor [10, 32]. Being expressed in different tissue, L1 protein has 2 isoforms: the full-length isoform (fl-L1), composed by 28 exons and present in neuronal and some cancer cell types and the short (sh-L1) isoform lacking two mini-exons (exon 2, encoding extracellular amino acids, and exon 27, encoding intracellular amino acid) expressed in non-neuronal cell types [33]. The expression of the two isoforms depends on the transcription factor REST and the splicing factor Nova2. In cells with high levels of REST, Nova2 is downregulated and alternative splicing

does not occur, leading to the predominant expression of the short isoform. In cell types with low levels of REST, as neuronal cells and cancer cells, Nova2 is present in high amounts and the splicing of L1 takes place, with the insertion of the two exons 2 and 27, resulting in the formation of the full-length isoform of L1 [33].

The importance of L1 for the development of the nervous system is also highlighted by the large number of neurological disorders in humans linked to mutations in the L1 gene. Mutations in the L1 gene cause a wide spectrum of syndromes, summarized as L1 syndrome, which is an X-linked recessive disorder that results in brain abnormalities and delay in the development of the nervous system. The main symptoms of the L1 syndrome are hydrocephalus, the stenosis of Sylvius's aqueduct, adducted thumbs, aphasia, shuffling gait and mental retardation, spastic paraplegia type 1 (SPG1) and agenesis of the corpus callosum and corticospinal tracts [34]. Other disorders linked to mutations in the L1 gene are fetal alcohol syndrome [35] and schizophrenia [36, 37]. To better understand the mechanisms underlying the L1 syndrome, L1 knock-out mice and mice carrying a disease-causing human mutation have been studied. As in humans with L1 mutations, these mice show hydrocephalus, alterations in axon guidance and neuronal morphology and hypoplasia [38, 39, 37, 40]. Moreover, L1 is associated with numerous kinds of cancer and it is used as marker for tumor progression and as an indicator of the prognosis. In most of the cancers, like ovarian and endometrial carcinoma, L1 expression is associated with poor prognosis, progression of the tumor cells to lymph nodes and metastasis [41]. Tumor cells expressing L1 show increased proliferation, motility and metastasis invasion of healthy tissues [42]. It is possible that in cancer cells L1 keeps tumor cells together, promotes an invasive phenotype, induces cell migration and therefore tumor growth, metastasis and chemoresistance [43]. In contrast to other cancer types, the expression of L1 in children affected with neuroblastoma, is an indication of good prognosis [44].

Putting together all the data from cancer research focusing on the role of L1, it is clear that this protein could be a potential target for cancer therapy, not only a biomarker [10]. Thus understanding L1's functions is a step forward for tumors treatment.

1.1.2   L1 and its proteolytic processing

The mechanisms and functions of L1 depend also on a highly regulated proteolytic process that controls the role of L1 and its location. The full-length L1 can be cleaved by different proteases and at different sites. One cleavage site is located in the third fibronectin domain at the dibasic sequence $_{858}$RKHSKR$_{863}$ (Figure 1.3) [45], and L1 is cleaved at this site by serine protease PC5a [46], plasmin [47, 48, 49] and trypsin [50, 51]. It was thought that Reelin also cleaves at this site, but recent studies suggested that Reelin is not cleaving L1 but the co-purified protease myelin basic protein [52, 45]. The cleavage of L1 by PC5a, plasmin and trypsin lead to the formation of one soluble fragment of 140 kDa containing the extracellular epitopes for the L1 antibodies 324, 555 and 557, and a transmembrane fragment of 80 kDa containing the intracellular epitopes for L1CAM-C2 and 172-R antibodies [45]. Full-length L1 can be also cleaved by members of the ADAM family, such as ADAM10 and ADAM17 [53] which are both involved in regulating neural cell adhesion, migration, and neurite outgrowth, or by neuropsin [54], resulting in the generation of a soluble 180 kDa, found in tumor cell lines and the developing mouse brain, and a membrane-bound 32 kDa fragment [55, 56]. Moreover, ADAM proteins can process the 80 kDa fragment, generating the 32 kDa fragment and an extracellular 50 kDa fragment [46, 50]. The 32 kDa membrane stump of L1 is further processed by presenilin/γ-secretase generating an intracellular 28 kDa fragment, which is transported into the nucleus, and contributes to the regulation of gene expression [55]. Another cleavage site is located in the first fibronectin domain at the position R$_{687}$V (Figure 1.3) [45] and myelin basic protein (MBP) cleaves L1 at this site [57].

The cleavage is preceded by a post-translational modification that leads to a sumoylated L1 full-length protein. The cleavage by MBP generates an extracellular fragment of 134 kDa, with the epitope for the L1 antibody 324, and a sumoylated fragment of 70 kDa, which contains not only the intracellular domain with the epitopes for the antibodies L1CAM-C2 and 172-R, but part of the extracellular domain with the extracellular epitopes for the antibodies 555 and 557 [26]. The L1-70 fragment has been shown to be transported into the nucleus [26] and into mitochondria [58]. In the cytosol, L1-70 can be further processed by cathepsin E leading to the generation of a sumoylated 30 kDa fragment which is transferred into the nucleus, playing a role in cell migration and axonal myelination [25].
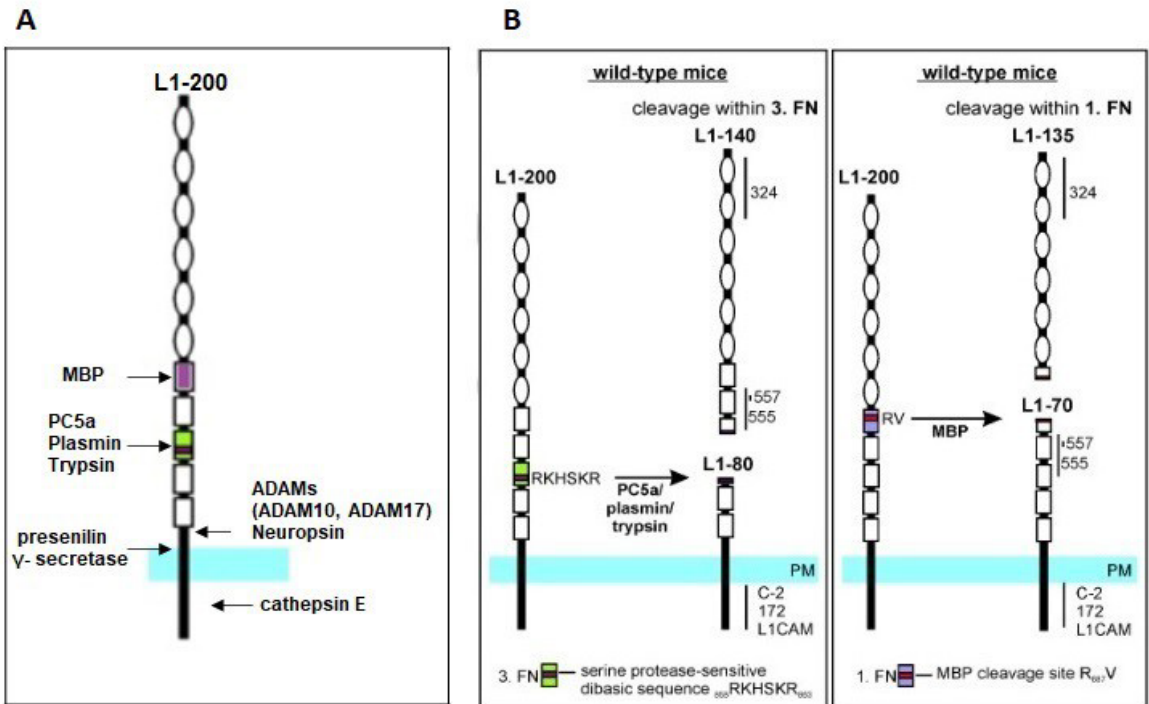
Figure 1.3: L1 structure and cleavage sites. A) Full-length L1 contains different cleavage sites within the fibronectin domains, close to or within the transmembrane domain. B) Cleavage site in the third FNIII domain within the dibasic sequence $_{858}$ RKHSKR$_{863}$, and in the first FNIII domain at the R$_{687}$ V position. Image modified from [45].

The mutations in the first fibronectin domain (from $R_{687}V$ to $A_{687}V$) and in the third fibronectin domain (from $_{858}RKHSKR_{863}$ to $_{858}SKHSSS_{863}$) prevent the generation of the L1-70 fragment, and mice with these mutations were used in this thesis.

1.2 Mitochondria

Mitochondria are considered the "powerhouse" of the cell, being the main source of adenosine triphosphate (ATP), produced through the oxidative phosphorylation mechanism (OXPHOS) [59]. Mitochondria have a central role in the energy metabolism: the energy produced by the oxidation of food is converted into ATP. Nicotinamide adenine dinucleotide (NADH) and flavin adenine dinucleotide ($FADH_2$) that are produced during the glycolysis and fatty-acid oxidation are used in the electron transport chain as electron donors [60]. Apart from cell respiration and ATP synthesis, mitochondria are involved in numerous and various cell processes as calcium homeostasis [61], programmed cell death [62], stem cell reprogramming [63] or innate immunity [64]. In addition, mitochondria are also involved in the production of metabolic precursors for proteins and lipids, DNA and RNA [65].

Mitochondria contain their own genome consisting of a double-stranded circular DNA (mtDNA), compacted by the mitochondrial transcription factor TFAM [66], and their own protein translation machinery, ribosomes, tRNAs and associated protein factors. From the mtDNA, transmitted only through the female germ line [67], a very low number of proteins (13 in humans) are synthesized in mitochondria from the mitochondrial genes located on mtDNA. In fact, 99% of mitochondrial proteins are encoded and produced by nuclear DNA in the cytoplasm and imported into the organelle through a set of protein translocases [68].

Mitochondria are double membrane organelles: they have an outer membrane that separates the organelle from the cytosol and an inner membrane that surrounds the mitochondrial matrix (Figure 1.4). The space between the two membranes is the intermembrane space. The outer membrane, that does not create a membrane potential, can be crossed by ions and small uncharged molecules that can freely move through porins and ions channels, such as the voltage-dependent anion channel (VDAC) [68, 69]. The inner membrane instead is a tighter barrier and molecules, especially proteins, can cross this membrane only through a specific transport machinery. The inner membrane has an electrochemical membrane potential (180 mV) and forms invaginations into the matrix called *cristae* where the oxidative complexes are located and where the ATP is synthesized [68]. The difference in pH between the mitochondrial matrix (7.9-8) and the intermembrane space (7.2-7.4) creates the electrochemical gradient that drives the synthesis of ATP.
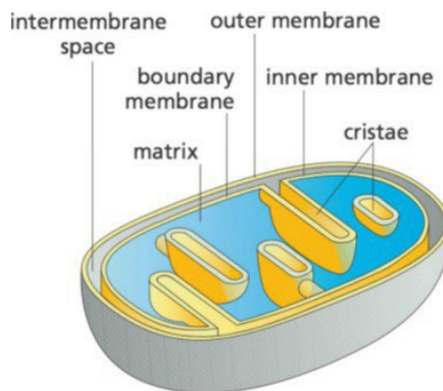
Figure 1.4: Mitochondrial structure. Mitochondria are double membrane organelles formed by an outer membrane that separates the mitochondria from the cytosol and an inner membrane that encloses the matrix containing the mtDNA. The inner membrane forms the cristae, invaginations of the membrane into the matrix where the ATP synthase machinery is located. The space between the membrane is the intermembrane space. Image modified from [68].

1.2.1   Import machinery

The majority of the proteins involved in OXPHOS are encoded by nuclear DNA, synthesized in the cytosol as precursors and then imported into the mitochondria by the import machinery. There are different ways through which proteins can be transferred into mitochondria (Figure 1.5):
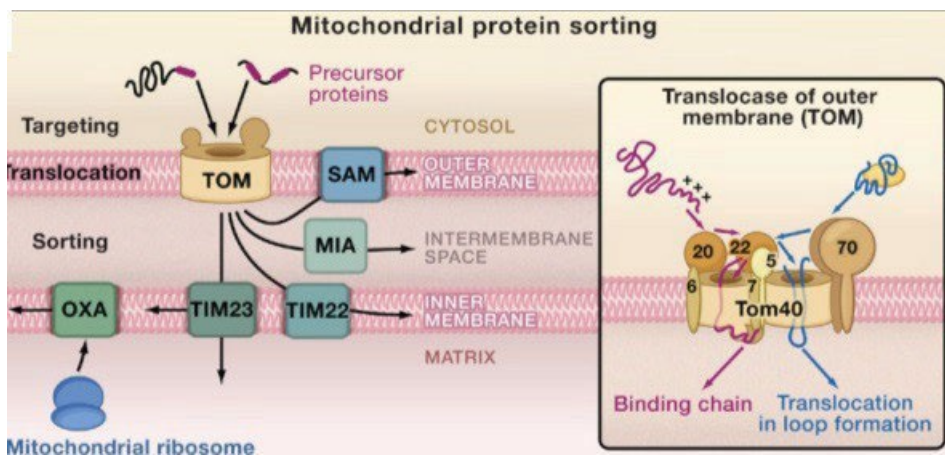
Figure 1.5: Overview of the import machinery of mitochondria. All proteins are imported first through the translocase of the outer membrane (TOM) and according to their destination are sorted out by different import mechanisms: oxidase assembly (OXA) translocase, insertase/export machinery of the inner membrane; translocase of the inner membrane (TIM) 23 complex, presequence translocase of the inner membrane for preprotein with an N-terminal target sequence; TIM22 complex, carrier translocase of the inner membrane for pre-protein with an internal targeting sequence; MIA, mitochondrial intermembrane space assembly for preprotein with cysteine motifs; SAM, sorting and assembly machinery for proteins inserted in the outer membrane. The TOM complex consists of seven different subunits: TOM20, TOM22, and TOM70 receptors, the channel-forming TOM40 and three small Tom proteins, TOM5, TOM6, and TOM7, involved in the assembly and dynamics of the TOM complex. Image modified from [70].

- Presequence pathway:
  The presequence pathway is responsible for the import of 60% of all mitochondrial proteins [71]. Proteins that are transferred through this pathway, are characterized by an N-terminal targeting sequence (15-50 amino acids), that forms an α-helix, and are recognized first by the translocase of the outer membrane (TOM) [72]. The TOM complex is composed of TOM20, TOM22, TOM70, which are receptors, TOM40 with a β-barrel structure forming the channel and small associated proteins TOM5, TOM6 and TOM7 that regulate the dynamics of the complex [70]. The presequence on the N-terminus of the preprotein is recognized by TOM20 [73] and TOM22, while TOM5 mediate the transfer of the protein to the TOM40 channel. The preprotein interacts with the TIM23 complex [72] which is composed of TIM23, TIM17, TIM50 and TIM21. TIM50 recognizes the presequence on the protein and blocks also the TIM23 channel in absence of preproteins [74], TIM23 and TIM17 form the channel and TIM21 connects the TIM23 complex to the III e IV supercomplex of the respiratory chain [72, 70]. The TIM23 complex is activated by the membrane potential of the inner mitochondrial membrane: the difference of charges across the membrane activates TIM23, which is voltage-dependent [75] and favors the transport of the positively charged targeting sequence across the inner membrane into the matrix [76]. The preprotein is transferred into the matrix by the presequence translocase-associated motor (PAM) [72]. The core of PAM is the molecular chaperone mitochondrial 70 kDa heat shock protein (mtHsp70) that drives the translocation of the protein into the matrix by an ATP-dependent mechanism [77, 70]. Once in the matrix, the signal sequence is proteolytic processed by the matrix protein peptidase (MPP) [70]. If the protein has to be inserted in the inner mitochondrial membrane, the protein is further synthesized on mitochondrial matrix ribosomes and translocated into the inner membrane by the oxidase assembly (OXA) [78].

- Carrier pathway:
  The carrier pathway is responsible for importing proteins that do not possess an N-terminal sequence mitochondrial target, but different internals target sequences [79]. The precursor of the protein is carried to the mitochondria by cytosolic chaperones (such as HSP70) [72], recognized by TOM70 and transferred into the matrix through the complex TIM22 activity. TOM70 presents two binding sites, one for the precursor protein and one for the cytosolic chaperone. When ATP is released, the precursor protein is released from the cytosolic chaperone and binds to TOM70, and is then transferred to TOM22, followed by the insertion in the TOM40 channel. From the TOM complex the protein is translocated to the TIM22 complex consisting of TIM22 that forms the channel and regulates the insertion of the protein in the inner membrane in a membrane potential-dependent way, the receptor-like TIM54, TIM18-Sdh3 module that is involved in the assembly of the TIM22 complex, and the TIM9-TIM10- TIM12 chaperone complex [72]. The carrier precursors proteins first bind to the Tim9–Tim10–Tim12 chaperone complex on the surface of the translocase and after the activation of TIM22, proteins are inserted into the channel and laterally released into the lipid phase of the inner membrane [72].

- Sorting and assembly machinery pathway:
  The proteins that have to be inserted in the outer mitochondrial membrane are characterized by a β-barrel structure and are integrated into the membrane, or an α-helix structure, which are the proteins anchored to the membrane by one or more transmembrane segments [72]. These proteins are transferred into the mitochondria with the sorting and assembly machinery pathway (SAM): first proteins with the β-barrel structure are recognized by TOM20, transferred to the TIM chaperons and then inserted into the membrane through SAM. The SAM complex consists of Sam50, which is a transmembrane protein, and Sam35 and Sam37 that are exposed to the cytosol.

The protein first binds to Sam35, is then folded by Sam50, and finally released into the membrane by Sam37 [70]. If the precursor protein has an α-helix structure, the insertion is mediated by the MIM complex: the protein is recognized by TOM70 and then transferred into the membrane through the mitochondrial import 1 (Mim1) subunit, which is present in different copy number and one copy of Mim2 [72].

- Mitochondrial intermembrane space assembly pathway: The import of proteins that are located in the intermembrane space into mitochondria is carried out by the mitochondrial intermembrane space assembly pathway (MIA). These proteins, characterized by cysteine motifs are in an unfolded state in the cytosol [80] and are oxidized by the MIA complex before getting released into the intermembrane space. The MIA complex consists of Mia40, which serves as receptor and the endogenous retroviral element 1 (Erv1), and it is supported by the helper of Tim of 13 kDa (HOT13). First the protein is transferred to the TOM complex, in particular just the TOM40 subunit is involved in this step [81]. Mia40 recognizes the cysteine residues and catalyzes the formation of disulfide bonds, stabilizing the protein. The formation of the disulfide bonds is mediated by Erv1, by the formation of transient disulfide bonds that are passed to Mia40 and then to the protein. This passage leads to the reduction of Mia40 which is oxidized again by Erv1 and HOT13. The oxidation and reduction mechanisms originate from a flux of electrons from Mia40 to Erv1, and then to O_2 and then cytochrome c, and finally to the respiratory chain [72, 82].

1.2.2   Oxidative phosphorylation complexes

The catabolism processes and the metabolism mechanisms of the cell such as glycolysis, transamination or β-oxidation produce molecules and substrates used by the electron mitochondrial chain (ETC) for the oxidative phosphorylation and the consecutive production of ATP by mitochondria [83]. The ECT is located within the inner membrane of mitochondria in proximity of the matrix, where the tricarboxylic acid cycle takes place (TCA or Krebs cycle) [83]. The ETC is formed by 5 different transmembrane complexes (I-V) and the electron carriers ubiquinone and cytochrome c, which move freely between the complexes (Figure 1.6) [84].
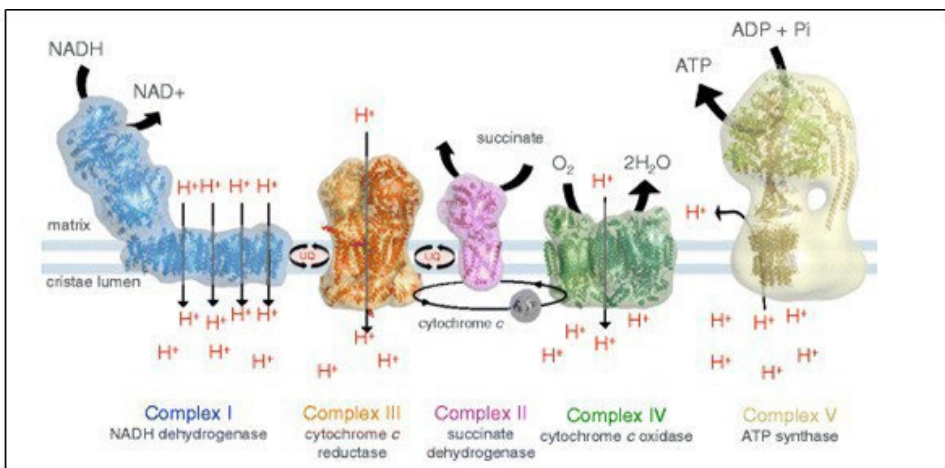
Figure 1.6: Overview of the complexes composing the mitochondrial respiratory chain. Complex I oxidizes NADH to NAD$^+$ by transfer of two electrons from NADH to ubiquinone forming ubiquinol. This reaction generates protons that are moved from the matrix into the intermembrane space. Complex II catalyzes the oxidation of succinate to fumarate and reduces ubiquinone to ubiquinol. No protons are transferred in this step. Complex III catalyzes the oxidation of ubiquinol and the reduction of cytochrome c with the translocation of protons in the intermembrane space. Complex IV transfers electrons from cytochrome c to O$_2$ and pumps protons across the inner mitochondrial membrane to generate an electrochemical proton gradient. The electrochemical proton gradient created across the intermembrane space by complex I, III and IV drives ATP synthesis by the ATP synthase (complex V). Image modified from [68].

The complexes are composed as follows:

- **Complex I (CI)**: CI or NADH-ubiquinone oxidoreductase, is the largest subunit of the ETC. It contains two domains: the membrane arm, which is the transmembrane portion of the subunit inserted into the inner mitochondrial membrane, and the matrix arm that extends into the mitochondrial matrix. The core of the complex is formed by 45 different proteins with 7 subunits in the matrix arm (comprehending NDUFV2), which are all encoded by the mitochondrial genome, and 7 hydrophobic subunits in the transmembrane arm [84]. The two arms, shaped like an L, have 3 different activity sites: 1) the N module, which contains the dehydrogenase site in the matrix arm, 2) the Q site in the junction between the two arms containing the site for the ubiquinone (CoQ) reduction and 3) the P module in the membrane arm, where the protons are released [85]. Basically, the NADH produced by the TCA binds to an ubiquinone site located in the junction between the two arms [84], and is oxidized to NAD^+ and the ubiquinone (CoQ) is reduced to ubiquinol (QH_2) [86]. The energy released by the electron flowing from NADH to CoQ drives the release of four protons from the matrix into the intermembrane space [84].

- **Complex II (CII)**: CII or succinate dehydrogenase ubiquinone–ubiquinol reductase is a component of the TCA cycle and the only membrane-bound member of the TCA cycle [86] linking the oxidative phosphorylation and the TCA processes [84]. This complex is composed of 4 subunits encoded by the nuclear genome and consists of a hydrophilic portion that projects into the matrix where the binding site for succinate is located [84], a hydrophobic tail within the inner membrane, containing the CoQ binding site [84], and of a short portion that projects into the intermembrane space [86]. CII catalyzes the oxidation of succinate in fumarate. This leads to the reduction of FAD to

$FADH_2$, after receiving the electrons from succinate, which are then transferred to CoQ that is reduced to QH_2. In this step there is no translocation of protons [84].

- **Complex III (CIII)**: CIII, also called ubiquinol–cytochrome c reductase, catalyzes the transfer of electrons from reduced ubiquinol to cytochrome c [84]. It is formed by a dimer, each monomer contains 11 subunits [87], of which only one, the cytochrome b, is encoded by mtDNA [83]. The catalytically active subunits are cytochrome b (b_L and b_H) and cytochrome c_1 [84]. CIII has two CoQ binding sites: one is the oxidation site (Q_0) on the intermembrane space, the other is the reduction site (Q_1) in the matrix space [84]. After the oxidation of ubiquinol, two protons are released from the matrix across the inner membrane into the intermembrane space. The electrons are transferred via cytochrome b_L, b_H and c_1 to cytochrome c in the intermembrane space [88].

- **Complex IV (CIV)**: CIV, also called cytochrome c oxidase, mediates the translocation of electrons from cytochrome c to the terminal acceptor O_2, thereby generating two molecules of H_2O_2 [84]. CIV is formed by 13 subunits, with the three largest ones encoded by mtDNA [83]. Cytochrome c, being loosely bound to the inner mitochondrial membrane can accept the 4 electrons from cytochrome c_1 of the CIII and then move along the surface to transfer the electron to a O_2 molecule that is thereby reduced to H_2O_2 [84, 88]. In this step a total of 8 protons are removed from the matrix of mitochondria, half of them are used to generate the two molecules of H_2O_2, while the other half are pumped into the intermembrane space [84].

- **Complex V (CV)**: CV or ATP synthase, uses the proton electrochemical gradient generated by the CI, CII, CIII and CIV to produce ATP [83]. The complex is formed by two domains, F_0 and F_1. F_0 is inserted in the inner mitochondrial membrane, while F_1 is located in the matrix [84]. The F_1 domain has three α subunits, three β subunits, which are

the catalytic core of F_1, one γ and δ subunit and one ε subunit, which connects F_1 to F_0 [89, 90]. The protons moved from CI, CIII and CV pass from the intermembrane space to the matrix through the F_0 domain which transfers the energy generated by the protons flux to F_1. This leads to a conformational change in the ATP synthase causing to phosphorylation of ADP to produce ATP [84, 90].

1.2.3   Mitochondrial dynamics

Mitochondria are highly dynamic organelles and all their mechanisms are regulated by a set of processes: fission, fusion, biogenesis, degradation, and intracellular transport [91]. The balance between these mitochondrial mechanisms regulates the number, shape and localization of mitochondria [92].

Mitochondrial trafficking

Mitochondria are transported and delivered to regions of cells that require energy. This is particularly true for neurons, where mitochondria are delivered to areas that require a high production of energy such as synapses [93] and active growth cones [94]. Long range movements need microtubule motors and adaptors of the kinesin or dynein family, while short-range movements are mediated by actin filaments [94]. Movement of mitochondria is saltatory and bidirectional [94] towards a "plus"-end directed to the terminals, called anterograde transport, and a "minus"-end directed towards the cell soma, called retrograde transport (Figure 1.7).

Generally, mitochondria with high membrane potential migrate in an anterograde direction, in regions with higher metabolic demand, while mitochondria with lower potential are mostly transported retrogradely [95]. The "plus"-end direction movements are mediated by kinesin, in particular kinesin-1 (kinesin heavy chain or Kif5). This protein has an N-terminal domain allowing movement in the "plus"-end direction, a large tail for dimerization and the C-terminus involved in cargo-binding regulation [93]. Kinesin binds to Milton, also called TRAK (trafficking protein kinesin- binding), which is expressed in two isoforms TRAK1 and TRAK2. Milton acts as adaptor between motor proteins, binds kinesin and thereby connects kinesin with Miro (also known as RhoT1/RhoT2). Miro is a Rho family GTPase, with two GTPase domains, a pair of Ca^{2+}-binding helix-loop-helix Ca^{2+} binding sites (EF hands) and is anchored to the outer mitochondrial membrane (OMM) through its C-terminal domain [95, 93]. Miro binds Ca^{2+} and acts as a sensor for the cytoplasmatic Ca^{2+} levels and ATP concentration. When cytosolic Ca^{2+} levels are low, Miro binds to Milton and when cytosolic Ca^{2+} levels are higher, Miro cannot bind Milton resulting in uncoupling of mitochondria from microtubules. This could explain the saltatory movements of mitochondria, which move when the cytoplasmatic Ca^{2+} levels are lower [95]. The "minus"-end directed or retrograde movements, are mediated by the dynein complex. The core of this complex is the dynein motor associated with dynactin, a multi-protein complex. Dynactin binds to the cytoplasmic dynein and microtubules, connecting the microtubules with mitochondria through the interaction with Milton [96]. Most mitochondria do not move in axons and constitute the steady and immobile mitochondrial pool. Regulation of the steady pool is controlled by syntaphilin (SNPH) [97]. SNPH is bound to the OMM of mitochondria and contains a microtubule-binding domain [93]. When cytoplasmatic Ca^{2+} concentrations are increased, Miro releases kinesin-1, which binds to SNPH, thereby inhibiting mitochondrial movements [97].
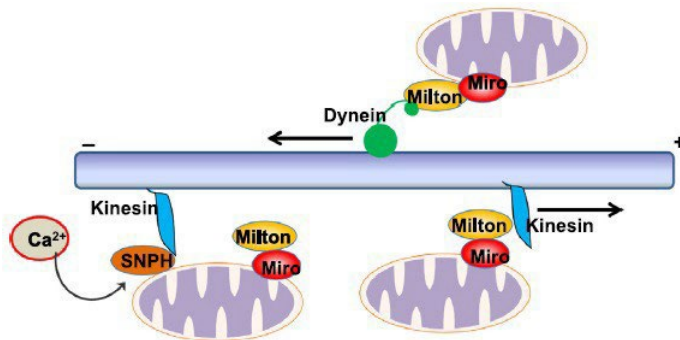
Figure 1.7: Overview of mitochondrial trafficking mechanisms:
Mitochondria are transported towards two directions, a "plus"-
end and a minus"-end. Two motor proteins regulate the
movements: kinesin mediates the movements to the "plus"- end,
while dynein regulates the movement to the "minus"- end. Binding
of mitochondria to the motor proteins is mediated by two anchors
and adaptors Milton, which links the motor protein to the OMM
and Miro which is bound to the OMM. Mobility of mitochondria is
regulated by syntaphilin (SNPH). Image modified from [97].

Fission and fusion

Fission and fusion of mitochondria are two opposite, but related
processes: morphology, number, shape and distribution of
mitochondria change according to the balance between these
processes, which are regulated by a series of GTPases for the
inner and the outer mitochondrial membranes (Figure 1.8) [98].
Mitochondrial fusion is coordinated by three large GTPase
proteins: mitofusin 1 and 2 (Mfn1 and Mfn2) and optic atrophy

1 (OPA1), which mediate the fusion of the OMM and inner
mitochondrial membrane (IMM), respectively [99].
Overexpression of both mitofusins leads to mitochondrial
aggregation around the nucleus [100], while knock-out of Mfn1 or
Mfn2 results in fragmented mitochondria or swollen and spherical
mitochondria, respectively [101]. Moreover, Mfn2 is also
involved in the mitochondria-ER interaction and facilitates the
Ca^{2+} intake [102]. Mitofusins are inserted in the OMM and carry an

N-terminus containing the GTPase site and two transmembrane

domains that separate two coil-coil heptad sequences, localized in the transmembrane domain (HR1) and at the C-terminal (HR2) exposed towards the cytosol, which functions in the mitochondrial tethering [103, 104]. Both proteins accumulate on the membranes of two adjacent mitochondria and establish homo- or heterotypic complexes leading to mitochondrial fusion [92], which is characterized by three steps: first two mitochondria bind in trans through the HR2 domains of mitofusin, then the attachment of the two membranes increases the contact site, finally the conformational changes due to the GTP hydrolysis lead to the fusion of the membranes [92]. OPA1 regulates the fusion of the IMM which occurs downstream of the OMM fusion [92]. Loss of mitofusins blocks both fusion of OMM and IMM, while in absence of OPA1 just the fusion of IMM is inhibited. Contrary to the OMM fusion that requires mitofusins on both mitochondria, the localization of OPA1 on just one of two mitochondria is sufficient for the IMM fusion [105]. OPA1 is inserted in the inner mitochondrial membrane and possesses an N-terminal domain facing the matrix and containing the target sequence, followed by a transmembrane domain facing the intermembrane space [92] and, interestingly, requires the interaction with Mfn1, not Mfn2, for the fusion process [106]. OPA1 exists in different isoforms generated by alternative splicing and the distribution and abundance of different OPA1 proteins affects the fusion process. Moreover, the membrane potential of the IMM can affect generation of OPA1 isoforms and their balance [107].

Mitochondrial fission comprises the division of one mitochondrion into two or multiple daughter mitochondria. This process requires the recruitment of the cytosolic protein dynamin-related protein 1 (DRP1). DRP1 contains an N-terminal domain with the GTP site, a middle domain followed by a GTPase effector domain (GED) at the C-terminal end [103]. During fission Drp1 is recruited to the OMM and forms a ring-like structure around the mitochondria on the fission site, where it forms dimers that surround and constrict the mitochondria.

After the hydrolysis of the GTP mitochondria are separated at the constriction site [99]. After the fission, Drp1 returns to the cytosol [103]. The localization and the activation of Drp1, as well as its pool, are regulated by different post-translational modifications as ubiquitination, phosphorylation or sumoylation [95]. Moreover, the recruitment of Drp1 on the mitochondria involves the interaction with accessory proteins as fission protein 1 (Fis1) or mitochondrial fission factor (MFF). Both Fis1 and MFF are anchored to the OMM and in particular MFF recruits Drp1 to the mitochondria while Fis1 is involved in the assembly of the fission apparatus [108].
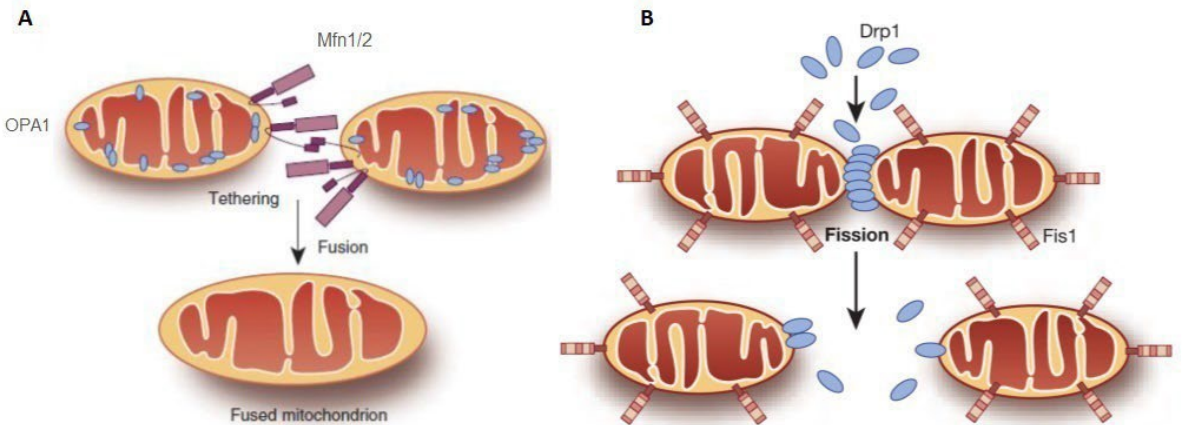
Figure 1.8: Overview of mitochondrial fission and fusion: a) Fusion is mediated by the GTPases Mfn1, Mfn2 and OPA1. Mitofusins are responsible for the fusion of the OMM, through t h e interaction of adjacent C-terminal HR2 regions in Mfn1 and Mfn2 and GTP hydrolysis. OPA1 regulates the fusion of the inner mitochondrial membrane. b) Fission is regulated by the GTPase Drp1, which is recruited to the outer mitochondrial membrane upon stimulation, interacts and oligomerizes with Fis1, leading to the constriction of the OMM through GTP hydrolysis and resulting in mitochondrial fission [103].

Mitochondria quality control and mitophagy

PINK1 and Parkin pathway: In order to function properly and to have a healthy pool of mitochondria, cells have quality control mechanisms that can recognize and remove damaged mitochondria. This process, defined as mitophagy, is a selective form of autophagy that prevents the accumulation of unhealthy mitochondria and removes impaired ones [109]. Different molecular mechanisms and pathways are involved in the mitophagy process. Fragmentation or fission of mitochondria with impaired membrane potential precedes mitophagy, while excessive fusion inhibits the degradation of mitochondria [110]. The main pathway of mitophagy involves two main proteins, PINK1 and Parkin, which respond to impairments in the mitochondrial membrane potential [110] (Figure 1.9). Parkin is an E3-ubiquitin (Ub) ligase that mediates the covalent binding of the C-terminal glycine residue of ubiquitin to the lysine residue of the target protein. Since ubiquitin itself contains 7 lysine residues, polyUb chains can be generated [111]. Parkin includes a Ub-like multiple RING domain containing a binding site for the E2 ubiquitin-ligase and the catalytic site, and a REP domain (repressor element of PARKIN domain). Parkin is normally inactive and auto inhibited in the cytosol through a repressor element that occludes both the catalytic site and the E2-ubiquitin ligase site [110]. The PTEN-induced putative kinase PINK1 is a serine/threonine kinase [112] containing a mitochondrial target sequence that mediates the translocation of PINK1 from the cytosol to the inner membrane of mitochondria through the TOM/TIM import pathway [109]. PINK1 levels are low in healthy cells, because the protein is rapidly transferred into mitochondria, cleaved by different proteases, such as the mitochondrial-processing protease (MPP) and the inner membrane presenilin-associated rhomboid like protease (PARL), and finally degraded [113, 114]. The loss of the membrane potential inhibits the translocation of PINK1 into the mitochondria, causing the accumulation of this protein on the outer mitochondrial membrane of damaged mitochondria [112, 115], marking them for degradation

and activating parkin [114]. To activate parkin and the cascade of events that leads to mitophagy of damaged mitochondria, PINK1 first phosphorylates itself at the S228 and S402 residues and this autophosphorylation enhances the ability to phosphorylate parkin [111, 116]. Parkin is phosphorylated by PINK1 at the N-terminus at the ubiquitin-like domain (Ubl) leading to its activation [111, 117]. The activation of parkin causes the ubiquitylation of mitochondrial targets. After its translocation to the mitochondria, activated parkin increases the E3 ubiquitin ligase activity [109]. Different targets are ubiquitinated by parkin, as Mfn1 and Mfn2, the voltage-dependent anion-selective channel protein 1 (VDAC1) [110], TOM20 and TOM70 [111]. The degradation of Mfn1 and Mfn2 lead to fragmentation of mitochondria that are then separated from the pool of healthy organelles [111]. By inducing the degradation of mitofusins, parkin inhibits the re-fusion of damaged and healthy mitochondria segregating the impaired ones for mitophagy [118]. Polyubiquitinated Mfn1 and Mfn2 are removed from the outer mitochondrial membrane and mitochondria are enclosed by the autophagosome for degradation [109, 118]. Moreover, the depolarization of mitochondria leads to the interaction of PINK1/parkin with mitochondrial Rho-GTPase Miro, which is involved in mitochondrial movement and trafficking. Miro is phosphorylated by PINK1 and then degraded in a parkin-dependent way. This process causes the loss of Miro and arrests the mitochondria motility, inhibits their fusion and separates the damaged from healthy mitochondria [109]. Furthermore, once the mitochondria are labeled for mitophagy, the ubiquitin-binding adaptor protein p62/SQSTM1 accumulates on mitochondria, thereby facilitating the recruitment of the autophagosome binding microtubule-associated protein 1A/1B light chain 3 (MAPLC3; also called LC3) [109, 114].
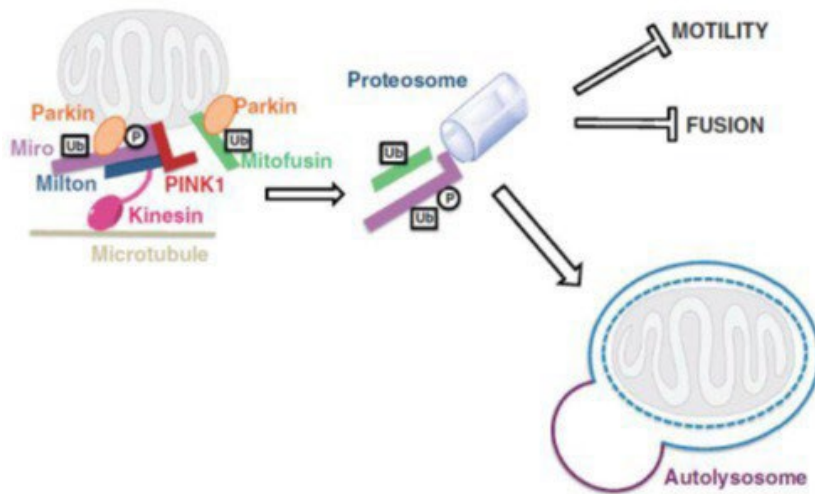
Figure 1.9: PINK1-parkin pathway. In depolarized mitochondria PINK1 accumulates on the OMM and recruits parkin. Parkin polyubiquinates mitofusin 1 and 2 and thereby inhibits mitochondrial fusion. Moreover upstream to degradation by the parkin-dependent way, Miro is phosphorylated by PINK1 disrupting the association of kinesins via the adapter protein complex of Miro and Milton with mitochondria. This results in blocking the motility of mitochondria. Image modified from [109].

LC3 pathway: MAP1LC3 or shortly LC3 is a soluble protein with a molecular mass of 20 kDa, which is present in all tissues. The human LC3 gene family has three members, LC3A, LC3B and LC3C. LC3A shows a perinuclear and nuclear localization, while LC3B and LC3C localize in the cytoplasm with LC3B present also in the nucleolar regions and LC3C is strongly expressed in the nuclei. Both LC3A and LC3B are expressed in normal tissues, while literature data report that LC3C is poorly or not expressed at all in most normal tissues [119]. LC3 is required for the elongation and maturation of the autophagosome. In the first steps of autophagy, a cup-shaped double membrane, the isolation membrane, is formed in the cytosol by the autophagy-related (Atg) proteins on the membrane formation site of the autophagosome. After its formation, the membrane elongates and closes, thereby engulfing cytosolic components and organelles.

Afterwards, the autophagosome fuses with the lysosome or with the endosome forming the autolysosome or an amphisome [120]. In the autolysosome the components and organelles enclosed in the double membrane are degraded by the lysosomal hydrolytic enzyme [120]. This steps are regulated by several Atg proteins [121], including LC3. Pro-LC3, is cleaved by the ATG4(B) protease exposing the C-terminal glycine residue forming the cytosolic form of the protein, LC3-I [122]. The cytosolic form of LC3 is further activated by Atg7 (E1-like enzyme) which transfers LC3-I to Atg3 (E2-like enzyme) and to the Atg12 complex to generate a membrane-bound form of LC3, LC3-II, which is conjugated to phosphatidylethanolamine (PE) [123] and localizes on both sides of the preautophagosomes and autophagosomes, making this protein a marker for autophagy [122]. LC3-II that localizes inside the autophagosome is degraded by lysosomal enzymes, while the portion outside is converted back to the LC3-I form and recycled [122]. The interaction between mitochondria and LC3 takes place through the binding of the p62 protein that functions as cargo [109, 114]. The binding of p62 and LC3 is mediated by the LIR domain (LC3-interacting region) that allows the docking of p62 to LC3. The C-terminus of LC3 includes a Ubl domain that contains a conserved 'ubiquitin fold', and the N-terminus contains two α-helices that are enclosed within the Ubl domain [124]. The interface of the N-terminal arm and the Ubl domain contains the LIR peptide with the sequence W/F/YxxL/I which mediates the interaction with LC3 for selective autophagy [110].

Different adaptor proteins involved in the mitophagy mechanisms contain a LIR motif that allows them to bind directly to LC3 and thus to label the mitochondria for degradation (Figure 1.10). The adaptors BNIP3/NIX or FUNDC1 are localized on the outer membrane of mitochondria [112]. The adaptor Bnip3 (Bcl-2/E1B-19 kDa interacting protein 3) and Nix contain a Bcl-2 homology 3 (BH3) domain, a C-terminal transmembrane domain and an N-terminal domain exposed to the cytoplasm. They act as pro-apoptotic mitochondrial proteins [112] and function as cell death

activators by inducing the opening of the mitochondrial permeability transition pore [125]. Both Bnip3 and Nix are not expressed under normal conditions, but during hypoxia their expression is highly induced [112]. FUNDC1 does not have a pro-apoptotic activity [125] and is highly expressed during hypoxia which leads to mitophagy [109, 112]. FUNDC1 and Nix/Bnip3 act as receptors and mediate mitophagy through the interaction with LC3 and the LIR domain [125]. The binding between FUNDC1 and LC3 is regulated by the reversible phosphorylation of FUNDC1 by PGAM5. Under normal conditions FUNDC1 is phosphorylated but in case of hypoxia, PGAM5 is activated and dephosphorylates FUNDC1 increasing its affinity for LC3. For Bnip3 instead, the affinity is higher after phosphorylation of Ser17 and Ser24 [71].
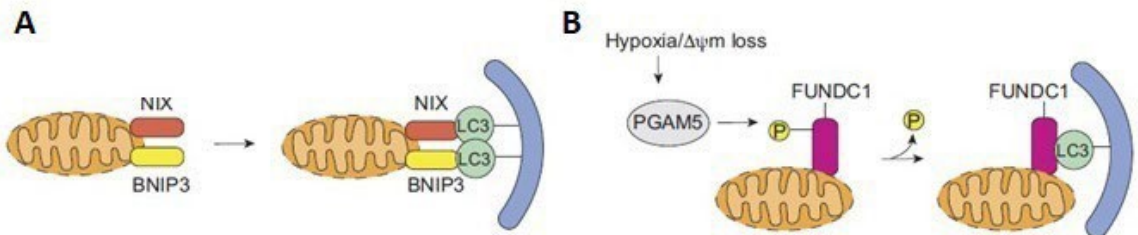
Figure 1.10: Overview of the autophagy LC3-dependent pathway. a) BNIP3 and NIX act as mitochondrial receptors and directly interact with LC3 through the LIR domain to induce mitophagy. b) Dephosphorylation of FUNDC1 by PGAM5 activates FUNDC1 that directly binds with LC3 via the LIR motif, to induce mitophagy. Image modified from [125].

1.3   L1 and mitochondria

A connection between L1 and mitochondria was previously established in our laboratory. It was shown that a fragment of L1, L1-70, which is the product of proteolytic activity of MBP [57], is imported from the cytoplasm into mitochondria [58]. In mice lacking L1, the activity of complex I, which is one of the complexes involved in generating the proton gradient [85, 84], is lower compared to that of wild-type mice and one subunit of the complex I, NADH dehydrogenase ubiquinone flavoprotein 2 (NDUFV2), was identified as binding partner of L1 indicating that L1-70 interacts with this complex I subunit to regulate its activity [58]. Moreover, the absence of L1 or prevention of L1-70 generation resulted in impaired mitochondrial membrane potential, associated with lower levels of fusion and higher numbers of fragmented mitochondria, as well as higher retrograde transport in cultured cerebellar neurons [58]. Additionally, results suggested that L1-70 interacts with Drp1 and Miro on the outer surface of mitochondria contributing to the fission–fusion cycles and mitochondrial trafficking [58]. In addition, the rotarod test performed on wild-type and L1-deficient mice showed that L1-deficient mice had a lower latency to fall from the rod than wild-type mice, which also performed better in subsequent trials, while mice lacking L1 did not show an improvement in the performance, suggesting an impaired motor function in L1-deficient mice [40, 126]. Impairments of mitochondrial functions, such as fission, fusion or mitophagy are implicated in neurodegenerative disease as Parkinson's, Alzheimer's and Huntington's diseases [109]. In particular, both PINK1 and parkin, which constitute the main mitophagy pathway for the clearance of damaged mitochondria, are associated with an early onset hereditary form of Parkinson's [109, 114]. Interestingly, it was shown that levels of full-length L1 and of the L1-70 fragment are reduced in a mouse model of Alzheimer's disease, and that overexpression of L1-70 had a protective effect on neurons in this model [26]. It is possible that the impairment of L1 or its fragments can contribute to the development of neurodegenerative diseases.

CHAPTER 2

AIM OF THE THESIS

Previous studies showed that L1 interacts with extracellular GAPDH [127] and adenine nucleotide translocator (ANT) isoforms ANT1 and ANT2 [128], which have major functions in mitochondria and metabolism. Moreover, previous studies in our group showed that a fragment of L1, L1-70, which is produced by MBP-mediated proteolytic cleavage [57], is transported into the mitochondria where it interacts with GAPDH, influences the mitochondrial membrane potential and complex I activity. Moreover, L1-70 is involved in regulating mitochondrial motility [58] and the motor activity of mice [40].
Based on these findings the aims of my study were:

Identifying binding partners of L1 involved in mitochondrial processes including mitophagy: this aim was addressed with immunostainings, immunoprecipitations and ELISA which allow to show binding of L1 to its mitochondrial interaction partners and their presence in a complex.

Studying the effects of the absence of the L1-70 fragment on mitochondrial metabolism: this aim was achieved through measurements of complex I activity, ATP levels, mitochondrial

membrane potential, motility of mitochondria and levels of mitochondrial interaction partners in neurons and mitochondria from wild-type mice and mice lacking L1-70.

Identifying potential differences in morphology: to achieve this goal, staining of tissue was performed to identify possible differences in the brain structure of L1-70 fragment-lacking transgenic mice in comparison to wild-type littermates.

Behavioral characterization of a L1-70-deficient mouse line: this aim was covered through behavioral experiments analyzing L1-70-deficient transgenic mice and wild-type littermates to gain insights into the functional role of L1-70 in behavior.

C H A P T E R 3

MATERIALS AND METHODS

3.1 Material

3.1.1 Chemicals

All chemicals, reagents and kits were purchased from the following companies: Abcam (Cambridge, UK) Addgene Inc. (Teddington, UK), Bioline (London UK), BioTek (Winooski, VT, USA), Bio-Rad Laboratories (Munich, Germany), Biozol (Eching, Germany), Carl Roth (Karlsruhe, Germany), Cayman Chemical (Ann Arbor, MI, USA), Corning (Wiesbaden, Germany), Dianova (Hamburg, Germany), Eppendorf AG (Hamburg, Germany), GE Healthcare (Chicago, IL, USA), Herolab GmbH, (Wiesloch, Germany), Invitrogen (Waltham, MA, USA), Jackson ImmunoResearch (West Grove, UK), LI-COR (Lincoln, NE, USA), Macherey-Nagel (Düren, Germany), Merck Chemicals (Darmstadt, Germany), New England BioLabs (Ipswich, MA, USA), PAN Biotech (Aidenbach, Germany), Promega (Madison, WI, USA), Qiagen (Venlo, The Netherlands), Santa Cruz Biotechnologies (Dallas, TX, USA), Sigma-Aldrich (Taufkirchen, Germany), ThermoFisher Scientific (Waltham, MA, USA), Roche Diagnostics (Mannheim, Germany).

3.1.2 Antibodies

- Primary antibodies:
  The primary antibodies used in this work are listed in the following table.

Table 3.1: List of all the primary antibodies used. Abbreviations: ELISA – enzyme-linked immunosorbent assay, IP – immunoprecipitation, PLA – proximity ligation assay, WB – western blot, FC - flow cytometry.

ANTIBODY	DILUTION
αTubulin (TU-02) #sc-8035 (Santa Cruz Biotechnology)	WB 1:500
6X His tag® antibody (HRP) #ab1187 (Abcam)	WB 1:1,000
BNIP3 polyclonal antibody #PAB1863 (Biozol), SH030611A	FC 1:50
CD171 (L1CAM) #MM-172R (Biolegend)	WB 1:2,000
CHL1 (C-18) #sc-34986 (Santa Cruz Biotechnology)	ELISA 1:1,000
LC3 Rabbit Polyclonal antibody #14600-1-AP (Proteintech)	WB 1:1,000 PLA 1:20
L1CAM antibody #A00729-1 (Bosterbio)	FC 1:200
Parkin (PRK8) #sc-32282 (Santa Cruz Biotechnology)	IP 1:200
PARK2/Parkin polyclonal antibody #14060-1-AP (Proteintech)	WB 1:500
Mouse IgG # 012-000-003 (Dianova)	IP 2.5 µg
NCAM-L1 (C-2) #sc-514360 (Santa Cruz Biotechnology)	WB 1:100 ELISA 1:1,000 PLA 1:30
TOM20 (F-10) #sc-17764 (Santa Cruz Biotechnology)	FC 1:200
TOM40 (D-2) #sc-365467 (Santa Cruz Biotechnology)	WB 1:500

- Secondary antibodies:
  The secondary antibodies used in this work are listed in table 3.2.

Table 3.2: List of all the secondary antibodies used.

ANTIBODY	DILUTION
HRP goat α-mouse IgG #926-80010 (LI-COR)	WB 1:10,000
HRP goat α-rabbit IgG #926-80011 (LI-COR)	WB 1:10,000
Cy2 donkey α-rabbit #711-225-152 (Jackson Immuoresearch)	FC 1:200
Cy5 goat α-mouse #115-172-146 (Jackson Immuoresearch)	FC 1:200
HRP goat α-mouse #115-035-174 (Jackson Immuoresearch)	ELISA 1:1,000
HRP donkey α-goat #705-035-003 (Jackson Immuoresearch)	ELISA 1:1,000

3.1.3 Buffers and reagents

- Reagents and buffers:
  All the buffers and reagents used for SDS-PAGE, western blot, ELISA, agarose gel electrophoresis and protein production are listed in the table 3.3.

Table 3.3: Buffers and reagents used in this thesis.
Abbreviations: APS – ammonium persulfate, ddH2O - double dis- tilled water, EDTA – ethylenediaminetetraacetic acid, NP40 – nonylphenoxypolyethoxylethanol, SDS – sodium dodecyl sulfate, TBS – Tris-buffered saline, TBS-T – Tris-buffered saline with Tween 20%, TEMED – tetramethylethylenediamine, BSA - bovine serum albumin, PBS - phosphate-buffered saline, RIPA - radioimmunoprecipitation assay.

BUFFERS AND SOLUTIONS	INGREDIENTS
Protease inhibitor solution	stock (in ddH$_2$O) and working solution (in RIPA or MIBA buffer) prepared according to the manufacturer's protocol
Laemmli buffer (4x)	250 mM Tris-HCl pH 6.8 8% SDS 40% glycerol 20% β-mercaptoethanol 0.1 % bromophenol blue
SDS 10 %	10 g SDS in 100 ml ddH$_2$O
SDS Running buffer 10x	250 mM Tris-HCl pH 8.3 1.9 M Glycine 0.1% SDS
SDS running gel 10 %	1.7 ml ddH$_2$O 2.0 ml 30% acrylamide-bisacrylamide (29:1) 2.3 ml 1 M Tris-HCl, pH 8.8 60 µl 10% SDS 15 µl 10% APS 6 µl TEMED
Stacking gel	1.6 ml dH2O 0.4 ml 30% acrylamide bisacrylamide (29:1) 0.3 ml 1 M Tris-HCl pH 6.8 30 µl 10% SDS 15 µl 10% APS 6 µl TEMED
Coomassie blue staining solution	20% methanol in ddH$_2$O 20% Roti-Blue in ddH$_2$O in 60 ml dd ddH$_2$O
Blotting buffer 1x (*Western Blotting*)	25 mM Tris 192 mM glycine 20% methanol 0.01% SDS
Blocking buffer *(Western Blotting)*	5% skim milk powder in 1x TBS-T

BUFFERS AND SOLUTIONS	INGREDIENTS
TBS 1x	10 mM Tris 0.15 M NaCl pH 7.5
TBS-T	1 ml Tween 20% in TBS1X
ELISA blocking solution	1% (w/v) BSA fatty acids-free in PBS with Ca^{2+} and Mg^{2+}
ELISA washing buffer (PBS-T)	0.005% (v/v) Tween 20 in PBS with Ca^{2+} and Mg^{2+}
OPD solution	0.5 mg/ml OPD Stable peroxidase buffer 10x
Stopping solution	2.4 M H_2SO_4
MIBA buffer *(mitochondria lysis)*	100 mM Tris-HCl 1 mM EDTA 0.2 M D-Mannitol 0.05 mM Sucrose 0.5 M Sodium orthovanadate 1 mM Sodium fluoride
RIPA *(for mithocondria)*	50 mM Tris-HCl pH 7.6 300 mM NaCl 0.5% sodium deoxycholate 1% NP40
Washing buffer *(for protein extraction)*	50 mM NaH_2PO_4 300 mM NaCl 30 mM Imidazole pH 8.0
Elution buffer *(for protein extraction)*	50 mM Tris-HCl 250 mM Imidazol pH 8.0
Lysis buffer *(for protein extraction)*	50 ml of washing buffer + 1 tablet protease inhibitors
50x TAE	2 M Tris 1 M acetic acid 50 mM EDTA pH 8.0
Agarose gel solution with Roti-GelStain	2.5% agarose standard 1xTAE 0.05 µl/ml Roti-GelStain

- Buffers, media and solutions for cell culture
  Buffers, solutions and media used for cell culture are listed
  and described in table 3.4.

Table 3.4: List of buffers, solutions and media used for maintenance and preparation
of cells.

Coating solution	Poly-L-lysine (PLL) in 0.01% in dH_2O
HBSS (cell washing)	Hank's balanced salt solution witout Ca^{2+} and Mg^{2+} containing 0.35 g/l $NaHCO_4$ and phenol red
Medium X-1 *(cerebellar granule cells)*	Neurobasal A containing: 1x Pen/Strep 0.1% BSA 10 µg/ml insulin 4 nM L-thyroxine 100 µg/ml Transferrin, holo 30 nM Na-selenite 0.5x Na-pyruvate 1x L-glutamine
Medium X-1 with serum *(cerebellar granule cells)*	Medium X-1 and 5% fetal horse serum
DNase I solution *(cerebellar granule cells)*	10 mg DNase I 50 ml glucose 20 ml Neurobasal A
Trypsin/DNase solution pH 7.8 *(cerebellar granule cells)*	0.3 g trypsin 30 mg DNase I 300 µl 80 mM magnesium chloride ($MgCl_2$) 30 ml HBSS

- Media and chemicals for bacterial culture
  Media used for bacterial culture are listed in the table 3.5.

Table 3.5: List of solutions and media used for bacteria cultures.

LB medium (lysogeny broth)	10 g/l bacto-tryptone pH 7.4
LB medium with kanamycin	50 µg/ml kanamycin in LB-medium
Agar plates with kanamycin	20 g/l agar 50 µg/ml kanamycin LB medium
S.O.C. medium	(Thermo Fisher Scientific)

- Buffers for tissue staining
  In table 3.6 all buffers and solutions used for tissue staining are listed.

Table 3.6: Solutions used in the thesis for staining of tissue.

8% fixing solution	8% (w/v) paraformaldehyde in PBS adjust to pH 7.5 with NaOH
4% fixing solution	4% (w/v) paraformaldehyde in PBS
Dehydrating solution	15%-30% (w/v) sucrose in PBS
Acetic Acid solution	acetic acid glacial 10% in ddH_2O
Luxol Fast Blue	0.1% luxol fast blue 95% ethanol 10% acetic acid in ethanol
Cresyl Violet Acetate	0.1 g cresyl violet acetate in ddH_2O
Lithium Carbonate solution	0.25 g lithium carbonate in ddH_2O
Ethanol	70% or 95% (Th. Geyer)
Xylene	Sigma Aldrich
Mounting medium	Eukitt quick-hardening mounting medium (Fluka Analytical)

3.1.4   Vectors and bacteria

- Bacteria
  The bacterial strains used in this work are listed in table 3.7.

Table 3.7: List of bacterial strains used in this work.

STRAIN	GENOTYPE
E. coli One Shot™ BL21 Star™ (DE3) Chemically Competent	F–, *omp* T, *hsd* S$_B$, (r$_B$-, m$_B$-) *gal*, *dcm*, *rne* 131 (DE3)
One Shot™ MAX Efficiency™ DH5α-T1^R Competent Cells	F- φ80*lac* ZΔM15 Δ(*lac* ZYA-*arg* F)U169 *rec* A1 *end* A1 *hsd* R17(r$_k^-$, m$_k^+$) *pho* A *sup* E44 *th* i-1 *gyr* A96 *re* lA1 *ton* A

- Vectors
  In this work the pet28a+_L1ICD (Addgene) plasmid was used. In figure 3.1 the vector map is shown.
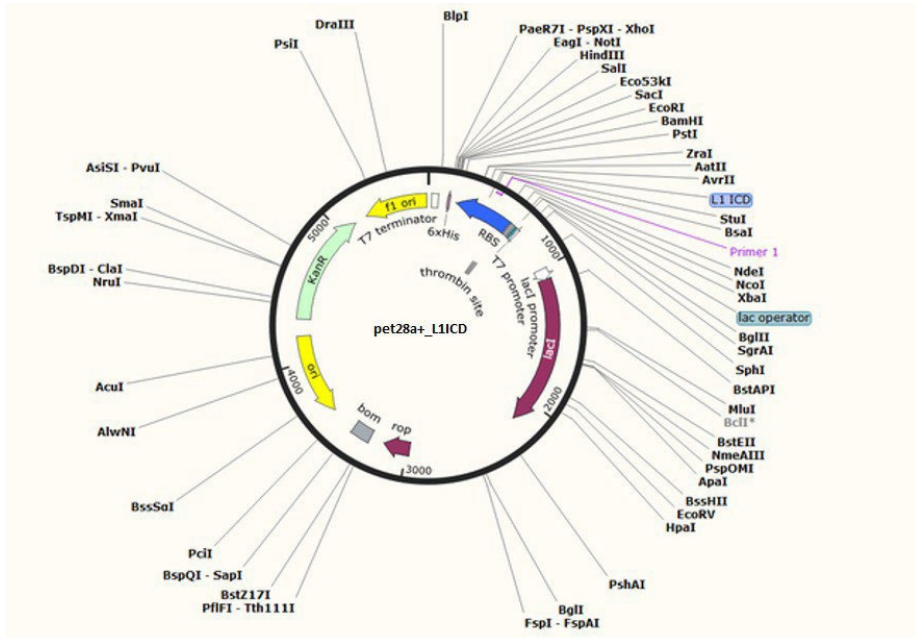
Figure 3.1: pet28a+_L1-ICD map.

3.1.5   Oligonucleotides

All the oligonucleotides used in this work are provided from Metabion International and listed in table 3.8.

Table 3.8: List of oligonucleotides used in this thesis.

L1arm2: 5′—GGA ATT TGG AGT TCC AAA CAA GGT GAT C-3′
L1 -5UP2: 5′—AGA GGC CAC ACG TAC CGC AGC ATC-3′
tTA-up3: 5′—TAC ATG CCA ATA CAA TGT AGG CTG C-3′

L1-RA fw: 5′—TGA GGA CAA GGA AAT GGC TCC-3′
L1-RA rev: 5′—GCT GTA GCA AGG ACA AGG AAC-3′

L1-DD 845 Tt L1 fw: 5′ TAA AGA GGA ATG TGA TAA TAT TGA 3′
L1 DD 845 Tt L1 rv: 5′ AAG GTT GAA GAA CAA CTG CTC TTT 3′

L1-LIR up: 5' CGAGACCTTCGGCGAGGCCAGGTCCGCGGAGAGTGACAATGAA 3′
L1-LIR dw: 5' TTCATTGTCACTCTCCGCGGACCTGGCCTCGCCGAAGGTCTCG 3'

3.2   Animals

3.2.1   Generation of L1-deficient mice

For the generation of L1-deficient (L1-/y) mice a tetracycline-controlled transactivator was inserted into the second exon of the L1 gene on the X chromosome [39, 129]. Wild-type males and heterozygous females (on 129SVJ background) were used for breading. Gene-edited mice expressing L1 with an arginine to alanine exchange at position 867 in the first FNIII domain (L1/687 mutant mice) or with a mutation of the dibasic sequence RKHSKR

to SKHSSS at position 858-863 in the third FNIII domain (L1/858-863 mutant mice) have been described [45]. Animals were housed at standard laboratory conditions with food and water supply ad libitum and with an artificial 12h light/dark cycle at the breeding facility of the University Medical-Center Hamburg-Eppendorf. All procedures used were approved by the responsible authorities of the State of Hamburg (Behörde für Wissenschaft und Gesundheit, Amt für Gesundheit und Verbraucherschutz, Lebensmittel-sicherheit und Veterinärmedizin; animal permit numbers ORG 1022, N19/004ZuchtNeuro, A 005/2019 and N 056/2019) and in agreement to the guidelines set by the European Union and Germany. Experiments were conducted and evaluated following the ARRIVE guidelines for animal research [130].

3.2.2   Genotyping of L1-deficient mice

The genotyping of L1-deficient mice was performed using tail biopsies and PCR using the MyTaq^{TM} Extract PCR Kit (Bioline). First the tail cuts were lysed using 20 μl of buffer A, 10 μl of buffer B and 70 μl of nuclease-free water for each sample. The tail cuts were incubated for 10 min at 75°C and 10 min at 95°C. Then, a mix was prepared using 12.5 μl of red mix, 5.5 μl of nuclease-free water, primers listed in table 3.8 (arm2 2.5 μl, up3 2 μl and up2 0.5 μl) and 2 μl of lysate product. A PCR was then performed using the following steps: 98°C for 3 min; 35 cycles: 98°C for 10 s, 65°C for 1 min, 72°C for 20 s; 72°C for 1 min; 4°C until further use. The DNA products were then applied to an agarose gel.

3.2.3 Genotyping of mutated L1 mice *(L1/687 and L1/858-863)*

- L1/687
  The genotyping of the L1/687 offspring was analyzed by PCR using the ThermoScientific Phire Animal Tissue Direct PCR Kit and tail biopsies. The primers, L1-RA fw *(5′-TGAGGACAAGGAAATGGCTCC-3′)* and L1-RA rev *(5′-GCTG TAGCAAGGACAAGGAAC-3′)* were used with the following program: 98°C for 5 min; 35 cycles: 98°C for 10 s, 56°C for 45 s and 72°C for 20 s; 72°C for 7 min; 4°C. Subsequently, the amplification product was digested with the restriction enzyme AciI (New England Biolabs) in CutSmart buffer (New England Biolabs) at 37°C for 2h. The 400 bp amplicon of mutant mice was cleaved into 107 bp and 293 bp products. The PCR and digestion products were visualized on 2.5% agarose gels stained with ethidium bromide.

- L1/858-863
  For the L1/858-863 genotyping, lysates of tail biopsies and the primers L1-DD fw *(5′-TAAAGAGGAATGTGATAATATTGA-3′; 73,857,992-73,858,015)* and L1-DD rev *5′- AAGGTTGAAGA ACAACTGCTCTTT-3′; 73,857,304-73,858,327)* were used for PCR with the ThermoScientific Phire Animal Tissue Direct PCR Kit (ThermoFisher Scientific) as follow: 98°C for 5 min; 35 cycles: 98°C for 10 s, 60°C for 45 s and 72°C for 20 s; 72°C for 7 min; 4°C until further use. The amplification product was digested with AvaI (New England Biolabs) in CutSmart buffer (New England Biolabs) at 37°C for 3 h or overnight. The 710 bp amplicon of mutant mice was cleaved into 210 bp and 500 bp products. An agarose gel of 2.5% was used for visualizing the PCR and digestion product and bands were stained with ethidium bromide.

3.3 Molecular biology methods

3.3.1 Agarose gel electrophoresis

DNA products were applied to an agarose gel of 2.5% positioned in a horizontal electrophoresis chamber (BioRad). A constant voltage of 150-170 was applied separating the DNA bands according to their size. Besides the samples, a DNA ladder was also loaded to assess the DNA bands size. The agarose gel was prepared as follows: first, agarose powder was dissolved in 1X TAE buffer while heating the solution and then for visualizing the DNA, Roti-Safe (Carl Roth) was added to the solution (7 μl Roti-Safe/100 ml of solution). The solution was subsequently poured in a casting tray and a 15-20 well comb was inserted for creating the wells for loading the samples. After the polymerization, the gel was inserted into the electrophoresis chamber and immersed in 1X TAE buffer. DNA samples mixed with 6X Loading Dye (ThermoFischer Scientific) were applied into the wells and the gel was run for 30-40 minutes until the dye reached the bottom. A picture of the gel was taken using the E.A.S.Y. UV-light documentation system (Herolab). For the transgenic lines L1/858-863 and L1/687, after the run the gel was stained with ethidium bromide for 20 minutes. The picture of the gel was taken by Gel Stick "Touch" (INTAS)

3.3.2 Mutagenesis and recombination reaction

For the production and the isolation of the plasmid containing the L1-ICD with mutated LIR domain the *OneShot^R* MAX *Efficency^R* DH5α^{TM} - *T* 1^R kit was used (Invitrogen). A reaction mix was prepared following the manufacturer's instructions and containing the L1-ICD encoding plasmid (previously produced in Prof. Schachner's lab by Gaston Castillo) with a final

concentration of 20 ng/μl, primer mix (10 μM each), 10x Enhancer, 10x *AccuPrime*^{TM} *Pfx* Reaction mix, DNA methylase (4 U/μl), 25x SAM, *AccuPrime*^{TM} *Pfx* (2.5 U/μl) and nuclease-free water. A PCR was then performed using the parameters indicated in Figure 3.2.

TEMPERATURE	DURATION	NUMBER OF CYCLES
37°C	12-20 min	
94°C	2 min	1
94°C	20 sec	
57°C	30 sec	
68°C	30sec/kb of plasmid	12-18 cycles
68°C	5 min	1
4°C	∞	1

Figure 3.2: PCR protocol for the mutagenesis reaction.

Then the PCR products were analyzed on a 1% agarose gel, using also the non-mutated L1-ICD plasmids as control. Next, recombination reaction was performed as indicated by the instructions from the distributor, with 5X reaction buffer, nuclease-free water, the PCR sample and 10X enzyme mix. The mix was incubated at room temperature for 10 minutes, then the reaction was stopped by addition of 1μl of 0.5 M EDTA. After, incubation on ice of the mix was used for the transformation step.

3.3.3   Transformation into E. coli DH5α

Subsequently to the mutation and recombination step, 2 μl of the recombination reaction were transferred into a vial containing 50 μl of DH5$\alpha^{T\,M}$ - $T\,1^R$ cells. The vial was incubated on ice for 12 minutes and then heat-shocked at 42°C for 30 seconds using a water bath and kept on ice for 2 minutes. Next 250 μl of SOC medium (Invitrogen), pre-warmed at room temperature, was added to the tube (Rxn1), which was incubated for 1 h at 37°C with gentle shaking using a Thermomixer 5436 (Eppendorf). After the incubation, the transformation reaction (Rxn1) was diluted in SOC medium, according to the plasmid size: 10 μl of Rxn1

+ 90 μl of SOC medium. Afterwards, 100 μl of transformed bacteria were applied in a T-streak to LB (lysogeny broth) agar plates containing kanamycin. The plates were inverted and bacteria incubated at 37°C for 20 hours.

3.3.4   Plasmid isolation

The agar plate was examined and single colonies were picked and transferred into bacterial culture tubes containing 9 ml of LB medium with kanamycin (final concentration 50 μg/μl) and grown overnight at 37°C under agitation ($\sim$ 180 rpm). In order to perform small scale bacterial plasmid isolation (Miniprep), the NucleoSpin Plasmid EasyPure (Macherey-Nagel) was used. The culture was centrifuged at 8,000 g for 10 minutes in order to pellet the cells and bacteria were lysed following the manufacturer's instructions: 150 μl of buffer A1 were added to the pellet and vortexed. Then 250 μl of buffer A2 were added, the tube was inverted several times and incubated at room temperature for 2 minutes. Finally, 350 μl of buffer A3 were added and the tube was inverted again until the lysate turned colorless. The sample was then centrifuged for 3 minutes at 4°C at 12,500 g and the supernatant was loaded on a spin column and centrifuged for 30 seconds at 1,000 g at room temperature. After discarding the supernatant 450 μl of buffer AQ were added to the spin column and columns were centrifuged for 1 minute at 12,000 g. For eluting the DNA the spin column was then transferred into a 1.5 ml microcentrifuge tube, buffer AE was added (50 μl) and samples were incubated at room temperature for 1 minute. Finally, a last centrifugation at 12,000 g for 1 minute was performed to collect the DNA.

3.3.5 Determination of DNA concentration and sequencing

The determine the DNA concentration the NanoDrop 1000 spectrophotometer (ThermoFisher Scientific) was used. A small amount of 1-2 μl sample DNA was used and the same amount of the diluent used in the sample was used as a blank control. The device uses the absorbance at 260 nm to estimate the concentration of DNA, and the ratios of absorbance 260/280 nm or 260/230 nm to evaluate purity [131]. The accepted 260/280 and 260/230 ratios for the DNA were approximately 1.8 and 2.0, respectively. Once the concentration was determined, the DNA was sequenced to verify the successful mutation process. To this aim, 500 ng DNA, 10 pmol primer and nuclease-free water were added to a 1.5 ml Eppendorf tube to a final volume of 8 μl. The samples were then sequenced by the ZMNH Core Facility Bioanalytics using the ABI PRISM Genetic Analyzer (ThermoFisher Scientific). The electronic data were analyzed with 'Benchling: Cloud-Based Informatics Platform for Life Sciences' and by performing a sequence alignment with the reference DNA sequences.

3.3.6 Expression and purification of recombinant protein

For protein expression 10 ng of plasmid DNA was transferred into a vial containing 50 μl of E. coli One$Shot^{TM}$ BL21 Star^{TM} (DE3) (ThermoFischer Scientific) and mixed by gentle tapping. The vial was incubated on ice for 30 minutes and heat shocked at 42°C for 45 seconds in a water bath. The vial was then placed on ice for 2 minutes and 250 μl of SOC medium were added to the tube. The tube was kept shaking for 1 hour at 225 rpm using the Thermomixer 5436 (Eppendorf). After this step, 50 μl of the transformation reaction were streaked on an LB agar plate

containing 50 μl/μg kanamycin and incubated for 24 hours at 37°C. Afterwards, a single colony was inoculated into an Erlenmeyer flask containing 10 ml of LB medium supplemented with 50 μl/μg kanamycin and grown overnight at 180 rpm and 37°C. A 7 ml aliquot of the culture was transferred then to a larger Erlenmeyer containing 300 ml pre-warmed LB medium supplemented with 50 μl/μg kanamycin and incubated at 37°C with agitation (190 rpm) until the optical density (OD600) value needed for protein induction was reached. The OD600 was measured every hour using a *μ-Quant^{TM}* Microplate Spectrophotometer (BioTek Instruments, Bad Friedrichshall, Germany), using LB medium as blank control. Once the OD600 had reached a value between 0.6 and 0.8, IPTG (isopropyl β-d-1-thiogalactopyranoside) was added to the culture at a final concentration of 1 mM. The culture was further incubated and each hour an aliquot of 2 ml of the culture medium was collected (before and after IPTG induction) as control and centrifuged at 6,000 g for 10 minutes. The pellet was then resuspended in 2X SDS-PAGE sample buffer, boiled at 98°C for 5 minutes and stored until needed for SDS-PAGE. After 4-5 hours the culture was centrifuged at 4,000 g for 10 minutes at 4°C. The supernatant was discarded, and the cell pellet was stored at –20°C until use. The cell pellet was resuspended in 5 ml lysis buffer (50 ml washing buffer + 1 tablet protease inhibitor, Roche) and kept on ice for 10 minutes. The sample was then sonicated 6x for 10 seconds at 200-300 W and then centrifuged for 30 minutes at 1,0000 g and 4°C. An aliquot of the supernatant (crude extract A, soluble protein) was kept as control for the SDS-PAGE, while the rest was stored on ice. The pellet was resuspended in 5 ml of lysis buffer (crude extract B, insoluble protein). For the subsequent step of purification Ni-NTA agarose beads (Qiagen) were centrifuged for 4 minutes at 1,000 g and 4°C and the supernatant was discarded. The beads were washed with washing buffer (50 mM NaH$_2$PO$_4$, 300 mM NaCl, 30 mM

imidazole, pH 8.0) for 30 minutes at 4°C. Centrifugation was again performed to remove the washing buffer. The crude extract A was incubated with the beads (1 ml beads for 5 ml crude extract A) overnight at 4°C with an upside-down movement.

Next, the agarose beads were pelleted down by centrifugation at 1,000 g for 4 minutes at 4°C and washed 3x for 10 minutes and then centrifuged again for 4 minutes at 1,000 g and 4°C. The beads were finally incubated with 1 ml of elution buffer (50 mM Tris HCl, 250 mM imidazole, pH 8.0) for 1 hour, and pelleted again by centrifugation for 4 minutes at 1,000 g and 4°C. This step was repeated two times in order to have two elutions. Both times an aliquot of the supernatant is diluted with 2X SDS-PAGE sample buffer, subjected to western blot analysis and Coomassie blue staining to evaluate the success of the protein production. Afterwards, the protein was concentrated using Viviaspin 20 columns (Satorius) with a cutoff of 5 kDa at 5,000 g.

3.3.7   Coomassie staining of polyacrylamide gels

After the SDS-Page electrophoresis, gels were stained with the RotiBlue kit (Carl Roth) overnight under gentle shaking. Gels were then washed multiple times with Coomassie washing solution in order to reduce the background. A light table was used for visualizing the stained protein bands.

3.4   Biochemical methods

3.4.1   Determination of protein concentration

For the determination of protein concentrations the Bicinchoninic acid (BCA) Protein Assay Reagent Kit (ThermoFisher Scientific) was used. First, standard solutions of bovine serum albumin (BSA) were prepared in concentrations of 62.5, 125, 250, 500, 1,000 and 2,000 $\mu g/\mu l$. A small aliquot of the samples of which the protein concentration had to be determined was diluted multiple times (2x, 4x, 8x) in distilled H_2O. In a microtiter 96-well plate, 10 μl of the blank control, the standards and the diluted and undiluted samples were loaded. The plate was incubated for 30 minutes at 37°C with 200 μl of a 50:1 mixture of solution A and solution B from the Protein Assay Kit (ThermoFisher Scientific), and the absorbance was measured at 562 nm using the μ-$Quant^{TM}$ spectrophotometer (BioTek Instruments). The calibration based on the absorbance curve of the BSA standards was used for determining the protein concentration of the samples.

3.4.2   SDS-polyacrylamide gel electrophoresis

For protein separation SDS-Page electrophoresis was performed using the Mini-Protean II system (Bio-Rad) with precast 4-20% gradient gels (BioRad) or self-made SDS-polyacrylamide gels, which percentage was chosen according to the size of proteins that had to be separated. The samples were diluted in 2X Laemmli buffer. In order to denature the protein the samples were heated at 95°C for 5 minutes and then 15-30 μg of protein/lane were loaded on tris-glycine SDS polyacrylamide gels. The PageRuler^{TM} Plus Prestained Protein Ladder (ThermoFisher Scientific) was used as molecular weight marker. A Power Pac 200 (Bio-Rad) was used to

run the gels with an initial voltage of 80 V for the first 20 minutes and then at 75-150 V for 60-90 minutes. When the gel was used for western blotting the SDS-PAGE was performed on ice.

3.4.3 Western blot analysis

As method for quantification of protein the western blot technique was used. The Mini Trans-Blot® blotting system (Bio-Rad) was used to transfer proteins to nitrocellulose membranes. According to the protein size two different types of nitrocellulose membranes were used: for proteins larger than 20 kDa 0.45 μm nitrocellulose Amersham^{TM} Protran^{TM} was used, while for proteins smaller than 20 kDa, 0.20 μm Protran^{TM} nitrocellulose membrane (GE Healthcare) was used. Membranes were first incubated in blotting buffer and then used to cast the blotting sandwich that was afterwards transferred to the blotting chamber, filled with ice-cold blotting buffer and placed on ice. Proteins were transferred at a constant voltage of 120 V for 1 h, 75 V for 30 minutes or 90 V for 90 minutes. Thereafter the membranes were placed in a glass container and blocked with 5% skim milk powder dissolved in TBS-T for 1 h at room temperature. Membranes were then incubated overnight at 4°C with primary antibodies, which were diluted in 5% skim milk powder in TBS-T. Afterwards the membranes were washed 3 times for 5 minutes with TBS-T and then incubated with HRP-coupled secondary antibodies for 1 h at room temperature. The membranes were washed again 3 times for 5 minutes with TBS-T and visualized with ECL select or ECL prime reagents (GE Healthcare Amersham^{TM}) and the LAS 4000 Mini camera (GE Healthcare).

3.4.4 ELISA

ELISA was used to determine binding between L1 and LC3. The assay was performed as follows: 10 μg/ml of recombinant protein LC3 (Ubiquigent, catalog number 60-0112-500, lot 30099) were applied to a 384-well high-binding polystyrene plate (Corning) overnight at 4°C in a volume of 25 μl per well. After one washing with PBS with Ca^{2+} and Mg^{2+} (pH 7.4), the plate was blocked with 2% bovine serum albumin in PBS for 1.5 h at room temperature and then washed with PBS-T (PBS with 0.01% Tween 20) for two times for 30 seconds. The ligands, (mutated or unmutated L1-ICD) and CHL1 intracellular domain (CHL1-ICD) (used as control) were added to the plate in increasing concentrations (25-500 nM), in a volume of 25 μl per well and incubated for 1-2 h at room temperature. Next, 3 washings with PBS-T for 5 minutes were performed and mouse monoclonal anti-L1-ICD antibody (NCAM-L1 (C-2), 1:1,000) or goat polyclonal anti-CHL1-ICD antibody (CHL1 (C-18), 1:1,000) were applied for 1 h at room temperature. Afterwards, the plate was incubated with either anti-mouse HRP- coupled secondary antibody (Jackson ImmunoResearch, 1:1,000 in PBS) or an anti-goat HRP-coupled secondary antibody (Jackson ImmunoResearch; 1:1,000 in PBS) for 1 h. Wells were washed again 3 times with PBS-T for 5 minutes and ortho-phenylenediamine dihydrochloride (ThermoFisher Scientific) was added at a concentration of 0.5 mg/ml and incubated in the dark for 1-5 minutes. Once the liquid in the wells changed its color, the reaction was stopped by addition of 25 μl of 2.5 M sulphuric acid per well and the absorbance was measured at 492 nm with an ELISA reader (μQuant microplate spectrophotometer, BioTek Instruments).

3.4.5   Co-immunoprecipitation

Brains from 7-day-old wild-type mice were removed and placed on ice, washed with ice-cold PBS with Ca^{2+} and Mg^{2+} (PAN Biotech) and then homogenized in RIPA buffer with protease inhibitors (Roche) and phosphatase inhibitors (Roche), both added just before use. For homogenization on ice a dounce homogenizer was used. Samples were centrifuged at 10,000 g and 4°C for. The obtained supernatant was removed and the samples were centrifuged again obtaining the total cell lysate. After determining the protein concentrations, an aliquot of 5 μg/μl was prepared to perform the co-immuno-precipitation and an aliquot of the supernatant was kept as input. Antibody against parkin was added to the supernatant and samples were incubated with gentle rotation for 2 h at 4°C in order to form the immunocomplex. Meanwhile magnetic protein G beads were cleared with 5 washings of PBS and then added to the immunocomplex and incubated at 4°C overnight with gentle rotation. The following day the beads were separated from the supernatant that was discarded. After 3 washings in ice-cold RIPA buffer and 1 wash in ice-cold PBS with Ca^{2+} and Mg^{2+} (PAN Biotech), the beads were transferred to a new tube and 4x Laemmli sample buffer was added. The samples were then heated up at 95°C for 5 minutes and the beads were separated from the immunocomplex that was transferred into a new Eppendorf tube for western blot experiments.

3.4.6   Mitochondria isolation

For isolating mitochondria, a kit from ThermoFischer Scientific was used (catalog number 89801) following the manufacturer's instructions. First, brains were isolated from male wild-type, L1-deficient and L1/687 or L1/858-863 transgenic mice (7- to 11-day-old or 4- to 6-month-old), cut into small pieces and transferred to a dounce tissue grinder and washed 2x with 2.5 ml of PBS.

Afterwards, 800 μl of BSA/Reagent A were added to each brain. A dounce homogenization was then performed with at least 20 strokes on ice with a Teflon pestle, before adding 800 μl of Reagent C. The homogenate was then transferred in a 2 ml Eppendorf tube and the tube was inverted several times in order to mix the reagents. Next, the samples were centrifuged at 700 g at 4°C for 10 minutes. The pellet was discarded and the supernatant was transferred into a new 2 ml tube before being centrifuged again at 5,000 g for 15 minutes at 4°C. Then the supernatant, which corresponds to the cytosolic fraction, was removed and stored and the mitochondrial pellet was obtained. The pellet was washed with 500 μl washing buffer (Reagent C + ultra-pure water) and centrifuged again at 12,000 g for 5 minutes. The supernatant was discarded and the pellet was kept on ice. For western blot analysis and complex I assay, mitochondria were lysed in 800 μl of 2% CHAPS *(3-((3-cholamidopropyl) dimethylammonio)-1-propanesulfonate)* (Merck) in TBS (25 mM Tris HCl, 0.15 M NaCl, pH 7.2) and vortexed for 1 minute. Following, the mitochondria were centrifuged at high speed for 2 minutes and the supernatant was used to determine the protein concentration.

3.4.7   Isolation of mitochondria for analysis in a flow cytometer

Male wild-type and L1-deficient littermate mice (3- to 5-month-old) were sacrificed and the brains were removed. The fresh mouse brains were washed once in PBS with Ca^{2+} and Mg^{2+} (pH 7.4) and immersed in MIBA buffer (10 mM Tris-HCl, 1 mM EDTA, 0.2 M

D-mannitol, 0.05 M sucrose, 0.5 mM sodium orthovanadate and 1 mM sodium fluoride; 3 ml/brain). Tissue was then homogenized with a Teflon pestle and a dounce homogenizer. The lysate was centrifuged at 500 g for 5 minutes at 4°C. Afterwards, the supernatant was transferred in a new tube and centrifuged at 8,000 g for 10 minutes at 4°C. Next, the supernatant was discarded and the mitochondrial pellet was washed three times with ice-old

MIBA buffer and resuspended in MIBA buffer (1 ml/brain). For determination of protein concentration, the samples were then tested with the BCA assay.

3.4.8 Flow cytometry

Subsequently to the mitochondria isolation, mitochondria (50μg mitochondrial protein in 40 μl MIBA buffer) were incubated at 4°C overnight with antibodies against L1 or BNIP3 (NCAM-L1 1:200, rabbit; BNIP3 1:50, rabbit), while an antibody against TOM20 (TOM20 (F10), catalog number sc-17764, D2318, mouse, Santa Cruz Biotechnology) was used as marker for mitochondria. Next, samples were stained with fluorescent secondary antibodies rabbit Cy2 (donkey anti-rabbit) and mouse Cy5 (goat anti-mouse) in MIBA buffer for 1 h at room temperature. Samples were then washed three times with ice-cold MIBA buffer by centrifugation at 8,000 g for 10 min at room temperature. Finally, samples were fixed with 4% formaldehyde and fluorescence was analyzed with a flow cytometer (BD Canto II, BD Biosciences). The samples were subjected to the flow cytometer by Susanne Roscher from the FACS Sorting Core Unit of the University Medical Center Hamburg-Eppendorf, who also extracted the resulting graphs. Experiments were performed three times independently.

3.4.9 Evaluation of complex I activity

Brains were isolated from 6- to 9-day-old or 4- to 6-month-old mice and frozen in liquid nitrogen. Mitochondria were then isolated using the Mitochondria Isolation Kit for Tissue from ThermoFisher Scientific, as previously described, and diluted in 2% CHAPS before proceeding to determine the protein

concentration and complex I activity. For determination of complex I activity, mitochondria were applied to the Mitochondrial Complex I Activity Assay Kit (Cayman Chemical, Ann Arbor, MA, USA). Experiments were carried out in duplicates and performed independently three times in a clear 96-well plate, following the manufacturer's instructions. Briefly, in a tube 910 μl of Complex I activity buffer assay, 20 μl of 100 mM KCN, 50 μl FF-BSA Reagent and 20 μl Bovine Heart Mitochondria assay buffer (solution A) were mixed. Next, 50 μl of the solution A were added in each well together with 20 μl of mitochondria, diluted in assay buffer, to a final protein concentration of 20 μg. Afterwards, 30 μl of a second solution (B) containing 625 μl of Complex I buffer, 30 μl NADH assay reagent and 20 μl of ubiquinone assay reagent was added to the well in a final volume of the assay of 100 μl per well. After adding the solution B, the absorbance at 340 nm was recorded for 15 minutes.

3.5 Cell culture methods and assays

3.5.1 Preparation of coverslips

Glass coverslips for primary cell culture and subsequent immunostaining were prepared as follows: coverslips were placed in an Erlenmeyer flask, covered with a 3 M hydrochloric acid solution and incubated for 30 minutes with gentle shaking at room temperature. The coverslips were then washed twice with ddH$_2$O and immersed in acetone for 3 h at room temperature with gentle shaking. Then, 5 washings with ddH$_2$O were performed and the coverslips were washed twice with ethanol for

10 minutes at room temperature. The Erlenmeyer flask containing the coverslips was then heated up to 160º C for 2 h. From this point the steps were performed under sterile conditions in a laminar flow hood. The coverslips were cooled down to room temperature and coated with sterile 0.01% poly-L-lysine (PLL) in ddH$_2$O overnight at 4ºC with gentle shaking.

Afterwards, the excess of PLL was removed and the coverslips were washed twice with ddH$_2$O and dried under the hood at room temperature. Finally, the coverslips were stored in a sterile 50 ml Falcon tube until used.

3.5.2 Primary cerebellar granular cells culture

For preparation of cerebellar granule cells, 6- to 8-day-old male wild-type and L1-deficient littermate mice, as well as male transgenic L1/687 and L1/858-863 mice and their male wild-type littermates were used. Mice were sacrificed by decapitation and cerebella were extracted and placed in a petri dish with ice-cold HBSS (Sigma Aldrich). Under a stereo-microscope cerebella were cleaned from blood vessels and meninges and transferred into a new petri dish containing ice-cold HBSS where they were cut into three pieces. The following steps were all performed under sterile conditions in a laminar flow hood: cerebella were transferred into a Falcon tube and washed once with 5 ml ice-cold HBSS per 3 cerebella, afterwards incubated with 1 ml trypsin/DNase solution per 3 cerebella for 15 minutes at room temperature and then washed three times with 5 ml ice-cold HBSS per 3 cerebella. Then, 1 ml DNase solution per 3 cerebella was added and cerebella were homogenized with 3 Pasteur pipettes with rounded tips and different diameters, by pipetting up and down for at least 10 times. The homogenates were then centrifuged for 15 min at 100 g at 4°C. Cell pellets were resuspended in pre-warmed medium (Neurobasal A medium supplemented with L-glutamine, penicillin/streptomycin, BSA, insulin, L-thyroxine, transferrin holo, Na-selenite, and Na-pyruvate) without serum for culturing of cells for two days, and with 5% of fetal bovine serum (FBS) for longer culture period. An aliquot of the cell suspension was mixed in a ratio of 1:2 with 0.4% trypan blue solution in order to determine the cell number with a Neubauer chamber. Cells were finally diluted to a cell number of 2 x 10^5 cells/ml (for proximity ligation assay), 1-2.5x 10^6 cells/ml

(for determination of membrane potential or mitochondrial movements) or 1-2.5 x 10^5 cells/ml (for ATP assay) and seeded on PLL coated 24-well-plates (for ATP assay) containing 15 or 22 μm coverslips (for membrane potential determination, mitochondrial movements and proximity ligation assay) and cultured for at least 24 h at 37°C, 5% CO2 and 90% relative humidity.

3.5.3 Proximity ligation assay (PLA)

The proximity ligation assay was performed using Duolink PLA products according to the manufacturer's protocol (Sigma-Aldrich; Duolink PLA technology). Cerebellar granule cells from male littermate wild-type, L1-deficient, transgenic L1/687 and transgenic L1/858-863 mice were seeded on PLL-coated glass coverslips in 6- or 24-well plates. After 24 h in culture, cells were either stimulated with 50 μg/ml L1-557 antibody for 1 h at 37°C, treated with 100 μM H_2O_2 for 3 h at 37°C or were left untreated. Then cells were fixed by addition of 1 volume of 8% formaldehyde to 1 volume of the medium and incubated for 20 minutes at room temperature. Cells were then washed 3 times with PBS for 5 min at room temperature. Afterwards, cells were blocked at 37°C using Duolink Blocking Solution, and then incubated overnight at 4°C with mouse L1 antibody C-2, rabbit LC3 or rabbit Parkin antibody, diluted in Duolink Antibody Diluent (L1-C2 1:30; LC3 1:20; Parkin 1:50), followed by 3 washing steps for 5 minutes at room temperature with Duolink Washing buffer A. Next, cells were incubated at 37° C for 1h with secondary antibodies conjugated with oligonucleotides (Duolink anti-mouse PLA probe MINUS and Duolink anti-rabbit PLA probe PLUS) diluted in Duolink Antibody Diluent. Cells were then washed at room temperature with Duolink Washing buffer A, incubated for 1 h at 37°C with Duolink Ligase diluted in Duolink Ligation Buffer and RNase-free water (Qiagen) and washed again with Duolink Washing buffer A at room temperature. All the following steps

were performed in the dark: Amplification Buffer, Duolink Polymerase and RNase-free water (Qiagen) were applied to the samples and incubated at 37°C for 100 minutes. Finally, cells were washed once with Duolink Washing buffer B and with 0.01% Duolink Washing buffer B in PBS, followed by an incubation for 15 minutes at room temperature with 5 μg/ml DAPI. Ultimately, coverslips were mounted with mounting medium (Shandon ImmuMount, ThermoFisher Scientific). Experiments were repeated three times independently and in triplicates.

3.5.4 Mitochondrial membrane potential

To measure the energetic state of mitochondria a cell-based assay was used: JC-1 iodide *(1,1′,3,3′-tetraethyl-5,5′,6,6′-tetrachloroimidacarbo-cyanine iodide)*, a cyanine dye (Santa Cruz Biotechnology, catalog number sc-364116, CAS n. 3520-43-2) was used to stain and measure the membrane potential of the organelles. JC-1 permeates into mitochondria and shows a potential-dependent accumulation: in healthy cells it forms red aggregates, *"j-aggregates"* within the mitochondria (emission at 590 nm) while in cells with impaired mitochondrial membrane potential the compound leaks from mitochondria forming green monomers (emission at 529 nm) in the cytosol. Consequently, mitochondrial depolarization is indicated by a decrease in the red/green fluorescence intensity ratio. Cerebellar granule cells from 6- to 7-day-old male littermate wild-type, L1/687 and L1/858-863 mice were plated on to 22 μm PLL coated coverslips in serum-free medium and left in culture for two days. Afterwards, cells were incubated with JC-1 in HBSS with phenol red at a final concentration of 3 μM for 30 minutes at 37° C, 5% CO2 and relative humidity of 90%. After a washing the cells with HBSS without phenol red for 15 minutes, cells were observed under a spinning disk microscope (Visitron, Puchheim, Germany) with a 60x objective. For detection of mitochondria with high mitochondrial membrane potential a rhodamine filter set was used

together with the fluorescein filter for detection of depolarized mitochondria with low mitochondrial membrane potential. Experiments were performed three times independently in duplicates.

3.5.5 ATP assay

ATP levels were determined using the BacTiter-Glo® 2.0 Cell Viability Assay (Promega, Walldorf, Germany; catalog number G8230). Cerebellar granule cells were cultured in serum-free medium at a density of 2.5 x 10^5 cells/well in 48-well plates for 1 day. Afterwards cells were scraped off in serum-free medium and 100 μl of the cell suspension was transferred into a white 96-well plate and 100 μl of BacTiter-Glo was added to the wells. Plates were incubated for 5 min at room temperature with gentle shaking. Finally, luminescence was measured using a luminometer (Mithras LB943; Berthold Technologies, Bad Wildbad, Germany). Experiments were carried out three times independently in triplicates.

3.5.6 Mitochondrial movements

For studying the mitochondrial movements, mitochondria were labeled with MitoTracker® Red CMXRos (ThermoFisher Scientific; catalog M7512). A stock solution of 1 mM was prepared and diluted in pre-warmed cerebellar neuron culture medium to a final concentration of 50 nM. Cerebellar granule cells from 7-day-old male littermate wild-type and L1/687 mice (1-2 x 10^6 cells/ml) were cultured for 48-72 h in medium containing 5% horse serum. The medium was replaced with serum-free medium and the cells were incubated with 50 nM Mitotracker for 30 minutes at 37°C. This solution was then replaced with fresh serum-free medium, and the cells were analyzed at 37°C under a 5% CO_2 atmosphere by time-lapse imaging using an upright Nikon Eclipse Ti microscope

(Nikon Instruments, Amsterdam, The Netherlands) combined with spinning disk (Visitron, Puchheim, Germany) live-cell confocal technology (Visitron Systems) and a 100× objective. Images were taken with an interval of 2 s for 5 min, using a 561 nm argon laser at 10% intensity. Videos were acquired using the VisiView software (Visitron Systems). Experiments were carried out in duplicates and performed independently three times.

3.5.7   Kymograph analysis

For the analysis of the mitochondrial dynamic parameters the ImageJ software was used [132]. Evaluation of velocity, mobility and direction of the transport (anterograde/retrograde) of mitochondria was performed using the kymograph (time-space plot) plugin from ImageJ [132]. Areas with visible mobile mitochondria were used as regions of interest and a segmented line was drawn in the time-series. Grey values along a segmented line for each frame were generated using the kymograph plugin to create a new image (kymograph). The kymograph consists of a horizontal line on top, which represents the first time point, followed by different time points below that line. The kymograph uses the x-axis as indication of the distance and the y-axis as representation of the time. Vertical lines represent static mitochondria, while diagonal lines indicate mobile mitochondria. The direction (right or left) of diagonal lines indicates retrograde or anterograde transport, which depends on the position of the cell soma [133]. Segmented lines were drawn along the diagonal lines of the kymograph to calculate the motility and the velocity and the respective tools from ImageJ [132] were used for the quantification of the motility. Experiments were carried out three times independently in duplicates and the analysis was performed by Ludovica Congiu (Senior Gruppe Biosynthese Neuraler Strukturen, ZMNH, UKE, Hamburg).

3.6 Immunohistochemistry

3.6.1 Perfusion of mice brains

Adult male and female wild-type, transgenic L1/687 and L1/858-863 mice were anesthetized with an intraperitoneal injection of ketamine (80 mg/kg body weight) and xylazine (10 mg/kg body weight). To verify that the anesthetic worked, the pinch-response method was used: if there was no response, the mouse was fixed to a plastic surface with adhesive tape. A lateral incision of 5 cm beneath the rib cage and through the integument and abdominal wall was performed. Next, the diaphragm was separated from its connection to the thoracic pleura and the liver was disjointed. The ribs were then cut from both sides and a hemostat was clamped to the sternum and placed over the head of the mouse to expose the heart. A small incision was made on the posterior end of the left ventricle and an olive-tipped perfusion needle, fixed in the position by using a little bulldog forceps, was passed through the ventricle into the ascending aorta. Another small incision on the right atrium was performed in order to start the perfusion. A syringe containing PBS was attached to the needle and 10 ml of the buffer were pumped (with a pressure of 80-130 mm Hg), followed by 50 ml of 4% formaldehyde solution used as fixative. Finally, brains were removed and incubated in 4% formaldehyde solution for at least 24 h at 4°C. Afterwards the brains were immersed in 15% sucrose in PBS solution for at least 24 h at 4° C and then immersed in 30% sucrose in PBS for cryoprotection for 2 days at 4º C. Brains were then frozen for 2 min in 2-methyl-butane pre-cooled to -80° C and stored at -80° C until further use.

3.6.2   Tissue cryosectioning

Formaldehyde-fixed brains were dehydrated for 1 day at 4° C in 15% sucrose and then for 3 days in 30% sucrose. Afterwards the brains were then shock-frozen in -80° C cold isopentane (Sigma-Aldrich) for 2 min and stored dry at -80° C. Prior to cryosectioning, the chamber of the cryostat (Cryostar Nx70, Thermo Fisher Scientific) was cooled down to -21° C, as the tissue holder, and the blade was cooled to -15° C. Brains were attached on the tissue holder, covered with a solution of Tissue-Tek OCT (optimal cutting temperature) Compound (Sakura Finetek) and covered with the same solution. Once the Tissue-Tek OCT Compound covering the brain was frozen, the brains were cut into 40 μm thick coronal sections and collected in section storage buffer (0.02% sodium azide in PBS) and stored at 4° C.

3.6.3   Luxol fast blue-Cresyl violet staining

Free-floating cryosections were mounted on glass slides (Super-frost Plus, ThermoFisher Scientific) and stained with a luxol fast blue solution (0.1% luxol fast blue in 100 ml of 95% ethanol and 10% acetic acid in distilled water) at 57° C overnight. Sections were then washed in 95% ethanol and distilled water before being stained in a 0.05% lithium carbonate solution for 3 minutes. Next, sections were incubated with 70% ethanol and distilled water. After these steps sections were stained in a 0.1% cresyl violet acetate solution at 57°C for 5-10 minutes. The cresyl violet acetate solution was pre-warmed and filtered just before use. Finally, sections were incubated with 95% ethanol, in several changes, dehydrated in 100% ethanol, cleared in xylene and mounted with Eukitt quick-hardening mounting medium (Fluka Analytical). After the staining, the hippocampal area was measured as follows: a mask was created around the hippocampus region and the area of the hippocampus was established (Figure 3.3).

The program (CellProfiler) recognized the section established and calculated the area of the selected pictures.
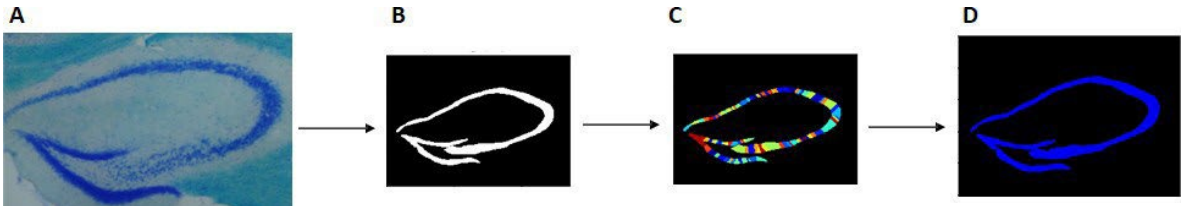
Figure 3.3: Representative scheme of the analysis of the staining. A) After the staining pictures of the hippocampal area were taken at the microscope B) and afterwards a mask was created around the region of interest. C) The images were processed with CellProfiler program, which recognized the section and D) calculated the area of the region.

3.7   Behavioral tests

3.7.1   Animals

Adult wild-type and transgenic L1/687 males and wild-type heterozygous and homozygous L1/687 females (3- to 4-month-old) were transferred from the pathogen-free breeding facility into a vivarium with an inverted 12 hour light–dark cycle (light off at 7:00) and maintained in groups of three to six siblings under standard-housing conditions (23°C $\pm$ 1°C, 40–50% humidity, food and water *ad libitum*). After one week of adaptation, mice were handled every day for one hour for one week and after this week of handling, they underwent the experiments that were performed between 10:00 and 15:00 in a room adjacent to the vivarium and illuminated with dim red light. All the mazes used for behavioral analyses were cleaned between mice with soap and water and with 70% ethanol. Care was taken to minimize pain or discomfort for the animals.

3.7.2   Open Field

The open field test is commonly used to evaluate activity levels, exploration habits and anxious-like behavior [134]. The open field (OF) consisted in an arena of 50 x 50 cm enclosed with 50 cm high walls, illuminated with 50 lux. The mouse was placed in a Plexiglas cylinder located in one corner of the arena. When the cylinder was lifted, the mouse could freely move in the arena for 20 or 30 minutes. Videos of the experiment were produced with the software EthoVision (Noldus). Different variables were evaluated and analyzed as the time spent in the center of the arena, the distance moved, the velocity and the average distance from the wall. Moreover, specific behavior parameters were analyzed with The Observer for the first 5 min of the test: rearing on wall (vertical exploration by standing on the back paws with one or two forepaws touching the wall), rearing off wall and self-grooming.

3.7.3   Elevated plus maze

Another test for evaluating anxious-like behavior is the elevated plus maze [135]: the arena for this test had a shape of a plus, with four arms, 30 cm long and 5 cm wide, connected with a center zone of 5x5 cm. Two opposing arms were bordered with a 2 mm rim (open arm), while the other two arms had a 15 cm high wall (closed arm). The plus maze was elevated 75 cm from the floor and illuminated with 10 lux. For the test male and female wild-type and L1/687 transgenic mice were used. The mice were transported to the room of the elevated plus maze and left for 10 minutes for habituation and after they were placed in the center of the maze facing the open arm observed for 5 minutes. The following parameters were analyzed with The Observer: open and closed arm entries (calculated when all the four paws were inside the arm), stretch attend posture (SAP, calculated when the mouse stretched forward and retracted to the original position

without forward locomotion [136], self-grooming, and head dips (exploratory head movement).

3.7.4 Social interaction

For the social interaction test, the arena used for the open field test (50 x 50 cm) was divided into two identical compartments by a 40-cm-high wall with an opening in the middle allowing the mouse the access to both compartments. A metal cup with a metal mesh allowing the tested mice to see and smell the mouse inside the cup was located in one corner of each compartment containing either one familiar or one unfamiliar mouse. The familiar mice were recruited from heterozygous female or wild-type male siblings living in the same cage as the test animal. In some cases wild-type and transgenic siblings from the same cage had to be taken as familiar mouse, but this was counterbalanced between genotypes. Heterozygous or wild-type mice from different cages that were not used as subjects in the behavior tests served as unfamiliar mice. First the familiar and unfamiliar mice were placed under the cups counterbalanced between the two compartments to avoid any bias due to the location, and then the subject mouse was placed in the arena and left free to move between compartments for 20 minutes. The room was illuminated with 5 lux. Videos were recorded with the software EthoVision (Noldus) and a different set of parameters was analyzed: distance moved, time spent in each compartment, and time spent in proximity of the two cups. The time spent in the transition zone in the middle, for moving from one compartment to the other was not in the calculation.

3.7.5 Marble burying test

The test was performed under red light and in a bigger cage, different from the home-cage of the mice (dimensions: 42 × 24 × 12 cm).

A 5 cm thick layer of bedding covered the floor of the cage and 20 black marbles (diameter 1.5 cm) were placed on top of the bedding. Wild-type and transgenic L1/687 mice were brought into the room of the experiment 5 minutes prior to the test for habituation. The mice were then placed in the corner of the cage and left for 30 minutes alone and free to explore and move. The test is used to measure repetitive or compulsive digging behavior and activity levels [137].

3.7.6 Rotarod

The rotarod test is used to evaluate motor coordination, impairment in locomotor activity and motor learning in mice [126]. Male and female wild-type and L1/687 mice were trained on a rotarod (Rota-rod for mice, UGO BASILE S.R.L., Germany) for two days with 2 trials with constant speed (4 rpm) for 2 minutes and 3 trials of training with acceleration (4-40 rpm) in 4 minutes. After every training trial, the training was stopped for an interval of 10 minutes before continuing with the next training phase. For the next 3 or 4 consecutive days mice were subjected to the test: mice were located on the 3 cm diameter rod which was subjected to an acceleration from 4 to 40 rpm within 300 sec. The tests were performed with just the red light and the running time (latency to fall from the rod) was recorded.

3.7.7 Beam walking and pole test

The pole test is commonly used to evaluate movement disorders in mice [138]. The test evaluates the ability of a mouse to grasp a pole and make a t-turn in order to climb down to its home cage. Wild-type and L1 transgenic mice were placed with their head oriented upward on top of a vertical pole of 48.5 cm length x 0.3 cm diameter and made of rough wood. The time needed to

climb down the vertical pole was measured. Another test used for assessing motor impairment is the beam walking test: mice were placed on a beam made of wood, 90 cm long with a width of 5 cm and suspended 50 cm from the floor. The mice, wild-type and transgenic L1/687 mice, males and females, were recorded from behind while walking on the beam, from the experimenter to the home cage, which is placed at the end of the beam. From the videos different parameters were analyzed such as the heal-tail angle and the foot-base angle. Experiments were performed under 50 lux light.

3.7.8 Home cage activity

Male and female wild-type and L1/687 mice were recorded for 24 hours using the MOUSE-E-MOTION software (Infra-e-motion GmbH, Hamburg, Germany). Mice were first placed into a single standard cage (15 x 20 x 23 cm) for 3 days for habituation before starting to monitor the home cage activity for 24 hours. The recorder, MOUSE-E-MOTION Universal Data Logger (Infra-e-motion GmbH, Hamburg, Germany) was placed on top of the cage and the activity of the mice was recorded every 4 minutes, for a whole day with a 12-hour light and 12 hour night cycle.

3.8 Statistical analysis

All numerical data are presented as group mean values with standard error of the mean (S.E.M.). Statistical tests used for comparisons are indicated in the text and figure legends. Analyses were performed using the SPSS or GraphPad software.

C H A P T E R 4

RESULTS

4.1   Interaction with mitochondrial proteins

4.1.1   L1 is present on the surface of mitochondria

Previous studies have shown that L1 is imported into mitochondria, where it interacts with GAPDH and the complex I subunit NDUFV2 [58]. To have a better understanding of the localization of L1 in regard to mitochondria and its transport, the location of L1 was further investigated using a flow cytometer. Isolated mitochondria from wild-type and L1-deficient mice were stained with different antibodies against proteins of interest and TOM20, which is localized in the outer mitochondrial membrane and used as marker for mitochondria. Mitochondria from male wild-type mice were positive for L1 and TOM20, while mitochondria from male L1-deficient mice were positive only for TOM20 (Fig. 4.1). In the graphs the values of the X-axis and Y-axis indicate the fluorescence intensity for L1/Cy5 and TOM20/FITC staining, respectively. Unstained mitochondria with low intensities for both staining were found in the Q3 quadrant.

Mitochondria positive only for L1 or TOM20 were found in the quadrant Q1 or Q4, respectively. In the quadrant Q2 TOM20- and L1-positive mitochondria were found. Mitochondria from wild-type mice were either unstained (9.2%), only L1-positive (38%), only TOM20-positive (65%) or positive for L1 and TOM20 (22.8%) (Fig. 4.1). Mitochondria from L1-deficient mice were unstained (13.6%) or only TOM20-positive (86.4%). These results indicate that L1 is present on the surface of mitochondria.
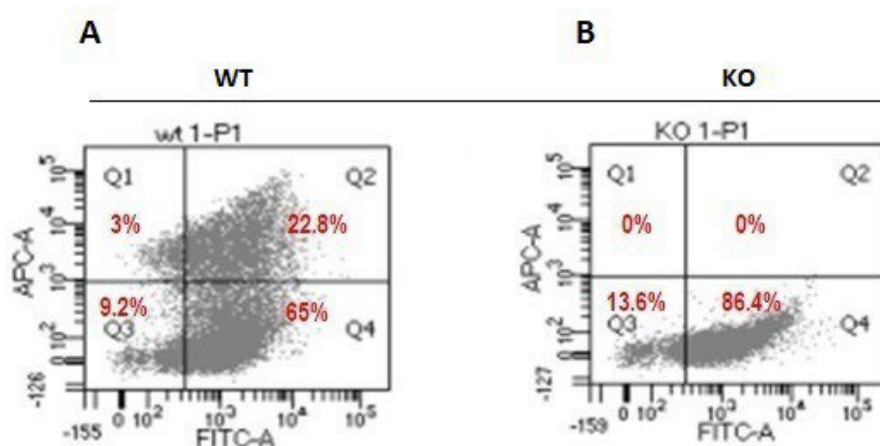
Figure 4.1: L1 is present on the surface of mitochondria. Mitochondria from brains of male wild-type and L1-deficient mice (3- to 5-month-old) were analyzed in a flow cytometer. A) Q1: mitochondria positive for L1; Q2: mitochondria positive for both L1 and TOM20; Q3: un-stained mitochondria; Q4: mitochondria positive only for TOM20. Mitochondria from wild-type mouse brains are positive for L1 and TOM20, indicating the presence of L1 on the surface of the mitochondria.   B)   In the mitochondrial   preparation   from L1-deficient mouse brains only a positive signal for TOM20 is found. Representative graphs of flow cytometry from three independent experiments are shown.

4.1.2   Levels of BNIP3 on the surface of mitochondria are higher in L1-deficient mice

Besides for L1, isolated mitochondria were stained with antibodies against proteins that are involved in mitophagy, such as PINK1, Parkin, FUNDC1 and BNIP3 [112] or in the fission/fusion process, such as Drp1, Mfn2, Fis1 and Rhot1 [95]. There were no differences in the levels of these proteins, between wild-type and L1-deficient mitochondria, except for BNIP3. The number of mitochondria stained with both BNIP3 and TOM20 were higher in the mitochondria from L1-deficient mice (86.7%) when compared to the numbers of mitochondria from wild-type littermates (28.1%), indicating that the levels of this protein on the mitochondrial surface are significantly higher in the mitochondria from L1-deficient mice compared to the wild-type mice (Fig. 4.2).
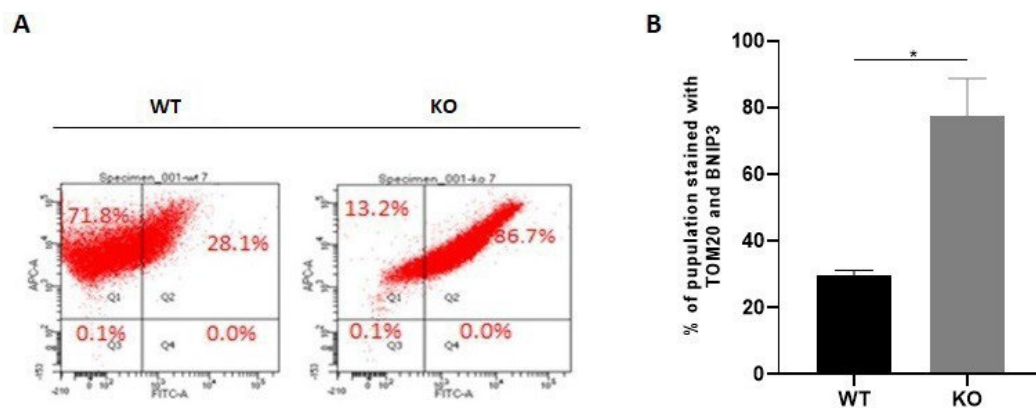
Figure 4.2: Levels of BNIP3 are enhanced on mitochondria from L1-deficient mice. Flow cytometry was performed using mitochondria isolated from brains of 3- to 5-month-old male L1+/y and L1-/y littermate mice. A) Q1: mitochondria stained with BNIP3; Q2: mitochondria stained with both BNIP3 and TOM20; Q3: unstained mitochondria; Q4: mitochondria stained with TOM20. Levels of BNIP3 are higher on the surface of mitochondria from L1-deficient mice compared to the levels on mitochondria from wild-type mice. Representative graphs from the analysis in a flow cytometer from three different experiments are shown. B) Quantification of the population of mitochondria stained with TOM20 and BNIP3 from wild-type and L1-deficient mice. The quantification is based on three independent experiments. Mean values ± S.E.M. are shown * p<0.05; unpaired t-test.

4.2   Interaction between L1 and LC3

Short linear motifs found in disordered regions of multidomain proteins have a central role in the network organization of protein–protein interaction. Important examples of motifs involved in protein-protein interactions are the LC3 interacting regions (LIRs). LC3 is one of the main proteins involved in the clearance and maintenance of a healthy pool of mitochondria [114]. LC3 is involved in the elongation of the autophagosome
[121] and anchors to damaged mitochondria through mitophagy proteins as BNIP3 and FUNDC1 [112], as well as mitochondria marked for degradation by PINK1 and parkin, in which pathway p62 acts as cargo between mitochondria and the autophagosome [109]. Since L1 contains a LIR motif W/F/YxxL/I in its intracellular domain composed as 5'- TGYLLSYhPVDG - 3', it was interesting to investigate if L1 and LC3 interact via this LIR motif. Furthermore, I determined if full-length L1 or the L1-70 fragment interacts with LC3. In addition, levels of LC3 on mitochondria of wild-type mice and of mice lacking L1-70 were analyzed to elucidate if lack of L1-70 leads to recruitment of LC3 to mitochondria and enhanced mitophagy.

4.2.1 L1-ICD directly binds to LC3

To test whether L1 directly interacts with LC3 binding between the intracellular domain of L1 (L1-ICD) and LC3 was first confirmed using an ELISA. Recombinant LC3 protein was immobilized and L1-ICD was used as ligand in increasing concentrations. CHL1-ICD served as negative control. The results showed a concentration-dependent and saturable binding of the L1-ICD, but not of the CHL1-ICD to the immobilized LC3 (Fig. 4.3, B). To further investigate whether the interaction between these proteins is mediated by a putative LIR motif in the L1-ICD, this motif was mutated by introducing

two-point mutations and an ELISA was performed using different concentrations of mutated L1-ICD and wild-type L1-ICD. Mutated and unmutated L1-ICDs showed similar binding curves, indicating that the mutation of the LIR motif in the intracellular domain of L1 does not affect the binding between L1-ICD and LC3 (Fig. 4.3, C). This result indicates that L1 directly binds to LC3 via its intracellular domain.
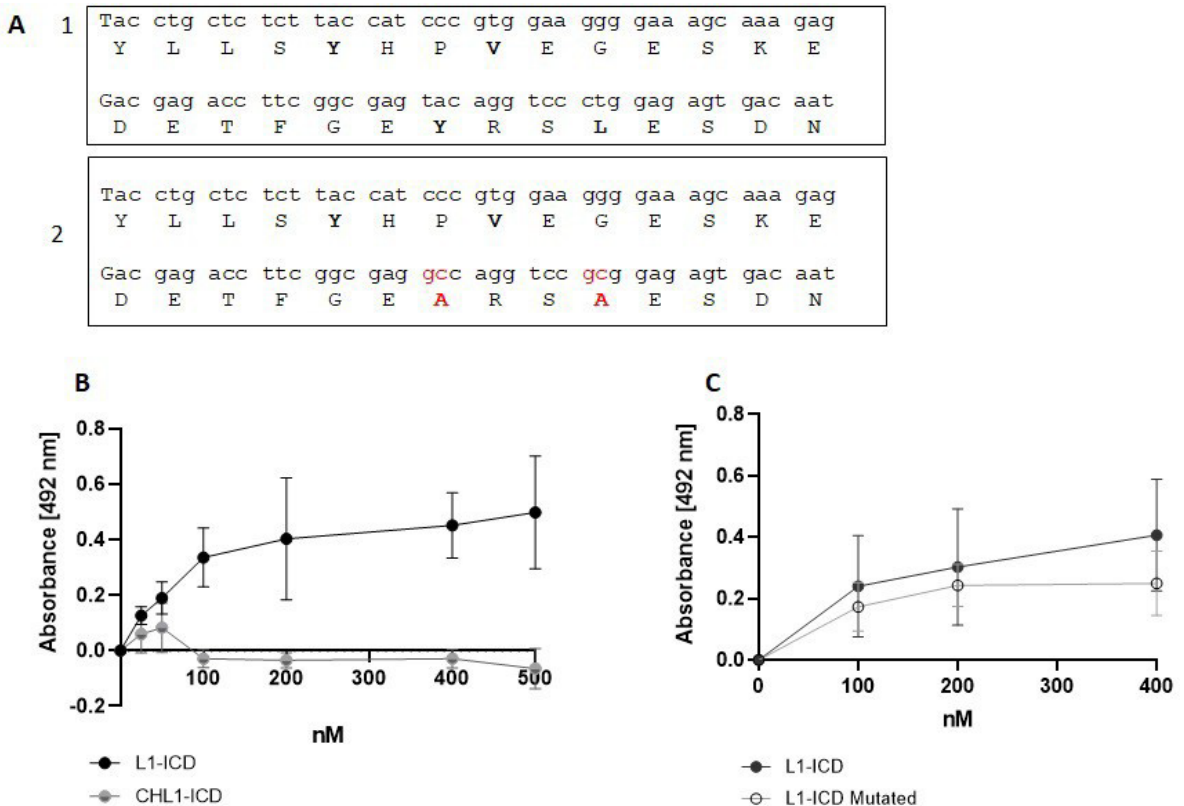
Figure 4.3 The binding of L1-ICD to LC3 is not mediated by the LIR- motif in the L1-ICD. Recombinant LC3 was substrate-coated and incubated with increasing concentrations of L1-ICD, CHL1-ICD and mutated L1-ICD. Binding was determined using mouse L1-C2 antibody, goat CHL1 antibody and horseradish peroxidase-conjugated secondary antibodies. A) Wild-type protein sequence of the unmutated LIR domain (1) with two-point mutations in red, leading to the exchange of a tyrosine and leucine by two alanine residues (2) B) L1- ICD, but not CHL1-ICD, binds directly to LC3. C) Binding between the L1-ICD and LC3 is not mediated by the LIR motif within the L1-ICD. Mean values ± S.E.M from three independent experiments carried out in triplicates are shown.

### 4.2.2   L1 binds to LC3 in a cellular context

The interaction between L1 and LC3 in a cellular context was next investigated in a proximity ligation assay (PLA) using a mouse L1 antibody and a rabbit LC3 antibody on cultured cerebellar granule cells from wild-type and L1-deficient mice. The PLA method allows the detection of proteins that are in close proximity of less than 40 nm. Cerebellar granule cells from wild-type mice showed L1/LC3 positive fluorescent signals as red dots while no red dots were detectable in the L1-deficient cerebellar granule cells (Fig. 4.4). The result indicates that L1 is in close proximity with LC3: positive fluorescent signals are observed in the cell body along neurites and especially around the nucleus.
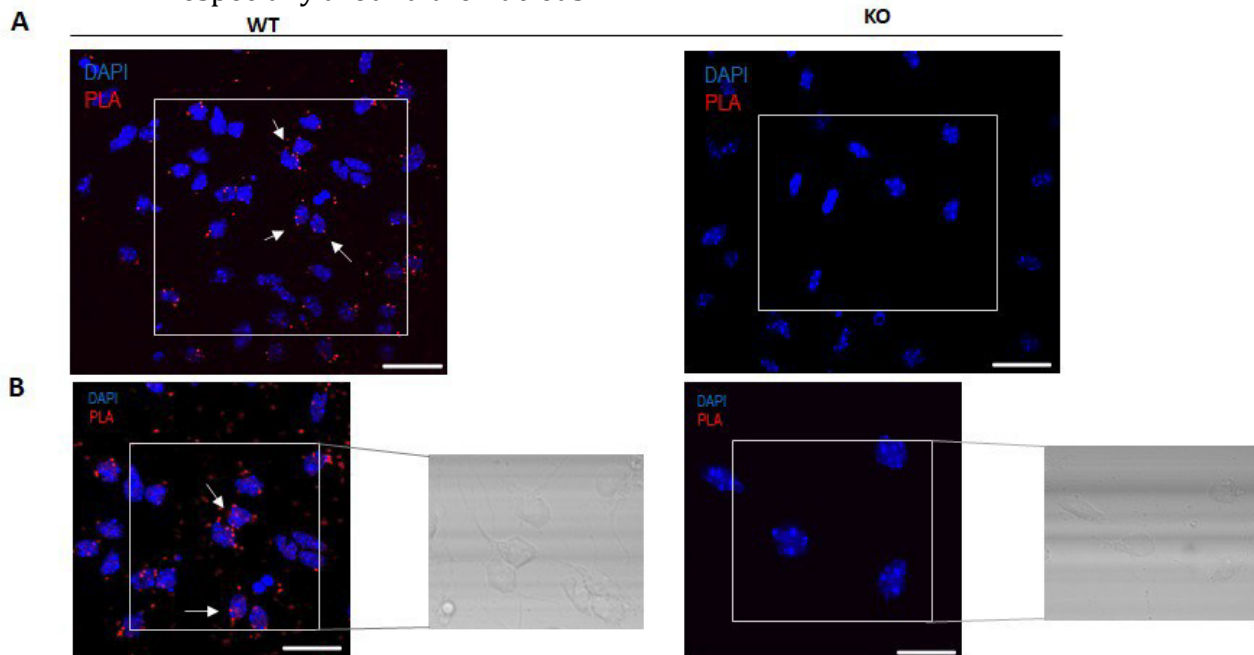
Figure 4.4: L1 and LC3 are in close proximity in cultured cerebellar granule cells. Proximity ligation assay was performed using cerebellar granule cells from 7-day-old male wild-type and L1-deficient mice. The assay was performed using primary L1 and LC3 antibodies. A) Representative pictures of wild-type and L1-deficient cerebellar granule cells from two independent experiments are shown. Nuclei are stained with DAPI (blue); red spots indicate close proximity between L1 and LC3 and are indicated with withe arrows. Scale bars, 20 μm. B) Close up and phase contrast images of cerebellar granule cells. Nuclei are stained with DAPI (blue), PLA signal is shown in red. Scale bars, 10 μm.

4.2.3 LC3 interacts with the L1-70 fragment

To understand if LC3 interacts with the L1-70 fragment, the binding between L1 and LC3 was further investigated using the mouse lines L1/687 and L1/858-863 in which the generation of L1-70 is prevented. Proximity ligation assay was performed on cerebellar granule cells from wild-type, L1/687 and L1/858-863 mice. L1- deficient mice were used as control. PLA signals were visible in cerebellar granule cells from wild-type mice, but not in cells from L1/687 and L1/858-863 mice (Fig. 4.5). This finding indicates that LC3 interacts with the L1-70 fragment.
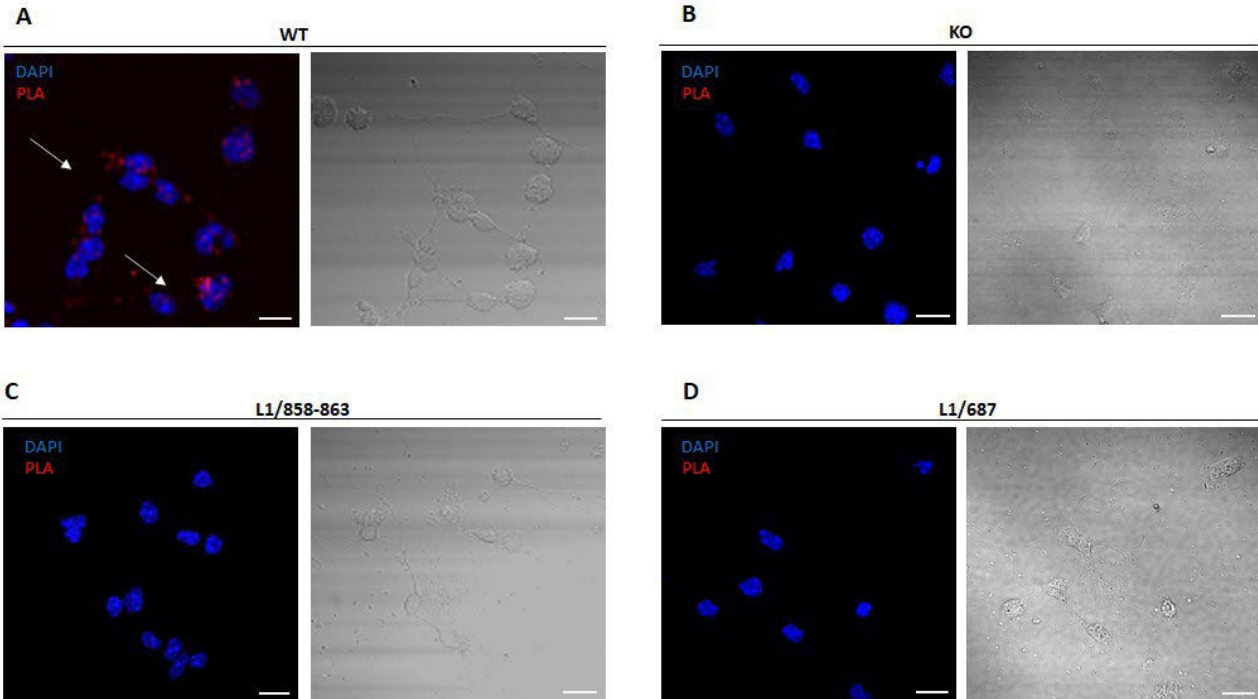
Figure 4.5: LC3 and L1 co-localize in cells from wild-type mice, but not in cells from mice lacking the L1-70 fragment. Proximity ligation assay was performed using cerebellar granule cells from 7-day-old male wild-type, L1-deficient, L1/687 and L1/858-863 mice. Primary antibodies against L1 and LC3 were used in the assay. Representative images of cerebellar granule cells from male wild-type mice (A) L1-deficient mice (B), L1/687 mice (C) and L1/858-863 mice (D) are shown. Nuclei are stained with DAPI (blue), red dots are indicative for the L1/LC3 interaction and are indicated by white arrows. Scale bars, 10 μm. Representative pictures from two independent experiments are shown.

4.2.4   Levels of LC3 in L1-70 lacking and L1-deficient mice

To further investigate the interaction between L1 and LC3, the mitochondria-associated levels of LC3 in wild-type mice, L1-deficient mice and the transgenic mouse lines were determined by western blot analysis using isolated mitochondria. For the L1-deficient mice, the analysis was performed using mitochondria of 6- to 10- day-old mice, while for the transgenic mice, mitochondria from 6- to 10-day-old and 4- to -6-month-old mice were used to investigate a potential age-related effect of lack of L1-70 on the LC3 levels. The levels of LC3 on the mitochondria from wild-type and L1-deficient mice did not differ (Fig. 4.6).
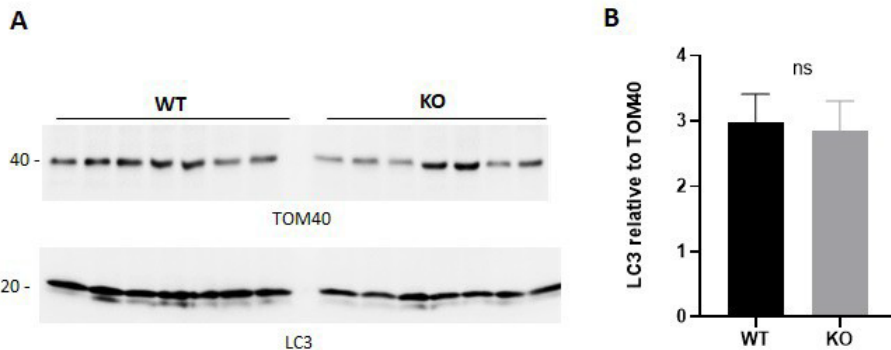
Figure 4.6: Levels of LC3 are normal on mitochondria from L1- deficient mice. Mitochondria were isolated from brains of 6- to 10-day-old male wild-type and L1-deficient mice and western blot with LC3 and TOM40 (loading control) was performed. A) Representative western blot from wild-type and L1-deficient mice using mitochondrial proteins. B) LC3 levels relative to TOM40 were calculated. Mean values ± S.E.M. ns: not significant; n= 7 animals for each genotype; unpaired t-test.

Western blot analysis was also performed with mitochondrial proteins from 6- to 11-day-old wild-type, L1/858-863 and L1/687 transgenic littermate mice and did not show differences in the levels of LC3 on mitochondria compared to the wild-type littermates (Fig. 4.7).
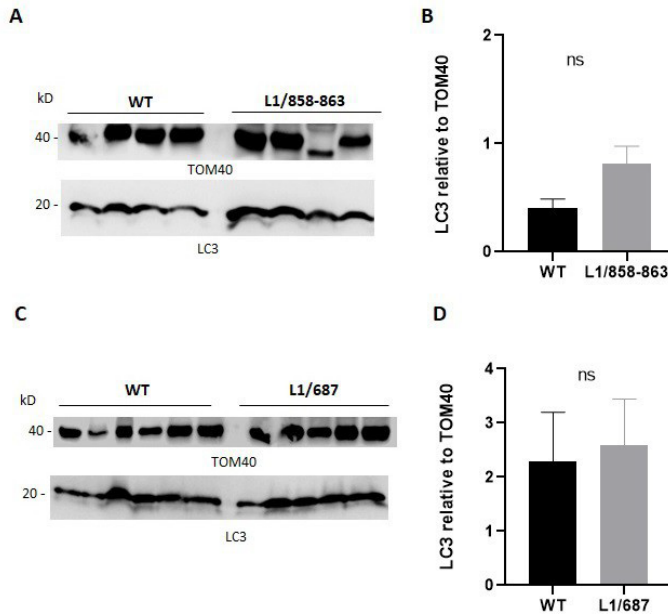
Figure 4.7: LC3 levels on mitochondria of wild-type, L1/858- 863 and L1/687 mice. Western blot analysis was performed using proteins from mitochondria from male wild-type, L1/858-863 and L1/687 mice. Mitochondria were isolated from brains of 6- to 11-day-old male wild- type, L1/858-863 and L1/687 mice. Western blots were performed using antibodies for LC3 and TOM40 as loading control. A) Representative western blot with mitochondrial proteins from wild- type and L1/858-863 mice. B) LC3 levels relative to TOM40 were calculated. n=4 animals for each genotype. C) Representative western blot on mitochondrial proteins of wild-type and L1/687 mice. D) LC3 levels relative to TOM40 were determined. N=6 animals per genotype. Mean values ± S.E.M. are shown; ns: not significant; unpaired t-test.

Western blot analysis of mitochondria from the L1/687 mice was performed on two different groups: brains were collected from male wild-type and L1/687 mice used for behavioral experiments (6-month-old) and mitochondria were isolated from one hemisphere and used to detect LC3 levels.
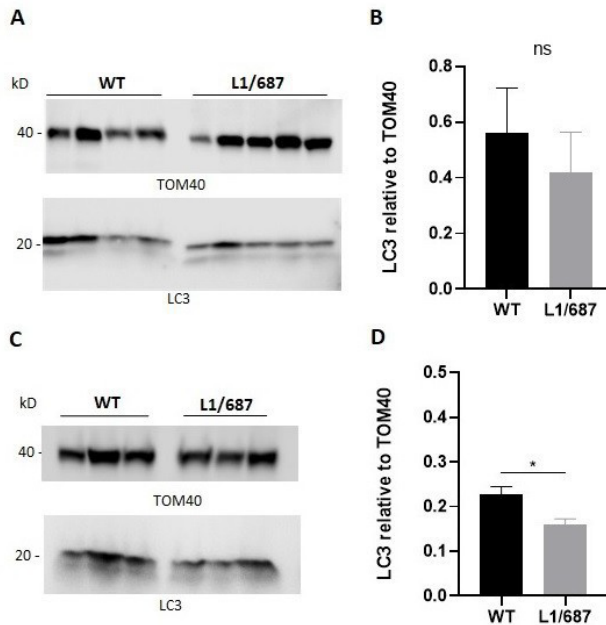
Figure 4.8: Levels of LC3 on mitochondria from L1/687 mice. Mitochondria were isolated from brains of wild-type and L1/687 male mice (4- to 6-month-old) and used to perform a western blot analysis to detect LC3 levels, using antibodies against LC3 and TOM40 as loading control. A) A representative western blot with mitochondria from 4-month-old mice using LC3 antibody and TOM40 as loading control is shown. B) Quantification of LC3 levels analysis relative to TOM40 levels was performed. Mean values with ± S.E.M. n= 4 wild-type and 5 L1/687 mice. Unpaired t-test. C) Representative picture of a western blot from mitochondrial proteins isolated from 6-month-old mice wild-type and L1/687 mice used for behavioral experiments before. D) Quantification of western blot signals. Mean values ± S.E.M. n=3 animals for each genotype *p<0.05 (p=0.03); ns: not significant; unpaired t-test.

Brains from 4-month-old mice which were not subjected to behavioral experiments were also analyzed. LC3 levels only showed a tendency to be lower in 4-month-old transgenic mice which were not used for behavioral studies (Fig. 4.8 A, B), whereas levels of LC3 are significantly lower in mitochondria of the 6-month-old transgenic L1/687 mice relative to those from wild-type littermates which both were previously used for behavioral experiments (Fig. 4.8 C, D). In contrast to the L1/687 mice, which show reduced levels of LC3, levels of LC3 on mitochondria of adult 5- to 6-month-old L1/858-863 mice, which were not used for behavior experiments, are higher compared to the levels of LC3 on mitochondria of wild-type mice (Fig. 4.9).
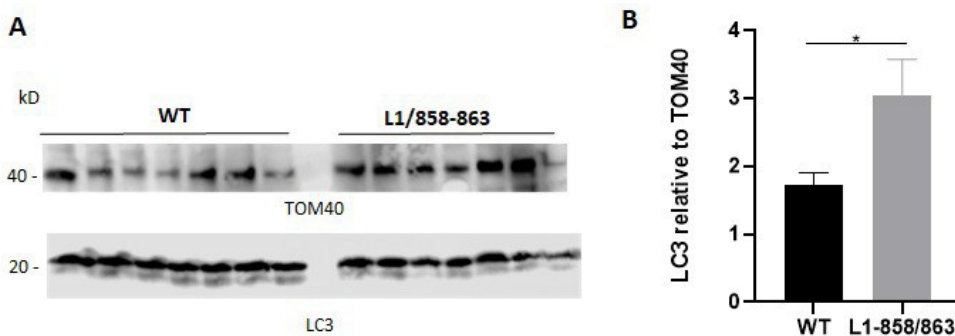
Figure 4.9: LC3 levels on mitochondria of wild-type and L1/858-863 mice. Mitochondria were isolated from brains of 5- to 6-month-old male wild-type and L1/858-863 mice and western blot was performed using LC3 and TOM40 (loading control) antibodies. A) Representative western blot on mitochondrial proteins from wild-type and L1/858-863 mice is shown. B) Quantification of LC3 level relative to TOM40 was performed. Mean values ± S.E.M. *p<0.05; unpaired t-test; n=7 animals for each genotype.

4.3 Interaction between L1 and Parkin

Besides LC3, other possible interaction partners of L1 were studied and investigated. It was previously shown that Drp1 and Miro co-immunoprecipitate with the L1-70 fragment and that in L1-deficient mice the activity of complex I is reduced and the mitochondrial membrane potential is impaired [58]. Basing on this data the interaction between L1 and Parkin was explored since an impaired membrane potential in a damaged mitochondrion activates the PINK1-Parkin pathway [112, 115, 116] for degradation of impaired mitochondria [114]. In this context it was important to analyze if L1 or its L1-70 fragment and its interaction with PINK1 and/or Parkin is involved in mitophagy.

4.3.1 L1 associates with Parkin

To have a better understanding of the role of L1 in the mitophagy process, a putative interaction between L1, PINK1 and Parkin was investigated. To this aim, co-immunoprecipitation experiments were performed using brain homogenates from wild-type mice. Full-length L1, but not L1-70, was detected in the Parkin immunoprecipitate, but it was not detected in the control immunoprecipitate obtained with non-immune antibody (Fig. 4.10). No co-immunoprecipitation with L1 was obtained using the Pink antibody. These results suggest that Parkin and L1 but not PINK1 and L1, are present in a complex that allows them to interact.
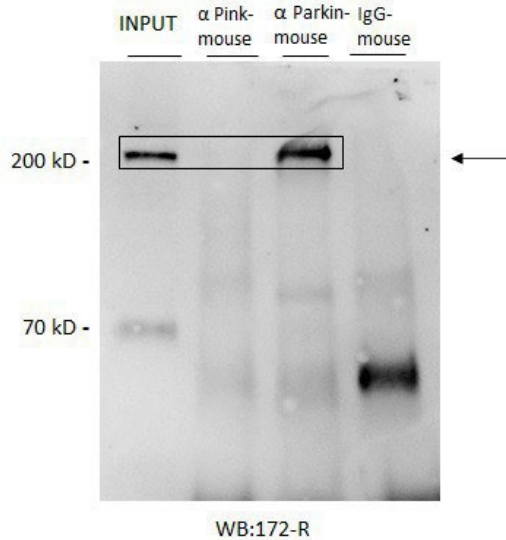
Figure 4.10: L1 and Parkin co-immunoprecipitate. Homogenates from brains of 2-month-old wild-type mice were used for IP with PINK1 and Parkin antibodies. Immunoprecipitates were subjected to western blot analysis with L1 antibody 172-R targeting an epitope in the L1 intracellular domain. Full-length L1, but not L1-70, is detected in the Parkin immunoprecipitate, but not in the PINK1 immunoprecipitate. Full-length L1 and L1-70 are present in the input but do not appear in the non-immune IgG control. A representative picture of two independent experiments is shown.

4.3.2 Parkin levels in L1-deficient mice are normal

Since L1 and Parkin can associate, the levels of Parkin were analyzed in brain homogenates of wild-type and L1-deficient mice, to determine if lack of L1 influences levels of parkin. Brains from 7-day-old male wild-type and L1 deficient mice were collected and the cytosolic fraction was used for western blot analysis with Parkin antibody and tubulin antibody as control loading. The levels of Parkin were not significantly different between wild-type and L1-deficient mice. (Fig. 4.11).
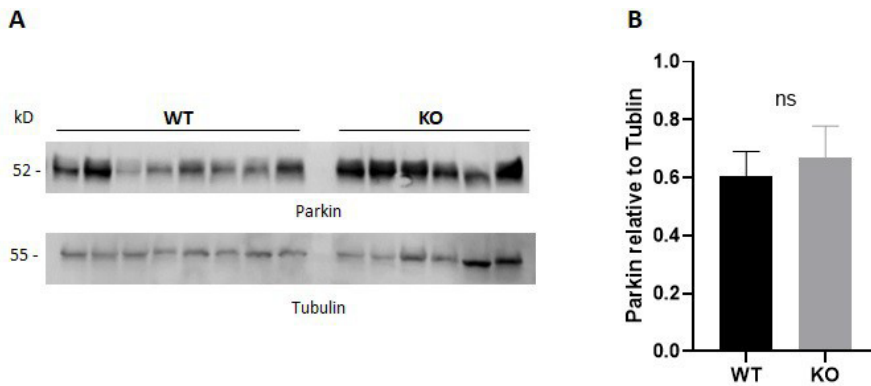
Figure 4.11: Cytosolic Parkin levels in wild-type and L1-/y mice. A) Representative picture of a western blot with cytosolic proteins from male wild-type and L1 deficient mice. B) Quantification of western blot signals using Parkin antibody and tubulin as loading control. Mean values ± S.E.M. ns: not significant; n=8 animals for wild-type and 6 animals for L1-deficient mice; unpaired t-test.

4.3.3 L1 is in close vicinity to Parkin in cerebellar neurons

To verify the interaction between L1 and Parkin in neurons, cerebellar granule cell cultures from wild-type and L1-deficient mice were used for proximity ligation assay with L1 and Parkin antibodies. Positive fluorescent signals for L1/Parkin complexes were observed as red spots in wild-type, but not L1-deficient cerebellar neurons (Fig. 4.12). This result indicates that L1 is in very close proximity to Parkin.
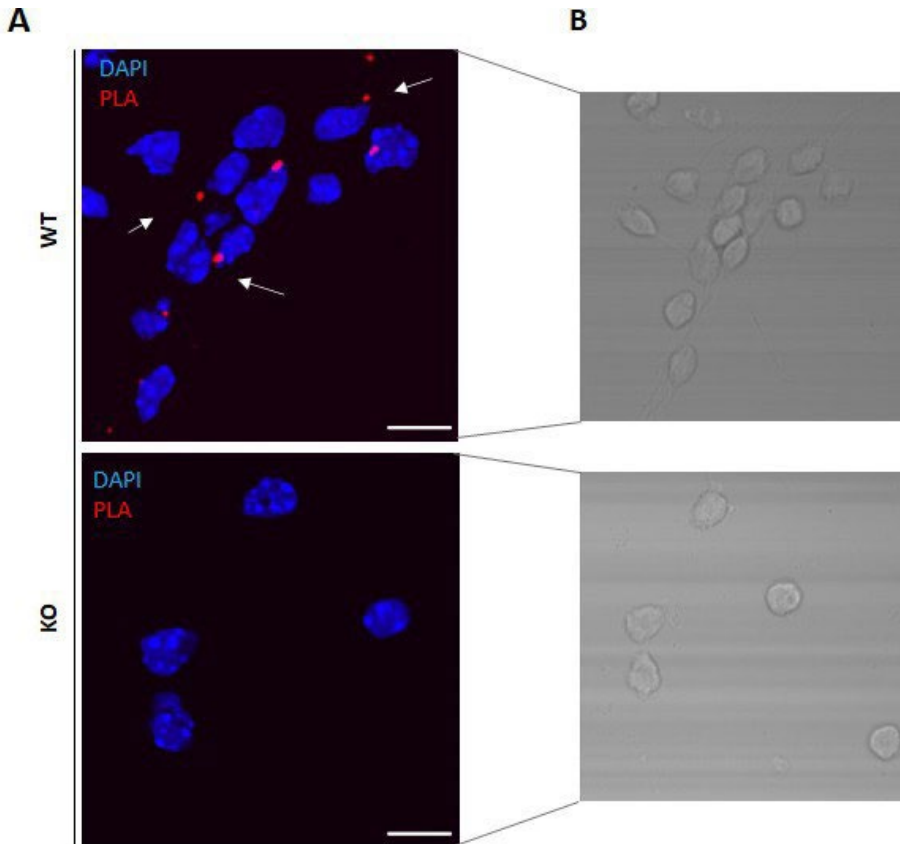
Figure 4.12: L1 and Parkin are present in close proximity in cerebellar granule cells from wild-type mice. Proximity ligation assay was performed using cultured cerebellar granule cells from 7-day-old male wild-type and L1-deficient mice and antibodies against L1 and Parkin. A) Representative pictures of wild-type and L1-deficient granule cells from two independent experiments are shown. Nuclei are stained with DAPI (blue); red spots, marked with withe arrows, indicate close proximity between L1 and Parkin. Scale bars, 20 μm. B) Phase-contrast pictures of cerebellar granule cells shown in (A). Scale bars, 10 μm.

4.4 Effect of L1-70 on mitochondrial dynamics

The role of L1 in mitochondrial dynamics was previously studied in our laboratory showing that in L1-deficient neurons motility of mitochondria was reduced as well as the membrane potential and the complex I activity, but no impairment in ATP synthase activity was observed. Moreover, results showed the import of the L1-70 fragment into mitochondria and the interaction of this L1 fragment with different proteins involved in mitochondrial dynamics as Drp1, Miro and NDUFV2 [58]. To better understand the role of L1-70 in mitochondria different mitochondrial parameters such as ATP levels, complex I activity and membrane potential together with mitochondrial dynamics as mobility, velocity and direction, were analyzed in mice lacking the L1-70 fragment.

4.4.1 Ablation of L1-70 affects complex I activity

In order to produce ATP, mitochondria use the oxidative phosphorylation machinery which includes the electron transport chain and the enzymes of complex I-V of the inner mitochondrial membrane. It was previously shown that the activity of complex I, but not that of the complexes II-V, was reduced in L1-deficient mice when compared to the wild-type mice [58]. CI, together with CIII and CIV, generates the electrochemical proton gradient across the inner mitochondrial membrane [85]. To test whether mitochondrial L1-70 has an influence on mitochondrial metabolism, the activity of CI was analyzed in transgenic mice lacking L1-70. To test the activity of this complex in wild-type and L1/687 mice, mitochondria were isolated from brains of young (6- to 9-day- old) and adult (4- to 6-month-old) wild-type mice and L1/687 littermates. The levels of NADH, which is oxidized by the CI, was then calculated by a decrease in absorbance at 340 nm, proportional to the activity of complex CI.

CI activity was not significantly different in L1/687 littermate mice compared to the wild-type mice at the age of 1-2 weeks or in adulthood (Fig. 4.13 A, B). The levels of CI activity had only a tendency to be lower in L1/687 mice. In mice subjected to behavioral experiments, the CI activity had a tendency to be higher in transgenic males compared to the wild-type males (Fig. 4.13 C) while complex I activity is significantly lower in L1/687 females compared to the wild-type females (Fig. 4.13 D).
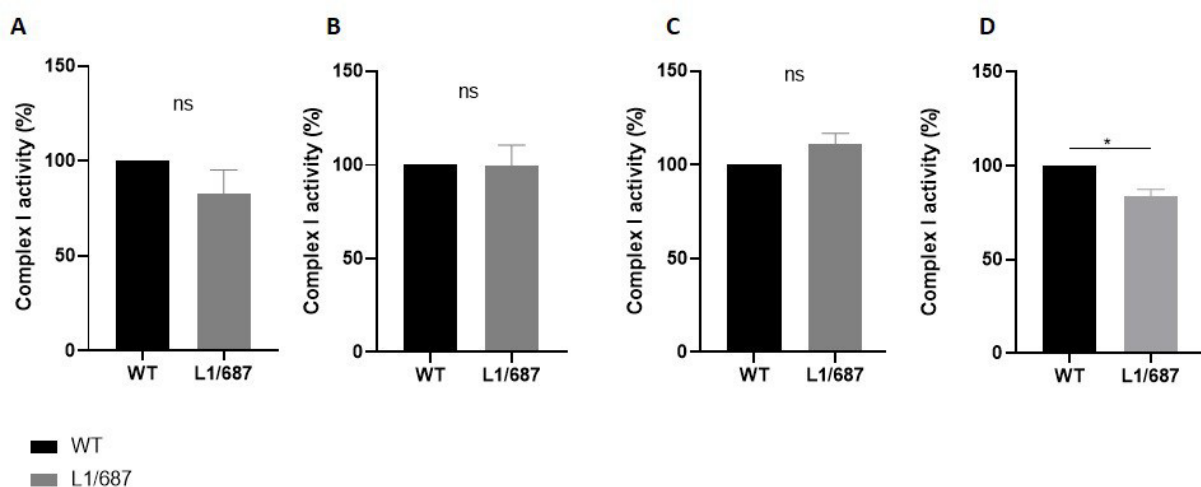
Figure 4.13: Complex I activity of mitochondria from L1/687 and wild-type mice at different ages. Mitochondria were isolated from wild-type and L1/687 mice at different ages and the oxidation of NADH was measured over 15 minutes. A) Analysis of CI activity from 6- to -9-day-old male L1/687 and corresponding wild-type littermates (n=6 per genotype). B) CI activity in 4-month-old male wild-type and L1/687 mice, not used for behavioral analysis (n=5 per genotype). C) CI activity in 6-month-old male wild-type and L1/687 littermate mice, previously used for behavioral experiments (n=3 per genotype). D) Activity of CI in adult 6-month-old female wild-type and L1/687 mice used for behavioral studies before. The activity is lower in L1/687 females compared to wild-type females (n=4 per genotype). Mean values ± S.E.M. are shown in all graphs; *p<0.05; ns: not significant; Mann-Whitney test.

4.4.2   Ablation of L1-70 affects ATP levels

Mitochondrial complex I is part of the respiratory chain that comprises the enzymes of complex I-V. Complex V catalyzes the synthesis of ATP from ADP and inorganic phosphate [141]. It was previously described that complex II/III and IV activity is not different in mitochondria of L1-deficient and wild-type mice. In addition, the results from the enzymatic assay for complex V showed no impairment of the ATP synthase activity in mitochondria of L1-deficient and wildtype mice [58]. Here, I analyzed levels of ATP in cerebellar neurons from male transgenic L1/687 and wild-type littermate mice, to understand if the lack of the L1-70 fragment can result in defects in the ATP production. Comparison of cultured cerebellar granule cells from wild-type and corresponding L1/687 littermate males showed that the levels of ATP are lower in cells from L1/687 mice compared to the cells from wild-type mice (Fig. 4.14). This result suggests that the lack of L1-70 affects the process of the ATP production.
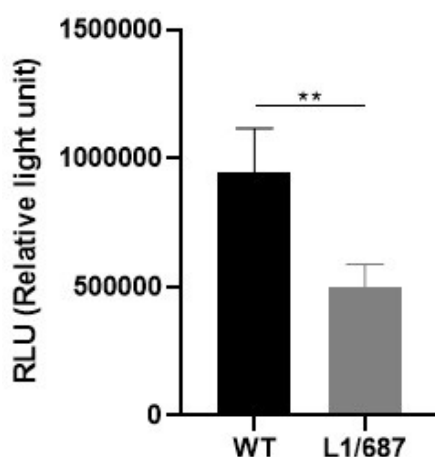
Figure 4.14: Measurement of ATP levels in wild-type and L1/687 neurons. Cerebellar granule cells from 7-day-old male wild-type and L1/687 mice were cultured for 24 hours and then the ATP assay was performed. Levels of ATP in neurons of transgenic mice are significantly lower compared to values of the neurons from wild-type mice. Mean values of three independent experiments and ±S.E.M. are shown; n=3 animals per genotype; $**p<0.01$; Mann-Whitney test.

4.4.3   Ablation of L1-70 affects the mitochondrial membrane potential

As previously shown, L1-70 is imported into mitochondria where it interacts with GAPDH [58], the enzyme that has a regulatory function in mitochondrial oxidative phosphorylation [142]. The energetic status of mitochondria from L1-deficient and wild-type mice has previously been analyzed and an impairment of the mitochondrial membrane potential in L1-deficient mice was found [58].

In order to better understand the role of L1-70 in mitochondrial metabolism, the energetic status of mitochondria was analyzed in neurons from wild-type and L1 transgenic mice, lacking the L1-70 fragment. The measurement of the energetic status of the inner mitochondrial membrane was investigated with a cationic carbocyanine dye, JC-1 iodide. The dye accumulates inside healthy mitochondria forming red fluorescent aggregates, while in mitochondria with lower membrane potential the dye is present as green fluorescent monomers that leak from the mitochondria and into the cytosol of cells. Cerebellar granule cells from wild-type, L1/858-863 and L1/687 mice were cultured for two days and stained with JC-1 iodide. Cerebellar granule cells from L1/858-863 and L1/687 mice displayed a lower red/green fluorescent ratio compared to the wild-type cells, indicating a reduced mitochondrial membrane potential (Fig. 4.15). Basing on this result, I assume that L1-70 has a direct or indirect effect on the mitochondrial health and the mitochondrial membrane potential and the absence of this fragment in the transgenic mice leads to an impairment of the membrane potential of the inner mitochondrial membrane.
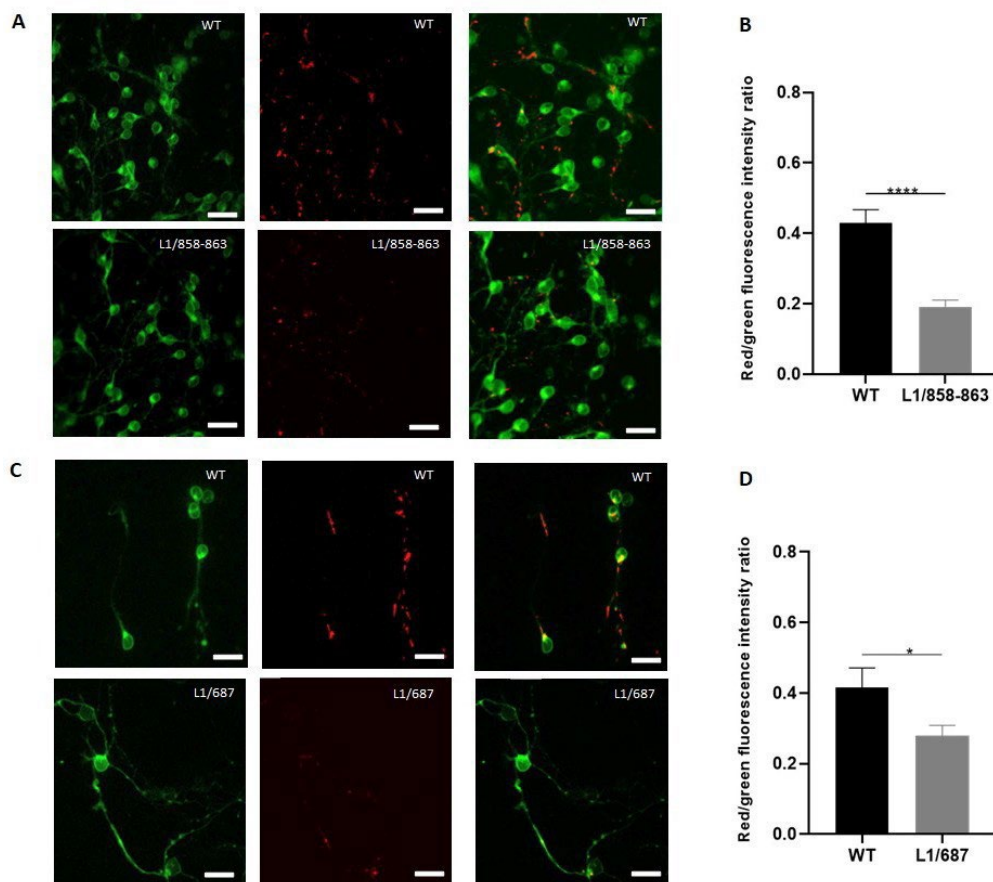
Figure 4.15: The mitochondrial membrane potential is reduced in transgenic mice lacking the L1-70 fragment. Cerebellar granule cells from 6- to 7-day-old wild-type and L1/687 mice were seeded on 22 μm coverslips coated with PLL in serum-free medium and left in culture for two days. Cells were then incubated with JC-1 (3 μM) in HBSS for 30 minutes and analyzed under a spinning disk. A) Representative images from three independent experiments with cerebellar granule cells from male wild-type and L1/858-863 mice are shown. From the left: green fluorescent monomers indicating impaired membrane potential; in the middle: red aggregates in healthy mitochondria; right: overlay. Scale bars, 20 μm. B) The membrane potential of L1/858-863 cells is lower compared to the wild-type cells. C) Representative images from three independent experiments with cerebellar granule cells from male wild-type and L1/687 mice are shown. From the left: green fluorescent monomers indicating impaired membrane potential; in the middle: red aggregates in healthy mitochondria; right: overlay. Scale bars, 20 μm D) The membrane potential of L1/687 cells is lower compared to the wild-type cells. The total cell fluorescence intensity was calculated for the green and red channels separately and then the ratio of red to green fluorescence intensity ratio was determined. Mean values ± S.E.M. from at least 15 images per group per 3 experiments obtained with cerebellar neurons are shown. **** $p < 0.0001$, *$p < 0.05$; unpaired t-test.

4.4.4 Effects of L1-70 ablation on direction of mitochondrial movements

An impaired mitochondrial membrane potential can affect different mitochondrial parameters, as fission and fusion and also mitochondrial transport. Mitochondrial depolarization can lead to disruption of the binding complex of kinesin/dynein motors and adaptor proteins, obstructing the mitochondrial transport [141]. The effects of the total absence of L1 were previously studied in L1-deficient mice. An enhanced retrograde transport of mitochondria in cerebellar granule cells from L1-deficient mice and a lower mitochondrial velocity compared to mitochondria of wild-type cells, with no effect of L1 on the mitochondrial mobility was observed [58]. In this thesis the experiments on mitochondrial motility were performed on neurons from wild-type and transgenic L1/687 mice, to further investigate the potential role of L1-70 in these dynamics. Mitochondria of cultured cerebellar cells were labeled with MitoTracker and mitochondrial transport was analyzed using time-lapse video microscopy and quantification by a kymograph. The term motility describes the velocity of dynamic mitochondria in axons and dendrites represented by diagonal lines in the kymographs, whereas the term mobility specifies the number of stationary or mobile mitochondria in neurons represented by vertical lines in kymographs. Unlike the mitochondria of L1-deficient mice, mitochondria from L1/687 mice did not show a significantly lower motility compared to the mitochondria of wild-type neurons (Fig. 4.16 A), but the absence of L1-70 had an effect on the direction of mitochondria. The percentage of anterogradely moving mitochondria was higher in wild-type neurons than in L1/687 cerebellar neurons, while the percentage of retrogradely moving mitochondria was higher in L1/687 neurons than in wild-type cerebellar neurons (Fig. 4.16 B). Moreover, the percentage of stationary mitochondria was higher in L1/687 neurons compared to the wild-type neurons (Fig. 4.16 C). These results show that the presence of L1-70 can affect mitochondrial transport by changing the direction of mitochondria.
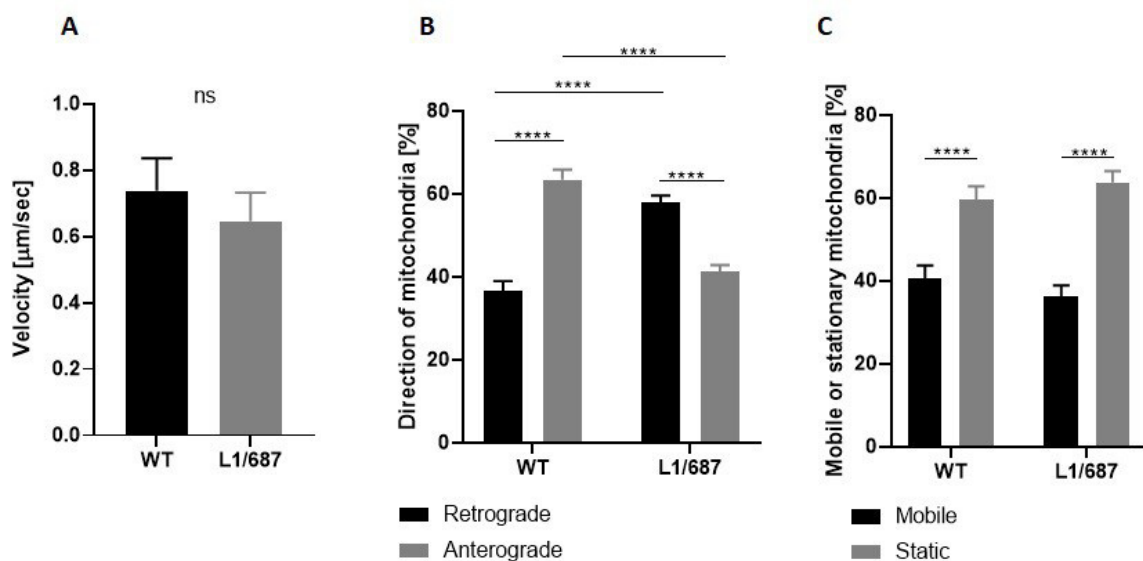
Figure 4.16: Mitochondrial motility and mobility in wild-type and L1/687 cerebellar granule neurons. Cerebellar neurons from 7-day-old male wild-type and L1/687 littermates were plated on 22 μm coverslips coated with PLL and cultured for two to three days in medium with 5% horse serum. Cells were then stained with 50 nM MitoTracker for 30 minutes at 37°C. The medium was replaced with fresh serum-free medium and cells were analyzed every 2 seconds for 5 minutes. A) Motility of MitoTracker-labeled mitochondria in wild-type and L1/687 neurons is similar. B) Percentage of anterograde and retrograde moving mitochondria in wild-type and L1/687 neurons. The number of mitochondria moving in the retrograde direction is higher in L1/687 neurons. C) Analysis of mobile and static mitochondria in wild-type and L1/687 neurons showed a higher number of static mitochondria in the transgenic cells. Mean values of three independent experiments and analysis of kymographs of 50 mitochondria in 5–10 neurons per group and experiment are shown. Mean values ± S.E.M. are represented; ****p<0.0001; ns: not significant; unpaired t-test (velocity), two-way ANOVA with Tukey's multiple comparisons test (direction and mobility).

4.5 Histology results

4.5.1 The area of the hippocampus is altered in transgenic mice

For assessing differences in the brain anatomy between wild-type, L1/858-863 and L1/687 mice, brain sections were stained with luxol fast blue and cresyl violet. Luxol fast blue stains the myelin sheaths, cresyl violet stains cell bodies. The hippocampal area was measured by creating a mask around the hippocampal region and quantifying the area of the section. As seen from the representative pictures (Fig. 4.17), the hippocampus shows diffused cells in the CA3 region of L1/858-863 mice compared to the CA3 region of L1+/y mice. The layers in the hippocampus in the transgenic mice are not as compact as in the wild-type mice and more dispersion is observed. This could be due to a migration problem of the cells or in compaction of the layers of the hippocampus.
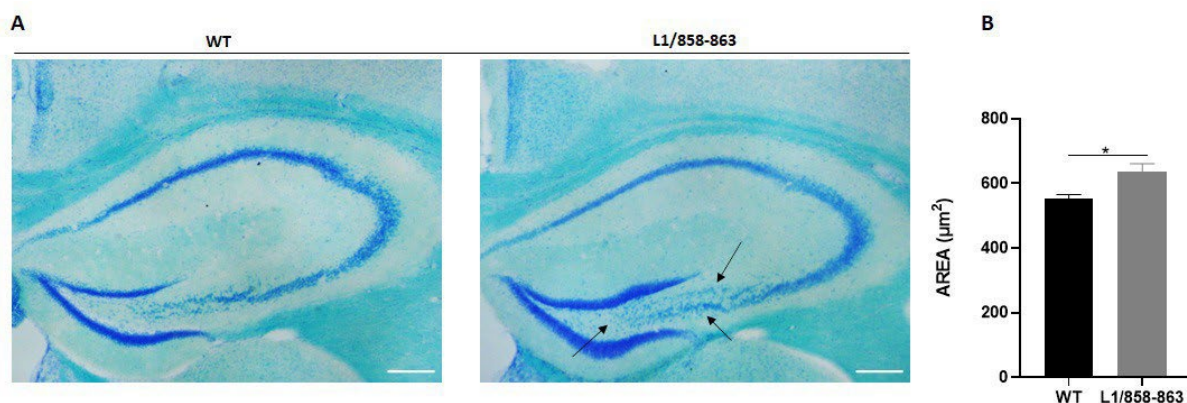
Figure 4.17: L1/858-863 male mice display a larger hippocampal area. Luxol fast blue staining of coronal sections from adult male L1+/y and L1/858-863 mice was performed and the hippocampal area was determined. A) Representative pictures of coronal brain sections from L1+/y and L1/858-863 mice (5- to 6-month-old). Magnification 6.3x. B) Quantification of the area of the hippocampus was performed. The area of the hippocampus is significantly larger in transgenic mice compared to wild-type mice (n=3). Scale bars, 100 μm. Bars represent ± S.E.M. *p<0.005; unpaired t-test.

For the L1/687 mice, the analysis did not reveal any differences in the area of the hippocampus (Fig. 4.18).
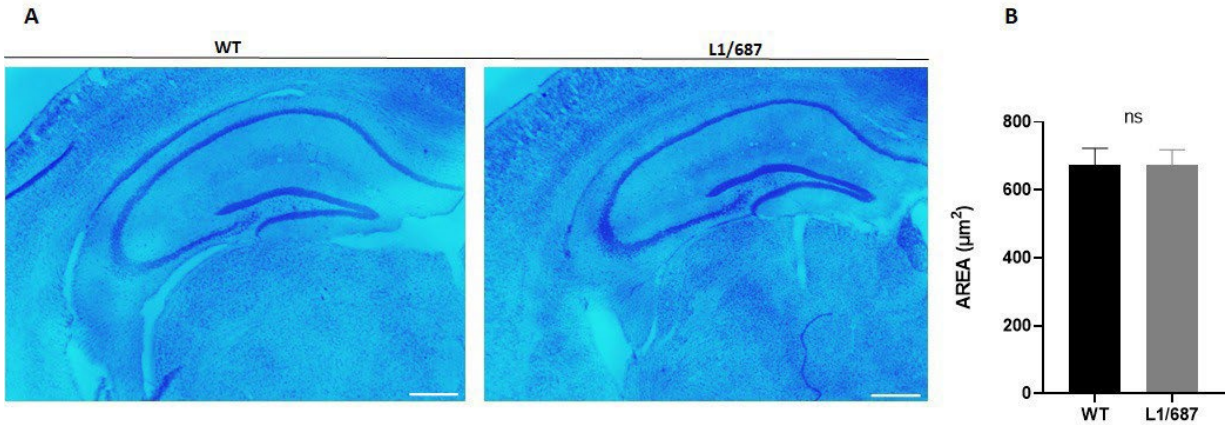
Figure 4.18: L1/687 male mice have a normal hippocampal area. Luxol fast blue staining of coronal sections from adult male L1+/y and L1/687 mice was performed and the hippocampal area was determined. A) Representative pictures of coronal brain sections from L1+/y and L1/687 mice (5- to 6-month-old). Magnification 6.3x. B) area of the hippocampus is similar between wild-type and transgenic mice (n=3). Error bars represent mean ± S.E.M; unpaired t-test; ns: not significant.

4.6   Behavioral studies

To better understand the role of L1 and in particular its L1-70 fragment in brain functions, different behavioral experiments were conducted using the L1/687 line. Previous motor experiments were conducted with wild-type and L1-deficient littermate mice [40], indicating that in L1-deficient mice motor coordination and learning memory were impaired.

Motor tests, together with behavioral experiments used to determine anxiety, circadian activity and sociability, were here performed using wild-type and L1/687 mice lacking the L1-70 fragment. Behavioral experiments were also performed on the L1/858- 863 line and analyzed by Ludovica Congiu (Senior Gruppe Biosynthese Neuraler Strukturen, ZMNH, UKE, Hamburg)

4.6.1   Open field

The open field (OF) is the most common test used to evaluate anxious-like behavior. Mice, both females and males, were recorded for 30 minutes and different parameters were analyzed: time spent in the center zone, distance from the walls, distance moved, time and speed, moving and not moving time. The total distance traveled in all 30 minutes was not different between transgenic male and female mice and wild-type (Fig. 4.19 A). The exploration of the wild-type and L1/687 males in the arena was not different when analyzing the first 15 minutes (Fig. 4.19 B). Whilst the analysis of the open field test with the wild-type and L1/687 females showed that the transgenic mice move a larger distance in the arena in the first 15 minutes (Fig. 4.19 B).
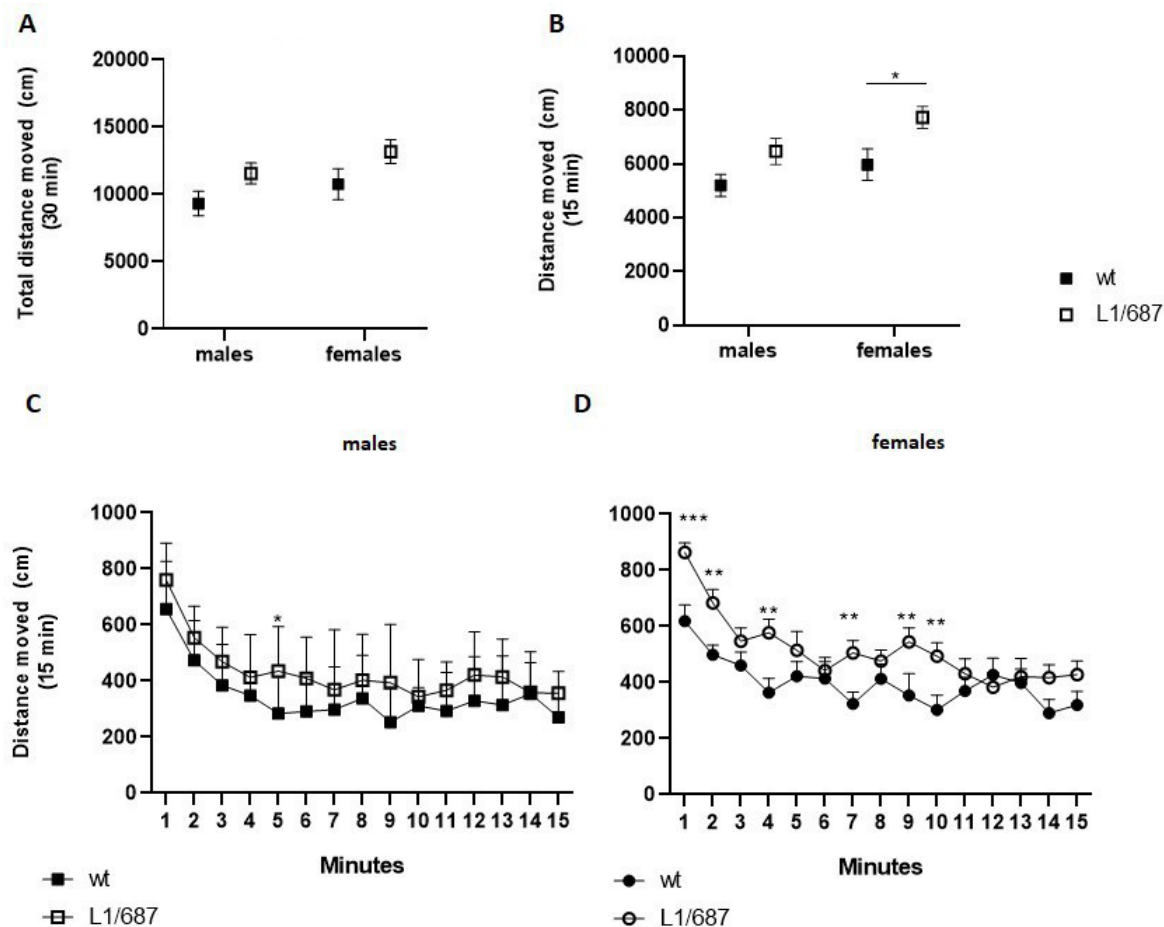
Figure 4.19: Total distance moved in the open field of wild-type and L1/687 males and females. Wild-type and L1/687 male and female mice were placed in the open field and the mice were left to move freely for 30 minutes. A) There was no significant difference in the distance moved in the overall 30 minutes of the test between wild-type and L1/687 male and female mice. B) In the first 15 minutes of the trial there was no significant difference in the ambulation between wild-type and transgenic male mice (p=0.06), while female transgenic mice moved more compared to the female wild-type mice. C) Line plot shows the distance moved (cm) in the first 15 minutes in the open field of male wild-type and L1/687. D) Line plot of wild-type and L1/687 female mice in the first 15 minutes. Mean values ± S.E.M. are represented in all the graphs; n=10 males and n=9 females per genotype; two-way and three-way ANOVA and Bonferroni Post Hoc Test; *p<0.05; **p<0.01; ***p<0.0001.

In the first 5 minutes the transgenic mice showed higher distances traveled compared to the wild-type mice (Fig. 4.20 A). Male and female L1/687 mice moved and explored more compared to wild-type littermates, indicated by the higher distance traveled in the arena in particular in the first five minutes of exploration. This is coherent with the exploration pattern of mice that is generally higher in the first minutes of the test. Moreover, in the first five minutes of the test the mean velocity was significantly higher in L1/687 male and female mice, compared to their wild-type littermates (Fig. 4.20 B).
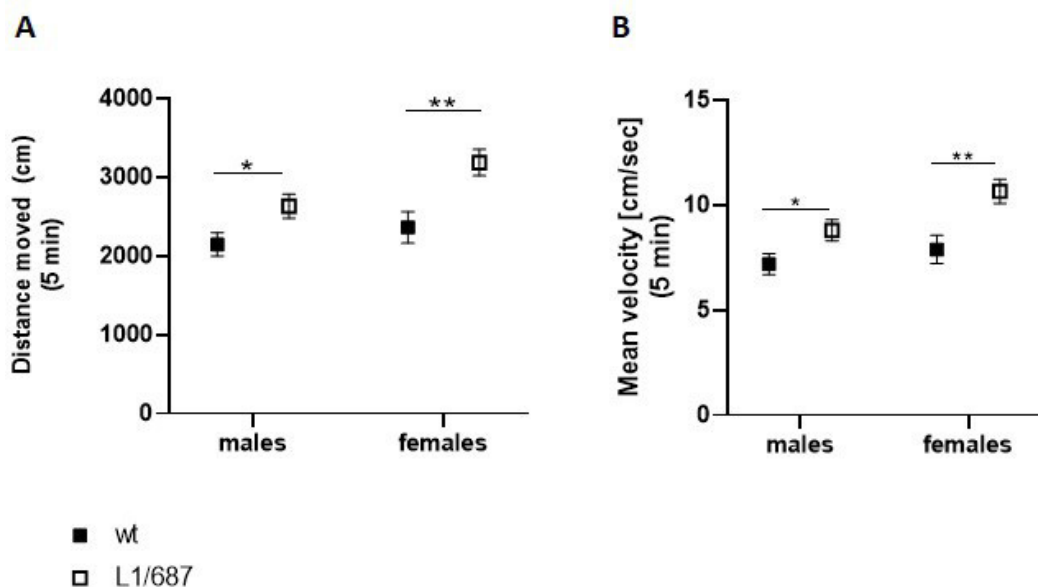
Figure 4.20: Distance moved in the open field of wild-type and L1/687 males and females and velocity. Wild-type and L1/687 male and female mice were placed in the open field and the distance moved and the velocity was analyzed. A) In the first 5 minutes of the test male L1/687 mice moved more compared to the wild-type littermates. The difference in distance moved between female wild-type and L1/687 mice was higher in the first 5 minutes of the test. B) In the first five minutes of the test L1/687 male and female mice had higher mean velocity compared to wild-type mice. Mean values ± S.E.M. are represented in all the graphs; n=10 males and n=9 females per genotype; two-way ANOVA and Bonferroni Post Hoc Test; *p<0.05.

4.6.2 Elevated plus maze

The analysis of the elevated plus maze with wild-type and L1/687 males and female mice highlighted that the wild-type males showed more immobility events and spent more time in an immobile status compared to the L1/687 males (Fig. 4.21 A, B). The immobility status of the wild-type mice in the elevated plus maze, combined with the distance moved in the open field, is an indication of higher locomotor activity and exploratory behavior in the transgenic mice. The females instead, showed no significant difference in immobility time but the wild-type females showed more stretched-attend postures, characterized by the elongation of the forepart of the body forward while the animal keeps a relatively safe distance from a possible threat which occurs during risk assessment [142], compared to the L1/687 females (Fig. 4.21 C).
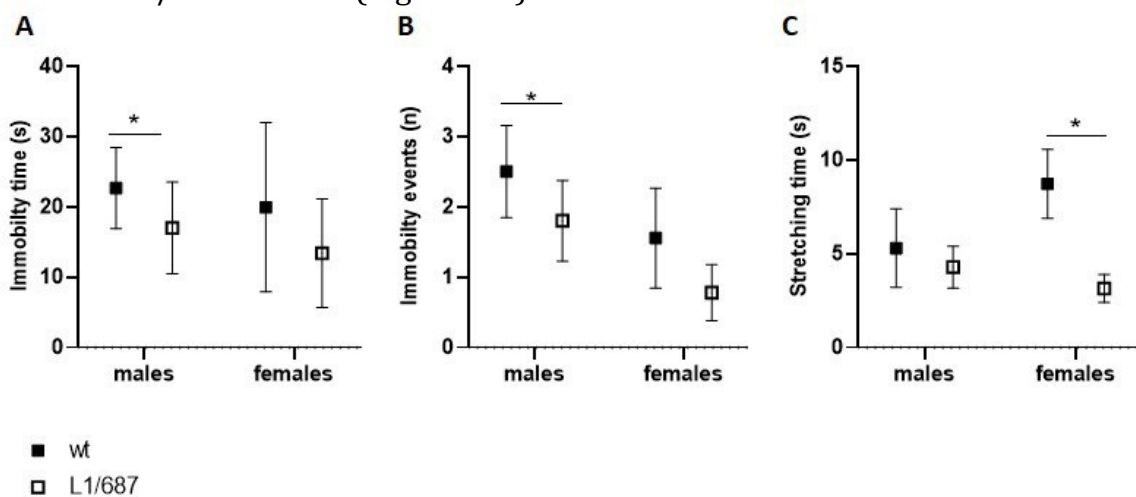
Figure 4.21: Elevated plus maze results from wild-type and L1/687 male and female mice. Mice were placed in the center of the elevated plus maze and their movements were recorded for 5 minutes. A) Male wild-type mice showed higher numbers of immobility events compared to male L1/687 mice, while no difference was seen in the immobility events in female mice. B) Compared to the male L1/687 mice, the L1 wild-type males spent more time in an immobile status while no difference in the immobility time was observed in the females. C) No difference in the stretching was observed for male wild-type and L1/687 transgenic mice. The L1/687 female mice showed a lower number of stretching compared to their wild-type littermates. N=10 males and n=9 females per genotype, Mean ± S.E.M. are represented in all the graphs; two-way ANOVA and Bonferroni Post Hoc Test; $*p<0.05$

There was no effect of the genotype in parameters observed as time and number of entrances in the open and closed arms (Fig. 4.22) and for other parameters as self-grooming and head dips (data not shown).
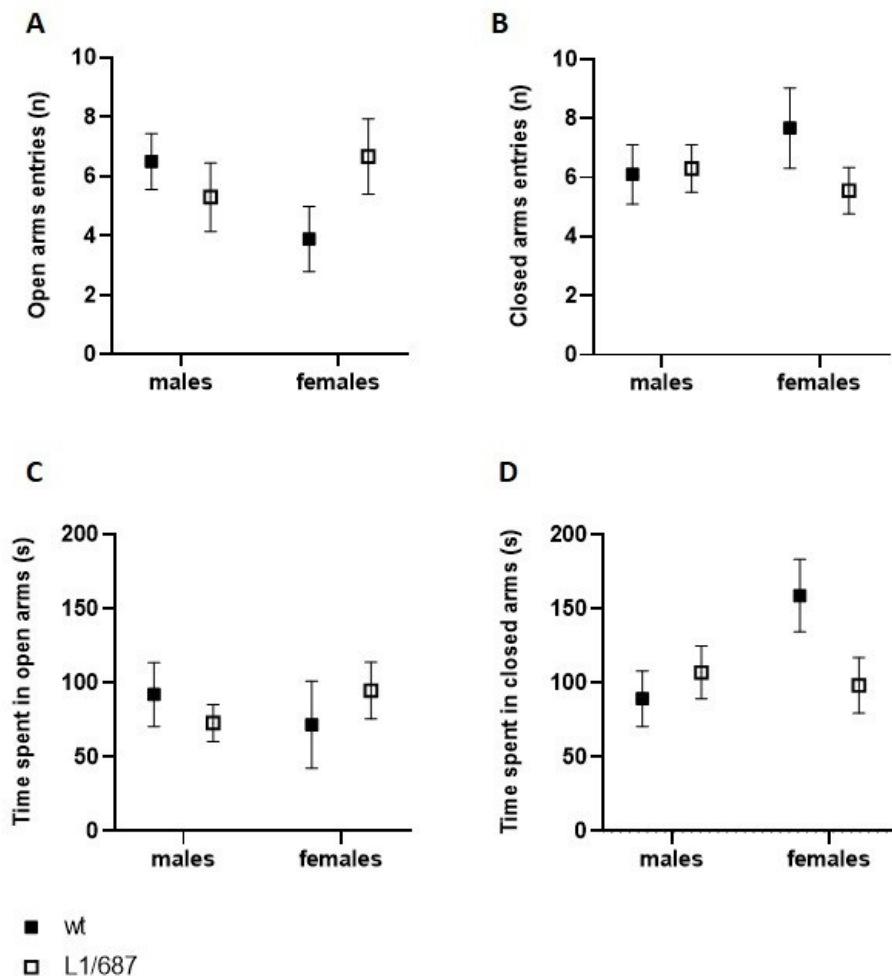
Figure 4.22: Elevated plus maze results from wild-type and L1/687 mice, males and females. Mice were subjected to the elevated plus maze and number of entrances into the open and closed arms and time in both arms were analyzed. There was no significant difference between genotypes in the number of entrances in the open (A) and closed arms (B). No difference between wild-type and L1/687 mice was detected in the time spent in the open (C) and closed arms (D) N=10 males and n=9 females per genotype. Mean values ± S.E.M. are represented in all the graphs; two-way ANOVA and Bonferroni Post Hoc Test.

4.6.3 Marble burying test

The marble burying test was conducted as additional test to evaluate anxiety-like behavior and behaviors seen in obsessive-compulsive disorders (OCDs) and autism-spectrum disorders (ASDs) [137]. The analysis of this test did not show a difference between the number of marbles buried by wild-type and L1/687 mice, males and females (Fig. 4.23)
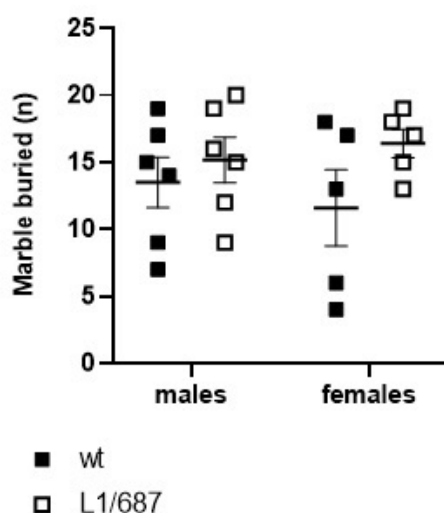
Figure 4.23: Male and female L1/687 mice showed no compulsive-like behavior in the marble burying test Wild-type and L1/687 mice were subjected to the marble burying test and the number of marbles buried was quantified and analyzed. There was no significant difference in the number of marbles buried between wild-type and L1/687 males and females. N=6 males and n=5 females per genotype. Mean values ± S.E.M. single values are represented in all the graphs; two-way ANOVA and Bonferroni Post Hoc Test.

4.6.4 Home cage activity

To investigate the overall spontaneous activity level of wild-type and L1/687 mice, the activity of mice was recorded in the home cage for 24 hours. The spontaneous activity of 5-month-old mice in their home cage was observed with an interval of 4 min (15 samples/hour) and 3 days after each mouse was placed in a fresh home cage alone. The analysis of the home cage activity was done considering two time frames:

-Dark phase (from 7:00 am to 7:00 pm) when the red light is on.

-Light phase (7:00 pm to 7:00 am) when the lights are on. As shown in the Figure 4.24, male and female L1/687 mice were more active in the dark phase as well as the wild-type mice. This result showed that there is no alteration in the circadian rhythm in the transgenic mice. Moreover, the activity of the transgenic female mice during the dark phase was significantly higher compared to the female wild-type mice, indicating more active behavior of the female L1/687 mice (Fig. 4.24).
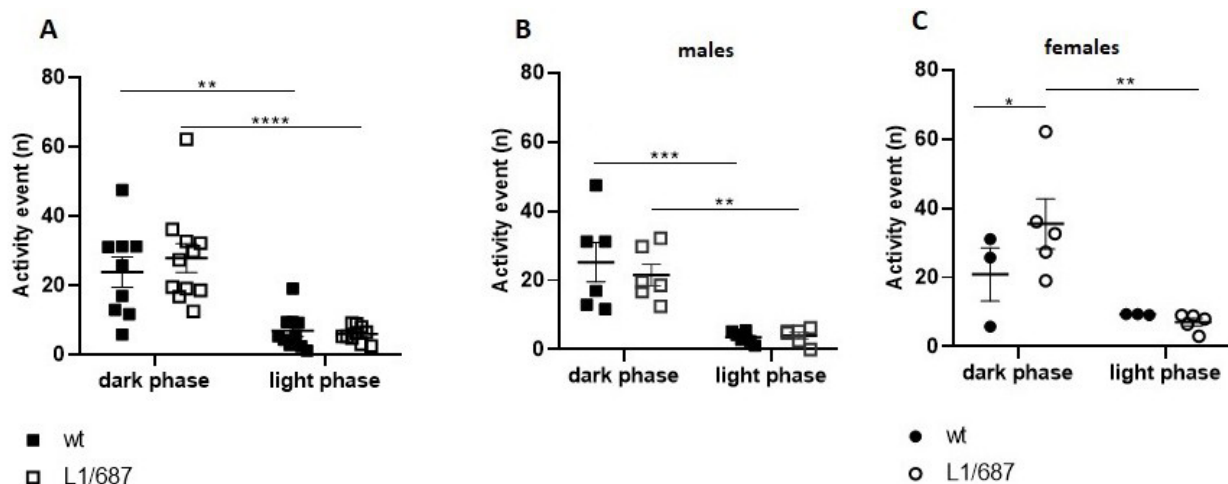
Figure 4.24: Home cage activity of wild-type and L1/687 mice. Home cage activity was recorded for 24 h during the dark and light phase. A) All mice showed higher activity during the dark phase. B) Male mice did not show differences in activity due to the genotype in the dark or light phase, but the activity of wild-type and L1/687 mice in the dark phase was significantly higher compared to the light phase. C) Female wild-type and L1/687 mice showed a significant difference in the activity in the dark phase, with significantly higher activity of the female L1/687 mice compared to the activity of the female wild-type mice. Besides, a higher activity of female wild-type and L1/687 mice in the dark phase compared to the light phase was found. N=6 males and n=3 (WT) and 5 (L1/687) females per genotype; three-way and two-way ANOVA with Tukey's multiple comparisons test and Bonferroni Post Hoc Test. Mean values ± S.E.M. single values are represented in all the graphs; *p<0.05, **p<0.01, ***p<0.001, ****p<0.0001.

4.6.5 Social interaction

As a next step the social interaction was analyzed. In this test the time spent next to a familiar or unfamiliar mouse, presented in a cup at opposite corners of the arena, is measured as an indicator for interest in social novelty. In social interactions, information processing is known to be strongly biased by emotional states, contexts and expectations and these could differ between wild-type mice and mice lacking L1-70.

As shown in Fig. 4.25 (A and B) both wild-type and L1/687 male mice were more distant from the familiar mouse during the first 10 minutes while there was no difference in the L1/687 male mice for the overall 20 minutes of the test. The wild-type females instead (Fig. 4.25 C, D) showed a significant larger distance from the familiar mouse in the first 10 minutes and in all 20 minutes of test whereas this parameter was only significantly larger for the total 20 minutes for the L1/687 females.
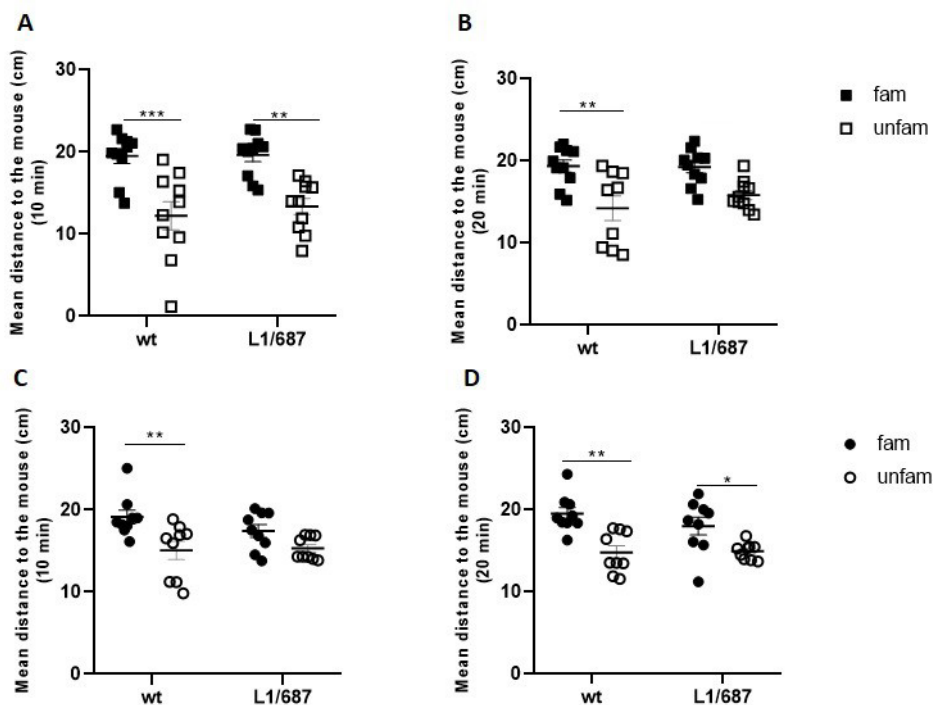
Figure 4.25: Wild-type and L1/687 mice stay closer to an unfamiliar mouse in the social interaction test. Male and female wild-type and transgenic mice were subjected to the social interaction test and distances to unfamiliar and familiar mice were determined. A) Male wild-type and L1/687 mice were more distant from the familiar mouse compared to the unfamiliar mouse in the first 10 minutes of test. B) This difference was present in all 20 minutes of the test for the male wild-type mice while no significant difference was found for the male L1/687 mice when comparing all 20 minutes. C) Female wild-type mice stayed closer to the unfamiliar mouse in the first 10 minutes of test, whereas the L1/687 females did not show a preference D) During the 20 minutes of the test wild-type and L1/687 female mice showed a preference for the unfamiliar mouse. Mean values ± S.E.M and single values are represented in all the graphs; n= 10 males and n=9 females per genotype; *p<0.05, **p<0.01, ***p<0.001; two-way ANOVA with Tukey's multiple comparisons test.

When the time and the frequency spent near the familiar and unfamiliar mouse were analyzed, no effect of the genotype was found. Males, both wild-type and L1/687, spent more time at the unfamiliar mouse compared to the familiar mouse. Also the frequency of visits to the familiar/unfamiliar mouse showed a higher number of visits to the unfamiliar mouse in both genotypes (Fig. 4.26 A, B). The analysis of the females instead showed a higher time spent at the unfamiliar mouse compared to the familiar mouse for the wild-type mice, but not in the L1/687 female mice. The frequency of the visits at the familiar and unfamiliar mouse was similar between wild-type and L1/687 females (Fig. 4.26 C, D).
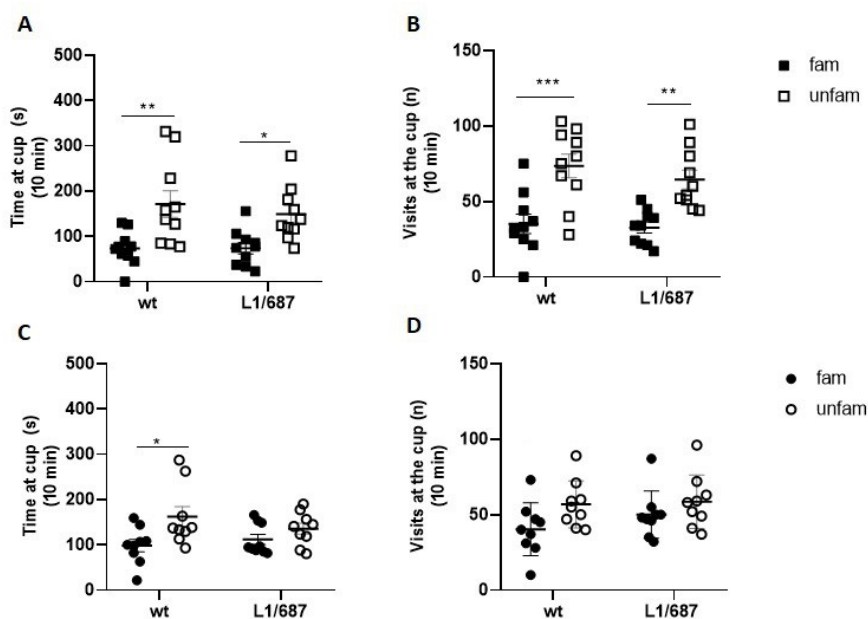
Figure 4.26: Male wild-type and L1/687mice spend more time close to the unfamiliar mouse in the social interaction test. Male and female wild-type and transgenic mice were subjected to the social interaction test and the time spent near each mouse and the frequency of the visits were analyzed. A) Male wild-type and L1/687 mice spent more time near the unfamiliar mouse compared to the familiar one. B) Also the frequency of the visits was higher for the unfamiliar mouse compared to the familiar mouse. C) Wild-type females also spent a longer time with the unfamiliar mouse while there was no difference for the L1/687 females. D) No difference was found for the frequency of visits at the familiar or unfamiliar mouse for the wild-type and L1/687 females. Mean values ± S.E.M. and single values are represented in all the graphs; n= 10 males and n=9 females per genotype; *p<0.05, **p<0.01, ***p<0.001; two-way ANOVA, Tukey's multiple comparisons test.

Next, the time spent in the arena containing the familiar or unfamiliar mouse was analyzed and no significant difference between genotypes was detected. Male mice, both wild-type and transgenic, spent significantly more time in the chamber with the unfamiliar mouse compared to the familiar (Fig. 4.27 A). Female wild-type mice showed a longer time spent in the arena containing the unfamiliar mouse but no preference was found for the L1/687 female mice (Fig. 4.27 B).
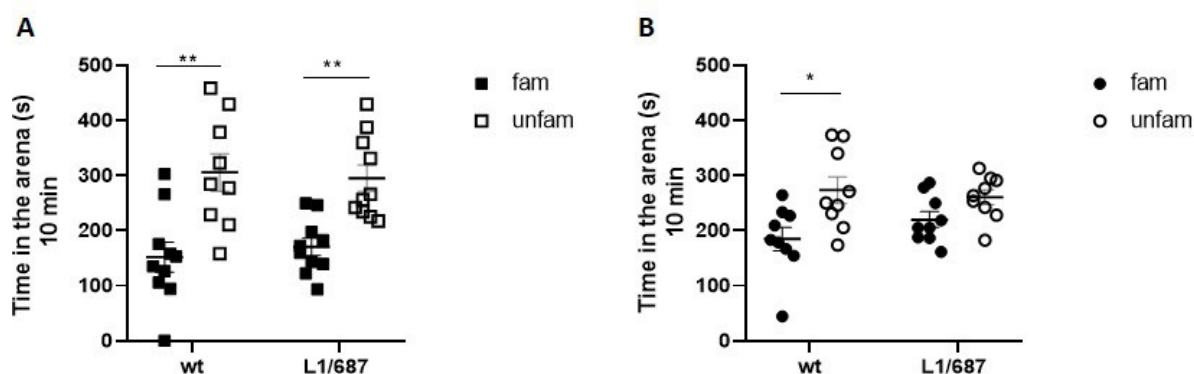
Figure 4.27: Time spent in the arena next to the familiar and unfamiliar mouse. Wild-type and L1/687 male and female mice were subjected to social interaction and the time spent in each side of the arena was analyzed. A) Male wild-type and L1/687 mice spent more time in the area containing the unfamiliar mouse compared to area with the familiar mouse. B) Wild-type females also showed longer time spent in the arena with the unfamiliar mouse compared to the familiar mouse, while there was no preference for the L1/687 females. Mean values ± S.E.M. and single values are represented in all the graphs; n= 10 males and n=9 females per genotype; *p<0.05, **p<0.01; ns: not significant; two-way ANOVA, Tukey's multiple comparisons test.

4.6.6 Motor activity

To investigate motor coordination and motor learning the rotarod test, beam walking test and pole test were performed. For the rotarod test, it was previously shown that wild-type mice exhibit motor learning, whereas L1-deficient mice did not show any improvement during subsequent trials. Moreover, L1-deficient mice transduced with adeno-associated virus coding for wild-type L1 performed as well as the wild-type mice, in contrast to L1-deficient mice transduced with virus coding for mutated L1 (L1/687) which did not improve their performance [40]. Here, the rotarod test was performed using 5-month-old wild-type and L1/687 mice, males and females. Male wild-type and L1/687 mice showed the same latency to fall and were spending a similar time on the rod. In addition, male wild-type and L1/687 mice also showed an improvement in their performance between the first and last trial (Fig. 4.28 A) Female wild-type and L1/687 mice showed a similar latency to fall, but no improvement of their performance, with no differences between the first and last trial (Fig. 4.28 B).
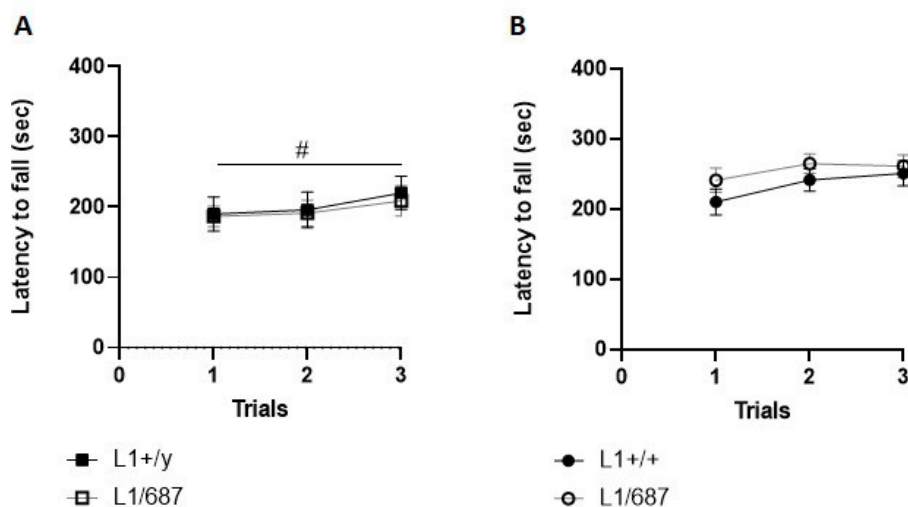
Figure 4.28: Rotarod test performed in 3 trials with 5-month-old wild-type and L1/687 mice. Mice were subjected to the rotarod and speed was accelerated from 4 to 40 rpm in 5 minutes. A) Male wild-type and L1/687 mice showed a similar latency to fall from the rod as well as motor learning. B) Female wild-type and L1/687 mice also showed a similar latency to fall but no motor learning. N=10 males and n=9 females per genotype; Mean values ± S.E.M. are shown. p<0.05; two-way ANOVA, Tukey's multiple comparisons test.

The rotarod performance was additionally executed with older mice (6- to 8-month-old). In this case wild-type male mice had a higher latency to fall compared to the male L1/687 mice and both genotypes did not show an improvement in their performance in subsequent trials. However, the latency to fall from the rod was significantly different between wild-type and L1/687 mice in each trial performed, with an overall effect of the genotype on the performance (Fig. 4.29 A). Female wild-type mice showed a lower latency to fall compared to the L1/687 females, although both wild-type and transgenic female mice did not show an improvement and learning during sequential trials. However, an effect of the genotype on the overall performance of female mice was found (Fig. 4.29 B).

A

B
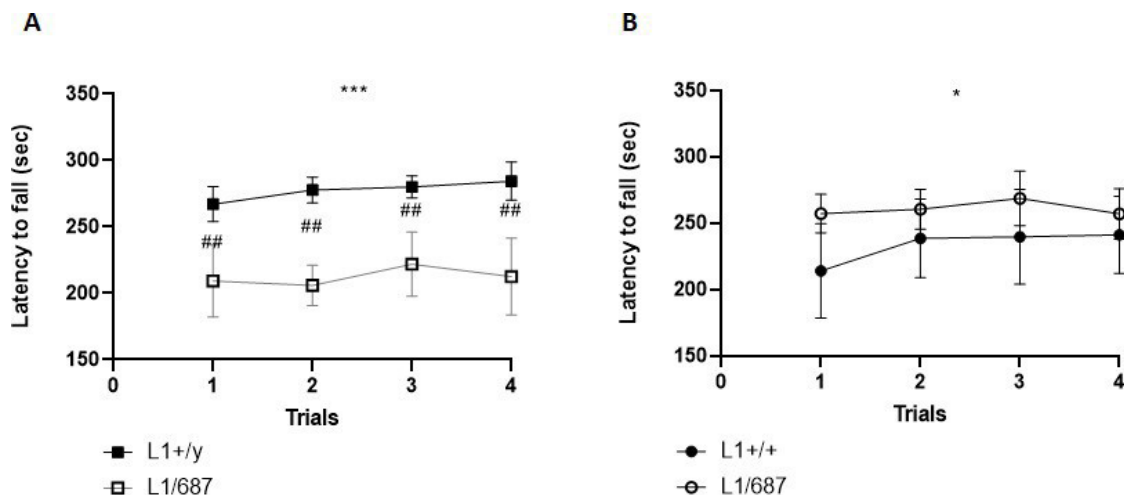
Figure 4.29: **Motor learning and motor coordination are impaired in 6- to 8-month-old L1/687 mice.** Rotarod test was performed with male and female wild-type and L1/687 mice. A) Male L1/687 mice showed a significant lower latency to fall from the rod compared to their wild-type littermates in each trial (##). The genotype had a significant effect on the performance (*** $p<0.001$). B) Wild-type female mice have a lower latency to fall compared to the female L1/687 mice, even though both genotypes did not show an improvement during subsequent trials. Also in this case, the genotype had an effect on the outcome of the test (*$p<0.05$). Mean values ± S.E.M. are shown. N=10 males and n=9 females per genotype; ##$p<0.01$; two-way ANOVA with Tukey's multiple comparisons test.

In addition to the rotarod test, the pole test was also conducted with 5-month-old male and female wild-type and L1/687 transgenic mice. The performance in the pole test did not show any difference or impairment in motor coordination of L1/687 transgenic mice (Fig. 4.30).
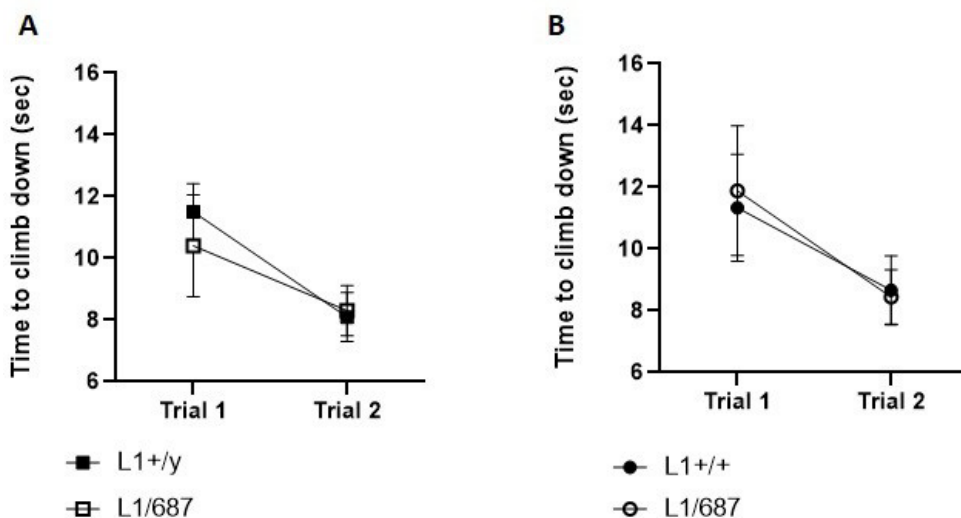
Figure 4.30: Pole test with male and female wild-type and L1/687 mice. There is no difference in the performance between wild-type and L1/687 male (A) and female mice (B). N= 10 males and n=9 females per genotype; Mean values ± S.E.M. are shown; two-way ANOVA, Tukey's multiple comparisons test.

To exclude that the performance of the transgenic mice on the rotarod was due to a physical impairment, the beam walking test was performed to analyze two parameters:

-Foot-base angle (FBA) measured when the ipsilateral foot has toe-off position and the contralateral paw is in a stance position. The angle is formed by the line symmetrically dividing the sole into two halves and the horizontal line [143];

-Heel tail angle (HTA) formed by the lines connecting the heels with a sagittal point on the animal's body corresponding to the external urethral orifice. The angle is measured at the position of the contralateral extremity when the swinging paw passes the stance-phase paw (maximal altitude of the heel) with the sole surface parallel to the transverse plane [144].

As shown in the Figure 4.31, L1/687 mice did not show an impairment in the plantar stepping abilities compared to the wild-type mice.
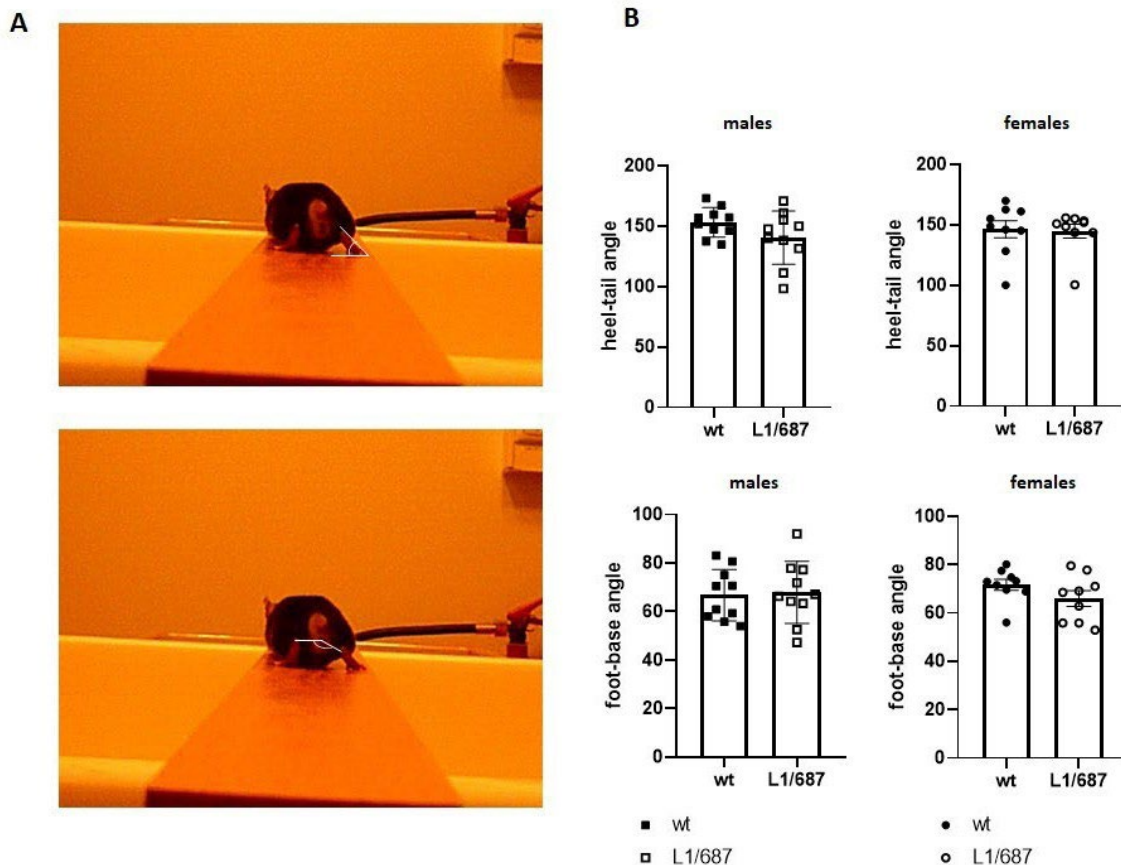
Figure 4.31: L1/687 mice show normal plantar stepping abilities. Motor abilities were determined in L1/687 and wild-type littermate mice using the beam walking test and FBA and HTA angles were determined. A) Images of mice crossing the beam walking and recorded from behind with the foot-base angle and heal-tail angle indicated. B) There was no difference in the locomotion between wild-type and L1/687 male and female mice and the angles of the paws. N=10 males and n=9 females; mean values + S.E.M. are shown; Mann–Whitney test.

C H A P T E R 5

DISCUSSION

The present study investigated three functional aspects of the L1-70 fragment:
1) role of the L1-70 fragment in mitochondrial dynamics and how the absence of this fragment affects mitochondrial processes and functions;
2) the influence of the L1-70 fragment on development and brain morphology;
3) the influence of the L1-70 fragment on mouse behavior: behavioral studies to characterize the transgenic mouse line L1/687 lacking L1-70 were performed.

5.1   Mitochondrial functions affected by absence of L1-70

5.1.1   L1 is present at the surface of mitochondria and interacts with mitochondrial proteins involved in mitophagy pathways

Previous studies conducted in our lab showed that a fragment of L1, L1-70, is imported into mitochondria and co-immunoprecipitation using mitochondrial lysates from wild-type mouse brains indicated that L1-70 interacts with Miro and Drp1 which are involved in mitochondrial process of motility and fission, respectively [58]. Both Drp1 and Miro are proteins located on the outer membrane of mitochondria. Analyzing immune-labeled mitochondria in a flow cytometer, I showed that L1 is present on the surface of mitochondria. Isolated mitochondria from wild-type mouse brains were immunopositive for L1 and the mitochondria marker protein TOM20, while in isolated mitochondria from L1-deficient mouse brains, immunopositive signals were just detected for TOM20. This result indicates that the L1-70 fragment is present at the surface of mitochondria, probably at the outer mitochondrial membrane.

 A previous study showed that the localization of the mitophagy marker protein LC3 on mitochondria was enhanced in HEK293 cells, which lack the L1 protein compared to HEK293 cells transduced to express L1. When HEK293 cells were transduced with a mutated form of L1 which does not allow generation of L1-70, the level of LC3 on mitochondria was enhanced in cells expressing the mutated L1 when compared to cells expressing wild-type L1 [147]. In addition, it has been shown that cerebellar granule cells from L1-deficient mice or lacking L1-70 have a more depolarized membrane potential compared to wild-type cells [58].

Since the absence of L1 leads to impaired mitochondria [58], and since literature data show that fragmentation or fission of mitochondria with impaired mitochondrial membrane potential precedes mitophagy [110], I investigated whether L1 interacts with proteins that are involved in the mitophagy process such as LC3, PINK1 and parkin [109], and whether L1 plays a role in mitophagy.

Many proteins interacting with LC3 contain a LIR domain which mediates the binding to LC3 [125]. L1 contains two LIR domains, one in the extracellular domain and one in the ICD. Since LC3 was suggested to interact with L1-70 and this fragment contains a LIR domain in the ICD I investigated if the L1-ICD binds to LC3 and if the LIR domain in the L1-ICD is involved in this interaction. By ELISA I showed that the L1-ICD binds directly to LC3 and that the mutation of the LIR domain does not affect the binding between LC3 and the L1-ICD. These results are an indication that the interaction between these proteins does not depend on the LIR motif of the intracellular domain of L1.

The LIR domain was originally mapped on the p62 protein and it has been shown that this motif is evolutionary conserved [148]. The canonical LIR domain consists of a $[W/F/Y]_0$-X_1-X_2-$[L/V/I]_3$ sequence with highly conserved positions at the X_0 and X_3, which are often acidic residues such as Asp, Glu, Ser or Thr residues that can be phosphorylated [148]. Autophagy receptors bind through the LIR motif to LC3 at the LIR docking site (LDS) formed by two hydrophobic pockets (HP1 and HP2) [149]. The interaction between LC3 and the autophagy receptors is mainly, and presumably, to scaffold and stabilize the autophagy complex to the growing phagophore [148] and is regulated by phosphorylation in different proteins such as BNIP3, FUNDC1 or Nix [126].

Although studies showed that the LIR motif is highly conserved, from yeast to mammals, it has been proven that not all the LIR motifs have the canonical sequence W/F/Y. Other types of bindings are described in the literature, as the one between the mitochondrial

protein cardiolipin, which binds to LC3 in a LIR–LDS independent manner because of the lack of the LIR sequence [148]. In addition, the binding between autophagy proteins and LC3 is highly specific and varies according to LC3 isoforms (MAP1-LC3A, B and C) [148, 120], for example the calcium-binding and coiled-coil domain-containing protein 2 (CALCOCO2$_2$) which binds exclusively to LC3C [148]. Moreover, the interaction of autophagy receptors and LC3 subfamily proteins probably does not only depend on the LIR sequence. A previous study showed the presence of short linear motifs, or the minimal essential region (MER), around the LIR domain of the Nix protein, which comprises three contiguous hydrophobic amino acid residues delimited by charged residues and has a role to stabilize the interaction [150]. The truncation of the LIR domain of Nix in mouse embryonic fibroblast causes a slight change in the activity of the protein, while the removal of the MER causes loss of activity [120].

Basing on these literature data it is possible that the binding between the L1-ICD and LC3 was not affected by the mutation of the LIR domain because of the presence of other specific binding residues that were not changed or because the specificity of the interaction of the LIR domain of the L1-ICD changes with different isoforms of the LC3 subfamily. It is also possible that, as for other proteins, the binding between L1 and LC3 is regulated by post-translation modifications which were also shown to increase or decrease the affinity between the LIR motif and the LDS. Moreover, L1 also contains a LIR domain in the extracellular domain, hence, an interaction between the extracellular LIR motif of L1 and LC3 could be further studied.

The interaction between L1 and LC3 was further investigated and confirmed by proximity ligation assay in cerebellar granule cells. Neurons from wild-type mice showed a positive signal indicating the close proximity of L1 with LC3. Signals showing this close contact were not detected in neurons from L1-deficient mice. The hypothesis that interaction between L1 and LC3 is probably

mediated by the L1-70 fragment was confirmed by my experiments, since in neurons from L1/858-863 and L1/687 mice, which lack the L1-70 fragment, no positive signals were detected indicating that the interaction in wild-type cerebellar granule cells depended on the L1-70 fragment. The western blot analysis of LC3 protein levels on isolated mitochondria from L1-deficient mice and wild-type mice showed similar amounts for both genotypes, indicating that L1 is not involved in the expression of LC3. In 6- to 11-day-old L1/858-863 and L1/687 mice, expressing full-length L1 but lacking the L1-70 fragment, levels of LC3 on isolated mitochondria did not differ to levels of LC3 on mitochondria of their respective wild-type littermates. The analysis of levels of LC3 on mitochondria from adult mice (5- to 6-month-old) determined by western blot revealed that LC3 levels were higher on mitochondria from L1/858-863 male mice compared to wild-type mice, while on mitochondria from L1/687 male mice, levels of LC3 were lower than LC3 levels on mitochondria of wild-type littermates. The difference in levels of LC3 on mitochondria between early postnatal and adult mice could be explained with different levels of L1 during postnatal development and in adulthood [37], whilst the opposite tendency in transgenic mice could be due to a different genetic background. The difference compared with the L1-deficient mice could be attributed to the fact that mitophagy does not happen just through one pathway, but also through different mechanisms that depend on the cause of the damage (e.g. hypoxia, depolarization of the mitochondrial membrane potential, starvation or ROS production [112]). Considering all this data, and knowing that L1-70 is imported into mitochondria [58], we can speculate that L1 binds to LC3 on the surface of mitochondria, maybe after an externalization process from inside the mitochondria, operating as cargo for LC3 to bind impaired mitochondria, but is not directly or indirectly influencing the expression of LC3.

In my studies I could show that levels of BNIP3, which is another mitophagy marker, are higher on the surface of mitochondria of L1-deficient mice compared to wild-type mice. BNIP3 belongs to the BH3-only subfamily of the Bcl-2 proteins and is formed by a single transmembrane domain inserted in the OMM, a cytoplasmatic domain which comprises the LIR domain and 10 amino acid residues protruding in the intermembrane space. Under normal conditions BNIP3 resides in the cytosol or is loosely attached to the OMM and the ER [151]. When apoptosis is induced, BNIP3 undergoes translocation from the cytosol to mitochondria, where it is inserted into the outer membrane to initiate mitochondrial mitophagy. The BH3 domain confers to BNIP3's pro-apoptotic functions, inducing the opening of mitochondrial permeability transition pores (MPT), disrupting the electron gradient across the inner mitochondrial membrane [126]. This leads to production of ROS, reduction of mitochondrial respiration and ATP levels [151], disruption of the fission/fusion balance and loss mitochondrial membrane potential ending with cell death [152].

Literature data show that dissipation of the mitochondrial membrane potential, as seen in neurons lacking the L1-70 fragment and neurons from L1-deficient mice [58], has been implicated in starting the necrotic and apoptotic neuronal cell death through the release of pro-apoptotic factors in the cytosol as cytochrome c and Ca^2+ [153]. Interestingly, it has been shown that overexpression of BNIP3 in mouse embryonic fibroblast cells reduces levels of proteins of the mitochondrial complex I and V involved in the mitochondrial respiration, which leads to reduced mitochondrial oxidative phosphorylation and cellular ATP production [154]. I hypothesize that the depolarization of the mitochondrial membrane potential of neurons of L1-deficient mice can activate the pro-apoptosis signal of BNIP3 that is transferred on damaged mitochondria to start the mitophagy process.

In the course of this thesis, I also showed a possible interaction between full-length L1 and parkin. In cerebellar granule cells from wild-type mice I could show L1 in close proximity to parkin. Interestingly, the levels of Parkin determined by western blot analysis in the cytosol from wild-type and L1-deficient mice were similar, demonstrating that L1 is not involved in Parkin protein expression. Literature data show that L1 plays a role in protection against oxidative stress and enhances neuronal survival [57]. It is worth to note that the PINK1-Parkin pathway is not only activated by an impaired membrane potential, but also high levels of ATP are required for its activation [155]. Whether the interaction of L1-70 with major mitochondrial proteins such as LC3 and parkin is required to balance mitochondrial mitophagy through its multiple pathways to defend cells from oxidative stress and death or if stimulation of L1 signaling cascades is responsible for the neuroprotective effect of L1 needs further investigation.

5.1.2   L1-70 regulates the mitochondrial membrane potential resulting in lower level of ATP

It was previously shown that in cerebellar granule cells from L1-deficient mice the mitochondrial membrane potential was impaired and lower compared to cells from wild-type mice and also the activity of complex I of the electron transport chain was reduced [58]. In addition, co-incubation of mitochondria from L1- deficient mice with the L1-70 fragment enhanced the complex I activity [58]. Similar results were obtained analyzing the mitochondrial membrane potential. Cells lacking L1 or expressing mutated L1, which cannot be cleaved to generate L1-70, had an impaired mitochondrial membrane potential [58]. These results suggested a role of L1, in particular of the L1-70 fragment, in mitochondrial functions. The role of L1 and the L1-70 fragment in regulating the mitochondrial membrane potential was furthered investigated using cerebellar granule cells from L1/858-863 and L1/687 mice. In the present study I could detect that cerebellar granule cells isolated from both transgenic mice

lacking the L1-70 fragment have an impaired membrane potential which is significantly lower compared to that of cerebellar granule cells from wild-type mice. In this study I also evaluated the activity of complex I on isolated mitochondria from wild-type and L1/687 mice. I could detect that the activity of complex I from 6- to 9-day-old L1/687 male mice was not significantly different compared to complex I activity of wild-type littermate mice, with a slight tendency to be lower in L1/687 mice. In adulthood, transgenic and wild-type male mice show similar complex I activities. When mice subjected to behavioral experiments were tested, the complex I activity showed a tendency to be higher in transgenic males compared to the wild-type males while female L1/687 mice showed a reduced activity of the complex I compared to wild-type females.

Mitochondrial functions, in particular the activity of the electron transport chain complexes I and IV, decline with aging in the brain and impairments in mitochondria are linked to development of neuropathologies and age-related disorders [156]. However, the activity of complex I in male mice subjected to behavior tests was slightly higher than the activity of complex I of wild-type male mice. It has been known for long time that exercise and physical activity have beneficial effects on metabolism and mitochondrial function, increasing mitochondria biogenesis and turnover [156, 157]. Data from literature report that behavioral exercise tests increased activity of complex I of mitochondria of brains from 24-month-old mice, which was lower prior to exercises compared to mitochondria from younger mice (4-week-old), without changes in markers for mitochondrial biogenesis [158].

Moreover, another study showed that moderate exercise prevents the decline of the complex I associated with age, increasing the activity of the enzymes of the electron transport chain [156]. We can speculate that the higher activity of the complex I of older male mice is a result of physical activity due to the behavior tests (rotarod and pole test). The analysis of how exercise can affect mitochondria metabolism needs to be evaluated also in female mice to understand the sex differences in mitochondrial function.

In addition, it is possible that the difference in the complex I activity between L1-deficient mice and L1/687 mice is due to different levels of L1 and its expression. In L1-deficient mice all L1 protein and all fragments are missing, while L1/687 mice lack only of the L1-70 fragment but express full-length L1 and other L1 fragments. Besides, levels of L1 change with the age of the mice [37].
Considering the expression of full-length L1 in L1/687 mice, other fragments of the protein can be generated by cleavage and it is possible that other L1 fragments have a role in mitochondrial function involving the complex I, or that L1-70 contributes to the complex I function but its absence does not affect severely its activity, possibly also through a compensatory mechanism.

Complex I is located in the inner mitochondrial membrane with an L-shaped structure that extends into the mitochondrial matrix, which contains different structures including the N-module on the peripheral arm. The N-module is the NADH-oxidizing dehydrogenase module and contains the NADH oxidation site and is formed by the NDUFV2 subunit. It was previously shown that the L1-70 fragment binds to the subunit NDUFV2 and to GAPDH [58]. It has been reported that mutations of the NDUFV2 subunit, which is highly expressed in the developing cerebral cortex, are involved in neuropathology as Parkinson, Alzheimer and schizophrenia [159, 160, 161]. Inhibition of NDUVF2 is reported to affect neuronal migration [162]. Interestingly, neurons which lack the L1-70 fragment exhibit reduced neurite outgrowth and migration [163]. Literature data report that mild deficiencies and reduction (even of just 20%), or conditions of complete inhibition of complex I activity, can cause a depolarization of the mitochondrial membrane potential [153, 164], leading also to a reduction in GAPDH activity [165].
It can be speculated that L1-70 binding to the NDUVF2 subunit of the complex I can contribute to its activity and in the absence of the L1-70 fragment the activity is reduced, but not severely affected, leading to a malfunction of the complex.

Studies report that the mitochondrial membrane potential is susceptible to depolarization after reduced complex I activity, rather than reductions in the activities of complex III and complex IV [153]. Post-mortem studies report that the complex I activity was reduced in the substantia nigra [159] and frontal cortex [160] from homogenates of Parkinson's patients and that depolarization of the mitochondrial membrane potential induces the activation of pro-apoptosis proteins, as BNIP3 [153]. It is likely that the mitochondrial membrane potential is disrupted due to the absence of the L1-70 fragment, affecting mitochondrial functions.

Reduced activity of complex I affects also GAPDH activity, maybe causing a double effect on the mitochondrial complex I and on the ATP levels. In this study I showed that in cerebellar granule cells of L1/687 mice, levels of ATP are lower compared to cells from wild-type mice. This reflects unhealthy mitochondria with impaired ATP generation or higher energy consumption in L1/687 cells lacking the L1-70 fragment. Reduced levels of ATP in L1/687 neurons could result from the decreased mitochondrial membrane potential, which is necessary for the ATP production. Production of ATP in neuronal cells is based mainly on oxidative phosphorylation [166], yet studies have demonstrated that the glucose metabolism, even though is not the primary source of ATP in neurons, is a key regulator for the process. In particular, one study showed that treatment with carbonyl cyanide m-chlorophenyl hydrazone (CCCP), which induces mitochondrial membrane depolarization, caused a drop in ATP levels in HeLa and MEF cells at low glucose concentrations. The same treatment performed under high glucose concentrations restored ATP levels [155]. To maintain glycolytic flux, the NADH produced by GAPDH must be oxidized to further progress in the glycolysis [166]. It has been shown that GAPDH binds to cytochrome c of the complex IV which stabilizes the complex I [167] and GAPDH protein damage results in decreased ATP levels [142]. Moreover the transfer of GAPDH into mitochondria has been linked to the induction of pro-apoptotic mitochondrial membrane permeabilization [165].

Considering that the activity of the ATP synthase in mitochondria from L1-deficient mice was not different from mitochondria of wild-type mice and that the activity of complex I is slightly lower in mitochondria from 6- to 9-day-old mice L1/687, we can hypothesize that lower ATP level in L1/687 neurons is the result of not only decreased membrane potential, but also a defect in the glucose metabolism. It has been recently shown that the complex I activity and ATP production are normal, with enhanced mitochondrial membrane potential in neurons from mice expressing another L1 mutation (D201N), in which the L1-70 fragment is produced [163].
This demonstrates that the absence of L1-70 has a role for the reduced membrane potential and, possibly as consequence, on the ATP production.

5.1.3   Cells lacking L1-70 have enhanced retrograde transport of mitochondria

Distribution of mitochondria in neurons is regulated by specific mechanisms to transport mitochondria to distal areas where ATP and Ca^{2+} are in high demand, such as synapses and axonal branches. Mitochondria move bidirectionally from the cell soma towards terminal areas (anterograde movement) and retrogradely towards the cell soma [94, 93], pause briefly, and move again, frequently changing direction [168]. However, in mature neurons, just a small percentage of axonal mitochondria is motile and the stationary mitochondria serve as energy sources for synaptic activity [168]. Previous studies have shown that in healthy neurons, 60-90% of mitochondria are stationary and 10-40% motile [93]. The balance between motile and stationary mitochondria is necessary for neuronal function and changes quickly in response to alterations in metabolic demands, under stress conditions or when they are impaired. Moreover, mitochondria need to be removed if they become aged or in case of dysfunction [168].

 In this study I investigated if the lack of the L1-70 fragment in cerebellar granule cells from L1/687 mice, affects mitochondrial motility. Analysis of different parameters showed that the values of static and motile mitochondria are comparable to the normal range values showing 30-40% motile mitochondria with an average velocity of 0.6-0.7 μm/sec, and 60-70% of stationary mitochondria in the analyzed cerebellar granule cells. I also showed that the number of mitochondria moving in the retrograde direction is higher in L1/687 neurons from 7-day-old mice. Not only the percentage of mitochondria moving towards retrograde direction is higher in transgenic cells compared to wild-type cells, but also the majority of mitochondria in L1/687 cerebellar granule cells are moving in the retrograde direction instead of the anterograde direction, showing an opposite tendency compared to the wild-type cells in which mitochondria move mostly anterogradely.

Previous studies showed that mitochondria with high membrane potential migrate in an anterograde direction, while mitochondria with lower or impaired membrane potential are mostly transported retrogradely to be degraded or repaired [95, 143]. Mitochondria are transported retrogradely to areas where the highest number of mature acidic lysosomes is located [168]. In addition, recent investigations support the idea that the change in the balance from motile to stationary mitochondria in axons could be a response to changes in axonal levels of AMP-activated protein kinase (AMPK), which is activated during stress conditions that lower ATP levels in the cell [168].

In basal conditions AMPK is sensitive to the AMP/ADP levels in cells [169, 170] and during stress states AMPK promotes local ATP generation and/or decreases biosynthetic pathways in order to increase availability of ATP while temporarily minimizing its consumption [169]. Data from literature report that AMPK signaling plays a role in regulating mitochondrial transport by suppressing mitochondrial mobility during periods of energetic stress [169, 170].

A deficit in mitochondrial ATP production, even without disruption in mitochondrial membrane potential or mitochondrial morphology, can cause impairment in mitochondrial mobility [169]. Moreover, AMPK also activates downstream pathways of autophagy mechanisms [169, 170, 171] also by stimulating fission through phosphorylation of mitochondrial fission factor [171]. It is possible that the higher retrograde movement of mitochondria in L1/687 neurons is due to lower levels of ATP that affect mitochondria motility and their transport. Loss of ATP promotes the activation of the AMPK pathway, leading to higher mitochondrial fission and activation of mitophagy, inducing retrograde transport of damaged mitochondria to preserve healthy mitochondria for energetic purposes. It has been showed that pharmacological activation of the AMPK pathway at the distal axon, and localized nutrient deprivation, enhance retrograde transport in primary mouse neocortical neurons [169] in the distal axon region. Hence, it is plausible that AMPK activation during energetic stress conditions has a neuroprotective effect, by accumulating mitochondria in the region subjected to the stress (e.g. lower ATP, loss of nutrient, fission, impaired membrane potential), resulting also in a mild depolarization of the mitochondrial membrane potential in this region [169].

Basing on this data, I can assume that in cells lacking the L1-70 fragment, mitochondria are in higher percentage stationary and more mitochondria are transported retrogradely, as reflection of an unhealthy pool of these organelles. Cerebellar granule cells from L1/687 mice show an impaired membrane potential and lower ATP levels, thus the sequestration and removal of damaged mitochondria through the lysosomal system may function as neuroprotective mechanism, since an alteration in the regulation of mitochondrial distribution and transport is implicated in the pathogenesis of several major neurological disorders [168]. Interestingly, L1/687 cerebellar neurons show normal outgrowth under stimulatory conditions when compared to wild-type neurons [172] strengthening the notion that cells can compensate for their impaired mitochondrial membrane potential.

Additionally, a recent study from our group showed that mitochondria of neurons with the D201N mutation, which produce the L1-70 fragment, also move more retrogradely than anterogradely which indicates that not the absence of L1-70 is responsible for the enhanced retrograde transport. This strengthens the idea that the higher retrograde movement is a possible consequence of impaired and damaged mitochondria that need to be eliminated in order to provide a healthy pool for synaptic and axonal functions.

5.2 Mice lacking L1-70 showed diffuse cells in the hippocampal region

During the development of the nervous system, neurons have to migrate to the target areas therefore cell migration is a key step for the correct development of the brain. In these first steps L1 together with other CAM proteins is responsible for the initial contacts and neuronal migration [1], with L1-deficient mice showing reduced size of the corpus callosum due to a failure of callosal axons to cross the midline [38] and an altered distribution of dopaminergic neurons [173]. In this thesis morphological differences were investigated in order to find possible differences and abnormalities in brains from the L1 mutants, L1/858-863 and L1/687, which lack L1-70 fragment, to understand the role of L1-70 during brain development. The analysis of the hippocampal area in coronal sections from adult wild-type, L1/858-863 and L1/687 mouse brains showed a layer of less compact cells in the transgenic brains compared to the wild-type brains. I observed that the CA3 area of the hippocampus shows diffuse cells in the CA3 region of L1/858-863 and L1/687 mice compared to the CA3 region of wild-type mice, detecting also a larger hippocampal area in L1/858-863 brains. The observed abnormal compaction of cells in transgenic mice could be caused by several factors. One cause could be a migration problem. Previous studies in our lab showed in fact that in the absence of L1-70 cerebellar granule cells migrate less and have shorter neurites [57].

Moreover, it was shown that L1 deletion in stem/progenitor cells increased the differentiation of progenitor cells into neurons with higher arborization and branching in immature neurons [174] and that L1-deficient mice present hydrocephalus, alterations in axon guidance, neuronal morphology and hypoplasia [38] and enlarged ventricles with a reduced number of pyramidal and granule cells in the hippocampus [39]. Hence, the diffusion of cells could be also due to damages from a possible hydrocephalus that creates liquor pressure in the areas around the hippocampus.

5.3 Behavioral studies

5.3.1 Exploratory and anxiety-related behavior

In this thesis, different behavior tests were performed to characterize the behavioral phenotype of the transgenic line L1/687. Mice have a natural interest to explore and investigate new environments. However, confrontation with an unknown situation can induce anxiety-like behaviors, which are also an adaptive behavior response. Therefore, behavior of mice in the open field and elevated plus maze is the result of the balance between the instinct of exploration and the level of anxiety [136, 137]. A number of varied factors can affect a mouse during tests for evaluation of exploratory and/or anxiety behavior such as previous exposure to the test, age, isolation or laboratory environment [175].

Through the open field I showed that in the first five minutes of the test, L1/687 mice, both males and females, explore more compared to their wild-type littermates, as shown by the larger distance moved in the arena. When the total 30 minutes in the open field were evaluated, the distance moved was comparable between wild-type and L1/687 mice. Moreover, L1/687 male mice showed

a higher distance moved in the center of the arena, a higher frequency to reach this area and a higher velocity. This enhanced exploratory behavior was confirmed also with the elevated plus maze test where wild-type male mice showed a higher immobility time. However, the amount of thigmotaxis, the distance to the wall and the time spent in the center zone in the open field were not altered between genotypes. Also, the amount of rearing, used as an ethological marker for novelty induced exploratory behavior [176], was not different between genotypes. Hence, no alteration in the anxiety levels was detected. In the elevated plus maze the choice between the open and closed arms is an example of the balance between the drive to explore versus being protected within a confined location. The number of entrances in the open arms and time spent in the open arms are in fact accepted measures to evaluate anxiety levels of rodents [137, 177]. Mice can distinguish between open and closed arms and decide to stay protected in the close arm, performing less risk assessment, or to enter in the open arm. Avoiding the open arms is interpreted as anxious behavior [177]. Since no differences in these parameters were found between genotypes, we can speculate that no anxiety-like behaviors are enhanced in the transgenic line. These results were also confirmed through the marble burying test [139], in which no difference was observed indicating that L1/687 mice do not have higher levels of anxiety. In addition, during the elevated plus maze, female wild-type mice showed more stretching. This behavior, characterized by the elongation of the forepart of the body forward while the animal keeps a relatively safe distance from a possible threat, generally occurs during risk assessment and could be an indication of more anxiety experienced [144].

Literature data report that lower levels of locomotion in the open field are a consequence of a higher level of anxiety, while extensive time spent or distance traveled in the center could be interpreted as a reduced state of anxiety-like behavior [178, 179, 180]. Moreover, exposure to an unknown environment is followed by high defecation as well as reduced ambulation, especially in the

central zone of the arena [180]. No differences in defecation and urination were found between genotypes in my study.

However, L1/687 mice exhibited higher locomotor activity, in the first five minutes of the test in males and females mice, and also in the first 15 minutes of the test in female mice, besides higher distance traveled in the center zone. This raises the question whether the increase in locomotion was linked to real exploratory behavior. Different mouse models for neuropathologies such as the attention deficit hyperactivity disorder (ADHD), characterized by hyperactivity, impulsivity and inattention [181], report phenotype results similar to the one obtained in this thesis. In particular, mice model for ADHD show higher distance traveled in the open field as well as higher velocity and absence of anxiety-like behavior in the elevated plus maze and open field and no impairment in motor test as rotarod and social recognition [181, 182]. Interestingly, the spontaneous/basal level of activity analyzed through the home cage activity test did not show differences in the activity of the male L1/687 mice but a slightly higher activity of the L1/687 females in the dark phase. This data holds true also for ADHD models, which exhibit normal and not altered levels of basal activity during home cage [182]. It is still debated whether ADHD is due to a hyperdopaminergic or hypodopaminergic defect [183], with hyperactivity usually associated with a hyperdopaminergic state [182]. Altered distribution of dopaminergic neurons was found in L1-deficient mice [173], hence analysis of the dopaminergic system could be also an interesting evaluation in L1/687 mice.

Summing up the results obtained from different tests (open field, elevated plus maze and marble burying test) we can hypothesize that no alteration regarding anxiety behaviors is observed in the transgenic mouse line. On the contrary, L1/687 mice seemed to be more active in some tests, with a higher drive to explore, but do not show strong alterations in exploration. Further studies are in need to evaluate the exploratory activity behavior of these mice, for example the spatial memory test, impulsivity test or tests for assessing attention could be performed in order to have a greater understanding of the phenotype.

5.3.2   Social behavior

Mice are social animals that live, in wildlife, in social groups sharing the same territory. Social recognition and interaction with other conspecifics are then fundamental for maintaining social hierarchy, for mate choice and for the organization and defense of the habitat [184]. Different neurological disorders are characterized by impairment in social behavior and recognition, as schizophrenia or autism spectrum disorders [184]. In this thesis a social interaction test was performed on male and female wild-type and L1/687 mice to analyze their social behavior. Analysis of different parameters evaluated showed no effects of the genotype regarding the "preference for social novelty", defined as propensity to spend time with a non-familiar mouse rather than with a familiar one that is already known [185]. Normally, mice tend to approach first the familiar subject and then direct their attention to the unfamiliar individual, showing more interest as enhanced investigation towards the unfamiliar mice [186]. Overall both transgenic and wild-type male mice were more distant from the cup containing the familiar mouse and spent more time near the unfamiliar mouse. Female wild-type mice also were more distant from the cup containing the familiar mouse, whilst the mean distance of L1/687 female mice was higher for the cup containing the unfamiliar mouse. The time spent near the cup containing the unfamiliar mouse was higher in male wild-type and L1/687 mice and in female wild-type mice, while L1/687 female mice were more distant from the cup. Differences were also detected in the frequency and the time spent near each cup for transgenic female mice. In general, male wild-type and L1/687 mice, spent more time in the chamber of the arena containing the unfamiliar mouse. This was true also for the wild-type females, but not the transgenic females. Basing on these data, we can speculate that L1/687 mice have intact social memory and predilection for novel

experiences, which is particularly true for the male mice. In fact, under normal situation wild-type rodents or mice with no social impairment prefer to spend time and investigate a novel subject, being able to distinguish between the familiar mouse, through social memory, from the unfamiliar mouse [184]. My work then shows no impairment in social memory and a normal preference for unknown subjects in the L1/687 transgenic line. However, the lack of preferences in female mice, expressed as time near the unfamiliar subject, frequency of visits and distance from the cup raises the question about the social ability of wild-type and L1/687 female mice. These could reflect less interest in the conspecific mice.

5.3.3 L1/687 mice show no impairment in the circadian rhythm compared to wild-type mice

To further characterize the behavioral phenotype of L1/687 mice, home cage activity was performed comparing the activity levels of L1/687 and wild-type mice during 24 hours period (12 hours of light and 12 hours of dark). The use of the home cage activity system allows observation of spontaneous behavior, reducing the novelty interference present when studying anxiety-like behavior. Having a baseline of activity levels facilitates the interpretation of tests for anxiety and exploratory behavior [187]. In the home cage activity test both L1/687 and wild-type mice did not show an alteration of the circadian rhythm. Both genotypes have higher levels of activity in the dark phase as expected. While in male L1/687 and wild-type mice no differences between genotypes were detected in the activity measured in the dark and light phase, female L1/687 mice showed a slight significant difference in the level of activity during the dark phase compared to wild-type females, although is a result that needs further investigation. Evaluation of the behavior outside a test situation helps to have a better understanding of the phenotype analyzed.

Based on home cage activity, open field and elevated plus maze, L1/687 show a phenotype characterized by higher locomotion with normal circadian rhythm and normal baseline activity in spontaneous situation.

5.3.4 Motor performance

Previous studies conducted in our group showed that male mice lacking L1 had impairments in motor function as shown by a lower latency in falling from a rotating rod than male wild-type mice, and wild-type mice were showing a better performance in subsequent trials whereas L1-deficient mice did not show an improvement. In this thesis the rotarod test was performed again using wild-type and L1/687 mice, males and females, at different ages. First, I showed that 5-month-old male wild-type and L1/687 mice showed an improvement between the first and the last trial on the rotarod and a similar latency to fall from the rotating rod, whereas female mice did not show improvements between trials. In addition, female L1/687 mice had the same latency to fall from the rotating rod as the female wild-type mice. The test was repeated with older mice of 6- to 8-month-old. Male wild-type mice had a higher latency to fall from the rod compared to L1/687 males while female L1/687 mice fall later from the rod compared to wild-type females. No motor learning was seen in the 6- to 8-month-old male and female L1/687 mice.

One explanation for the impairment of the motor coordination of older male transgenic mice could be due to the disturbed synaptic connectivity in the cerebellum of mice lacking the L1-70 fragment. A previous study showed through immunostaining that the climbing fibers contacting the dendritic trees of the Purkinje cells in the molecular layer were larger in male wild-type mice than in L1-deficient male mice and mice transduced to express L1/687. Moreover, the density of synaptic vesicles and of parallel fibers in contact with the Purkinje cells was higher in wild-type

males compared to L1-deficient males and in L1-deficient mice transduced to express L1 with the L1/687 mutation, as well as the density of spines of Purkinje cells [40]. Unfortunately, this analysis was performed only in male brains, and transduction of cells with L1 could also be not homogenous in all neurons, so further investigation is needed. Basing on this finding it is possible that the impairment seen in the male mice is due to poor innervation of the cerebellum that plays a key role in motor learning and motor activity.

The opposite tendency for the older transgenic female mice to have a higher latency to fall from the rod compared to wild-type females, even though no motor learning was detected in subsequent trials, could indicate a possible impairment in the learning circuit.

Literature data suggest that under standard conditions female rodents are more active than males, which is probably due to the need to provide resources for the offspring. Also, the variation of sex hormones with increased estrogen and decreased testosterone concentrations in females determines a higher activity and exploratory behavior in females, with female rodents performing better in tests of spontaneous activity and motor tests [188].

5.4 Final conclusions

Mitochondrial dysfunctions are one of the causes of neurological diseases. Literature data show an effect of L1 in Alzheimer's disease mouse model, with L1 binding to β-amyloid and reducing its aggregation. [189]. Also, increased amounts of soluble L1 fragments in the cerebrospinal fluid are associated with Alzheimer's disease and dementia syndromes [190]. In the present study, I investigated the role of L1 and its fragment L1-70 in mitochondrial dynamics strengthening the potential role of this protein in mitochondrial pathways and functions, offering new perspectives on the role of L1 in nervous system functions. In the first part of this study I showed that L1 is present on the surface of mitochondria, and is located on the outer mitochondrial

membrane, identifying a possible position for the interaction with proteins involved in the fission/fusion balance.

In addition I identified new potential binding partners of L1-70, LC3 and Parkin. These results highlight the neuroprotective effect of L1. Levels of LC3 on mitochondria are altered in both L1-70 lacking transgenic mouse lines, and in L1-deficient mice levels of BNIP3, another protein involved in the mitophagy process, are higher. Mitophagy may play a role in neurodegenerative diseases such as Alzheimer's disease, where β-amyloid fragments can target mitochondria and cause mitochondrial dysfunction. Also, it is known that some familiar forms of Parkinson's disease are provoked by mutations in PINK1 or Parkin [112]. This study reinforces the connection between L1 and mitochondria quality control, enhancing the idea that lack of L1 can affect mitochondrial health. Furthermore, I showed that the absence of L1-70 leads to an impaired and lower mitochondrial membrane potential. Also, the mitochondrial motility is affected by the lack of L1-70, with mitochondria from cerebellar granule cells lacking L1-70 being more static and moving in a retrograde direction, which is associated with an unhealthy pool of mitochondria being transported to the soma for degradation. Several studies have described that the alterations in mitochondrial dynamics and motility are linked to different pathologies [94]. The role of L1-70 for brain development was also investigated analyzing the brain structure of L1-70 lacking mice: I showed that in brains from both transgenic lines, in the CA3 area of the hippocampus cells are more diffused and not as compact as in the CA3 area of wild-type brain. Altogether this thesis reveals new aspects about the role of L1-70 in the central nervous system of mice. Further studies and investigation are required to fully understand the relationship between mitochondria and L1 in order to progress also in the knowledge of neurodegenerative diseases and identification of new potential drugs target.

In the second part of the thesis I performed behavioral experiments in order to characterize the behavioral phenotype of the L1/687 mice. I showed that L1/687 mice, males and females, do not have higher levels of anxiety-like behavior compared to wild-type mice, but the female transgenic mice have a higher basal level of activity. In addition, no impairment in the sociability and social memory was found in L1/687 mice.

Furthermore, motor tests were performed to investigate potential motor learning and physical impairment. I showed that older male L1/687 mice fall off the rotarod earlier than their wild-type littermates whereas the older female L1/687 mice showed a better performance as their wild-type littermates. This suggests that lack of L1-70 does not lead to a general impairment in motor coordination.

Further studies analyzing several aspects of behavior are necessary to fully understand how the absence of L1-70 can affect the behavior of mice.

SUMMARY-ZUSAMMENFASSUNG

The cell adhesion molecule L1 has a key role during the development of the nervous system and is involved in different neuronal process as migration, adhesion, cell proliferation, neuritogenesis, synapse formation and synaptic plasticity.

Basing on a previous work that showed the translocation of a fragment of L1, L1-70, into mitochondria, I showed in this thesis through flow cytometry that L1-70 is present on the surface of mitochondria and that interacts with different proteins involved in the mitophagy/mitochondrial quality control process.

The interaction between L1 and mitophagy markers as LC3 and Parkin has been confirmed in vitro using proximity ligation assay on cerebellar granule cells, ELISA and co-immunoprecipitation assays. Moreover, I showed alteration in the levels of another mitophagy protein, BNIP3, in L1-deficient mice.

To further determine the role of L1-70 in mitochondrial pathway, I used in this thesis two transgenic mice lines, expressing full-length L1, but no L1-70. To confirm the absence of L1-70 in the transgenic mice line, L1/687 and L1/858-863, proximity ligation assay was performed. The outcome of the experiment confirmed that the

interaction of L1 with LC3 was due to the L1-70 fragment. Levels of LC3 were also detected by western blot on isolated mitochondria from L1/687 and L1/858-863, showing an alteration of the protein levels, but not its production.

To understand the role of L1-70 in mitochondrial process, different assays were performed. I showed that in cultured cerebellar neurons lacking L1-70 fragment, mitochondria move more retrogradely, exhibit reduced mitochondrial membrane potential and had lower ATP levels compared to wild-type littermates. These results suggest that L1-70 is important for mitochondrial homeostasis and its absence reflects on the mitochondrial quality and stability.

In addition, with staining of coronal brain sections from L1/858-863 and L1/687, I showed that L1/858-863 brains, had diffuse cells and higher hippocampal area.

The role of the L1-70 fragment during was further analyzed with behavioral experiments in order to characterize L1/687 phenotype. Through open field, elevated plus maze and marble burying test I showed that L1/687 mice did not display anxiety-like behavior compared to wild-type mice, but higher locomotor activity, expressed by the higher distance traveled in the arena. Besides, with home cage activity test, I showed that L1/687 mice had a normal circadian rhythm, with L1/687 female mice being slightly more active compared to their wild-type littermates. In addition, with the social interaction test, I showed no alteration in social behavior of transgenic mice that exhibited unaltered social memory and predilection for novel experiences.

The use of motor tests as rotarod, beam walking and pole test highlighted that there was no physical impairment in L1/687 mice. Using the pole test and the beam walking, no differences were detected, suggesting that the absence of L1-70 does not lead to impairment in motor coordination, but more likely to a possible impairment in the learning circuit.

Altogether, the new findings of this study could help reveals new aspects about the role and the importance of L1 and the L1-70 fragment in the murine central nervous system. L1-70 has in fact a role in mitochondrial dynamics and a possible function in mitochondrial quality control. These findings can be relevant in further understanding neurodegenerative diseases associated with mitochondrial impairments.

Das Zelladhäsionsmolekül L1 spielt eine Schlüsselrolle bei der Entwicklung des Nervensystems und es ist an verschiedenen neuronalen Prozessen wie Migration, Adhäsion, Zellproliferation, Neuritogenese Synapsenbildung und synaptische Plastizität beteiligt.

Ausgehend von einer früheren Arbeit, in der die Translokation eines L1-Fragments, L1-70, in Mitochondrien nachgewiesen wurde, habe ich in dieser Arbeit mittels *flow cytometry* gezeigt, dass L1-70 auf der Oberfläche von Mitochondrien vorhanden ist und mit verschiedenen Proteinen interagiert, die an der Mitophagie bzw. mitochondrialen Qualitätskontrolle beteiligt sind.

Die Interaktion zwischen L1 und Mitophagie-Markern wie LC3 und Parkin wurde in vitro mittels *Proximity Ligation Assay* an Kleinhirn-Körnerzellen, ELISA und Co-Immunopräzipitation bestätigt. Darüber hinaus konnte ich bei L1-defizienten Mäusen eine Veränderung der Spiegel eines anderen Mitophagie-Proteins, BNIP3, nachweisen.

Um die Rolle von L1-70 im mitochondrialen Stoffwechselweg weiter zu bestimmen, habe ich in dieser Arbeit zwei transgene Mäuselinien verwendet, die L1 in voller Länge, aber kein L1-70 exprimieren. Um das Fehlen von L1-70 in den transgenen Mäusen L1/687 und L1/858-863 zu bestätigen, wurde ein *Proximity Ligation assay* durchgeführt. Das Ergebnis des Experiments bestätigte, dass die Interaktion von L1 mit LC3 auf das L1-70-Fragment zurückzuführen ist. Die LC3-Konzentrationen wurden auch mittels Western Blot an isolierten Mitochondrien von L1/687 und L1/858-863 Mäusen nachgewiesen, was eine Veränderung der Proteinkonzentrationen, aber nicht der Proteinproduktion zeigte.

Um die Rolle von L1-70 in mitochondrialen Prozessen zu verstehen, wurden verschiedene Tests durchgeführt. Ich konnte zeigen, dass sich in kultivierten Kleinhirnneuronen, denen das L1-70-Fragment fehlt, die Mitochondrien stärker retrograd bewegen, ein geringeres mitochondriales Membranpotenzial aufweisen und im Vergleich zu Wildtyp-Wurfgeschwistern niedrigere ATP-Werte haben. Diese Ergebnisse deuten darauf hin, dass L1-70 für die mitochondriale Homöostase wichtig ist und dass sich sein Fehlen auf die Qualität und Stabilität der Mitochondrien auswirkt. Darüber hinaus konnte ich anhand der Färbung von koronalen Hirnschnitten von L1/858-863 und L1/687 zeigen, dass L1/858-863-Gehirne diffuse Zellen und eine größere Hippocampusfläche aufweisen.

Die Rolle des L1-70-Fragments wurde mit Verhaltensexperimenten weiter analysiert, um den L1/687-Phänotyp zu charakterisieren. Mit Hilfe von *open field, elevated plus maze und marble burying test*, konnte ich zeigen, dass L1/687-Mäuse im Vergleich zu Wildtyp- Mäusen kein angstähnliches Verhalten zeigten, aber eine höhere Bewegungsaktivität, die sich in einer höheren zurückgelegten Distanz in der Arena ausdrückte. Außerdem zeigte ich mit dem homecage activity test, dass L1/687-Mäuse einen normalen zirkadianen Rhythmus hatten, wobei L1/687-Mäuseweibchen im Vergleich zu ihren Wildtyp-Wurfgeschwistern etwas aktiver waren.

Darüber hinaus habe ich mit dem Test zur *social intercation* konnte ich außerdem zeigen, dass das Sozialverhalten der transgenen Mäuse, die ein unverändertes soziales Gedächtnis und eine Vorliebe für neue Erfahrungen zeigten, nicht verändert war.

Der Einsatz von motorischen Tests wie Rotarod, beam walking und pole test zeigte, dass es bei L1/687-Mäusen keine körperlichen Beeinträchtigungen gab. Beim *beam walking* und beim *pole test* wurden keine Unterschiede festgestellt, was darauf hindeutet, dass das Fehlen von L1-70 nicht zu Beeinträchtigung der motorischen Koordination führt, sondern eher zu einer möglichen Beeinträchtigung des Lernkreislaufs führt.

Insgesamt könnten die neuen Erkenntnisse dieser Studie dazu beitragen, neue Aspekte über die Rolle und die Bedeutung von L1 und dem L1-70-Fragment im zentralen Nervensystem der Maus aufzudecken. L1-70 spielt in der Tat eine Rolle in der mitochondrialen Dynamik und hat möglicherweise eine Funktion in der mitochondrialen Qualitätskontrolle. Diese Erkenntnisse können für das weitere Verständnis neurodegenerativer Erkrankungen, die mit mitochondrialen Beeinträchtigungen einhergehen, von Bedeutung sein.

C H A P T E R 7

ABBREVIATIONS

AAV1 - adeno-associated virus 1
ADP - adenosine diphosphate
ANT - adenine nucleotide translocator
ANOVA - analysis of variance
AP-2 - adaptor protein 2
APS - ammonium persulfate
Arg - arginine
Asp - aspartate
ATP - adenosine triphosphate
BCA - bicinchoninic acid assay
bp - base pairs
BNIP3 - BCL2 Interacting Protein 3
BSA - bovine serum albumin
CA3 – cornu Ammonis 3
CAMs - cell adhesion molecules
CHL1 - close homolog of L1
CHL1-ICD – intracellular domain of close homolog of L1
Cy2 and 5 – cyanine fluorescent dyes 2 and 5
DAPI - 4,6-diamidino-2- phenylindole
ddH$_2$O – double distilled water
DNA - deoxyribonucleic acid

Drp1 - dynamin-related protein 1
ECL – enhanced chemiluminescence
EDTA - ethylenediaminetetraacetic acid
ELISA – enzyme-linked immunosorbent assay
ERM – ezrin-radixin-moesin
FADH$_2$ - flavin adenine dinucleotide
FNIII – Fibronectin type III domain
F - phenylalanine
FBS – fetal bovine serum
FGFR1 - fibroblast growth factor receptor 1
Fis1 - mitochondrial fission protein 1
FUNDC1 - FUN14 Domain Containing 1
GAPDH - glyceraldehyde 3-phosphate dehydrogenase
GED - GTPase effector domain
Gly - glycine
Glu - glutamic acid
HBSS – Hanks' Balanced Salt Solution
HEK293 – human embryonic kidney 293 cell
HeLa - Henrietta's cancer cells
HR1/2 - heptad repeat regions 1 and 2
HRP – horseradish peroxidase
I - isoleucine
Ig - immunoglobulin
IgCAMs – Cell adhesion molecules of the immunoglobulin super-family
IMM - inner mitochondrial membrane
IP - immunoprecipitation
IPTG - Isopropyl β-D-1-thiogalactopyranoside
JC-1 - 1,1',3,3'-tetraethyl-5,5',6,6'-tetrachloroimidacarbo- cyanine iodide
kDa - kilo Dalton
L - leucine
L1 - neural cell adhesion molecule L1
L1-/y- KO - L1-deficient mice
L1+/y - WT - L1 wild-type mice
L1-ICD – intracellular domain of neural cell adhesion molecule L1

LB – lysogeny broth media
LC3 - microtubule-associated protein light chain 3
LDS - LIR docking site
LIR - LC3-interacting region
Lys - lysine
MBP – myelin basic protein
MER - minimal essential region
Met - methionine
MFF - mitochondrial fission factor
Mfn1 and 2 - mitofusin 1 and 2
MIA - mitochondrial intermembrane space assembly
MIBA - mitochondrial isolation buffer
Mim1 - mitochondrial import protein 1
Miro - mitochondrial Rho GTPase 1
MPP - mitochondrial-processing protease
mtDNA - mitochondrial DNA
NAD$^+$ - oxidized nicotinamide adenine dinucleotide
NADH - nicotinamide adenine dinucleotide
NCAM - neural cell adhesion molecule
NDUFV2 - NADH dehydrogenase ubiquinone flavoprotein 2
NF-1A - nuclear factor 1-A
NP-40 - nonyl phenoxypolyethoxylethanol
OD – optical density
OD600 – optical density at 600 nm
OMM - outer mitochondrial membrane
OPA1 - optic atrophy protein 1
OPD - orthophenylenediamine
OXA - oxidase assembly
OXPHOS - oxidative phosphorylation
p62/SQSTM1 - ubiquitin-binding protein p62/sequestosome 1
PAM - presequence translocase-associated motor
PBS - phosphate buffered saline
PBS-T - phosphate buffered saline with 0.01% Tween 20
PCR – polymerase chain reaction
PINK1 - PTEN-induced kinase 1
PLL - poly-L-lysine

REST – RE1-Silencing Transcription factor
Rho - ras homolog family member
RIPA - radioimmunoprecipitation assay
RNA - ribonucleic acid
RNase – ribonuclease
SAM - sorting and assembly machinery
SDS – sodium dodecyl sulfate
SDS-PAGE – sodium dodecyl sulfate–polyacrylamide gel electrophoresis
SEM – Standard error of the mean
SNPH - syntaphilin
TBS – Tris-buffered saline solution
TBS-T – Tris-buffered saline solution containing Tween-20
TEMED – Tetramethylethylenediamine
TIM - translocase of inner mitochondrial membrane
TOM - translocase of outer mitochondrial membrane
TRAK - trafficking protein kinesin- binding
V - voltage
VDAC - voltage- dependent anion channel
W - tryptophan
Y - tyrosine
X - any amino acid

Bibliography

[1] Murray P., Frampton G., and Nelson P.N. Cell adhesion molecules. sticky moments in the clinic. *BMJ (1991)*, 319(7206):332–334.

[2] Maness P. F. and Schachner M. Neural recognition molecules of the immunoglobulin superfamily: signaling transducers of axon guidance and neuronal migration. *Nature Neuroscience (2007)*, 10(1):19–26.

[3] Harjunpää H., Llort Asens M., Guenther C., and Fagerholm SC. Cell adhesion molecules and their roles and regulation in the immune and tumor microenvironment. *Frontiers Immunology (2019)*, 10(1078).

[4] Togashi H., Sakisaka T., and Takai Y. Cell adhesion molecules in the central nervous system. *Cell Adhesion and Migration (2009)*, 3(1):29–35.

[5] Yamagata M., Sanesy J.R., and Weiner J.A. Synaptic adhesion molecules. *Current Opinion in Cell Biology (2003).*, 15(5):621–632.

[6] De Grandis M., Lhoumeau A.C., Mancini S. J., and Aurrand-Lions M. Adhesion receptors involved in HSC and early-B cell interactions with bone marrow microenvironment. *Cellular and molecular life science (2015)*, 73(4):687–703.

[7] Wei C.H. and Ryu S.E. Homophilic interaction of the L1 family of cell adhesion molecules. *Experimental and molecular medicine (2012)*, 44(7).

[8] Hortsch M. Structural and functional evolution of the L1 family: Are four adhesion molecules better than one? *Molecular and Cellular Neuroscience (2000)*, 15(1):1–10.

[9] Kenwrick S., Watkins A., and De Angelis E. Neural cell recognition molecule L1: relating biological complexity to human disease mutations. *Human molecular Genetics (2000)*, 9(6):879–886.

[10] Samatov T.R., Wicklein D., and Tonevitsky A.G. L1CAM: cell adhesion and more. *Progress in Histochemistry and Cytochemistry (2016)*, 51(2):25–32.

[11] Hortsch M. The L1 family of neural cell adhesion molecules: Old proteins performing new tricks. *Neuron (1996)*, 17(4):587–593.

[12] Kleene R., Yang H., Kutsche M., and Schachner M. The neural recognition molecule L1 is a sialic acid-binding lectin for CD24, which induces promotion and inhibition of neurite outgrowth. *Journal of Biological Chemistry (2001)*, 276(24):21656–21663.

[13] Brümmendorf T., Kenwrick S., and Rathjen F. G. Neural cell recognition molecule L1: From cell biology to human hereditary brain malformations. *Current Opinion in Neurobiology (1998)*, 8(1):87–97.

[14] Castellani V., De Angelis E., Kenwrick S., and Rougon G. Cis and trans interactions of L1 with neuropilin-1 control axonal responses to semaphorin 3A. *The EMBO Journal (2002)*, 21(23):6348–6357.

[15] Yip P.M., Zhao X., Montgomery A.M.P., and Siu C.H. The Arg-Gly-Asp motif in the cell adhesion molecule L1 promotes neurite outgrowth via interaction with the alphavbeta3 integrin. *Molecular Biology of the Cell (1998)*, 9(2):277– 290.

[16] Donier E., Gomez-Sanchez J.A., Grijota-Martinez C., Lakomá J., Baars S., Garcia-Alonso L., and Cabedo H. L1CAM binds ErbB receptors through Ig-like domains coupling cell adhesion and neuregulin signalling. *PLoS One (2012)*, 7(7): e40674.

[17] Schäfer M.K.E. and Frotscher M. Role of L1CAM for axon sprouting and branching. *Cell and Tissue Research (2012)*, 349(1):39–48.

[18] Kulahin N., Li S., Hinsby A., Kiselyov V., Berezin V., and Bock E. Fibronectin type III FN3 modules of the neuronal cell adhesion molecule L1 interact directly with the fibroblast growth factor FGF receptor. *Cellular and Molecular Biology Letters (2009)*, 37(3):528–536.

[19] Hortsch M., Nagaraj K., and Godenschwege T.A. The interaction between L1-type proteins and ankyrins–a master switch for L1-type CAM function. *Molecular and Cellular Neuroscience (2008)*, 14(1):57–69.

[20] Dickson T.C., Mintz C.D., Benson D. L., and Salton S.R. Functional binding interaction identified between the axonal CAM L1 and members of the ERM family. *The Journal of Cell Biology (2002)*, 157(7):1105–1112.

[21] Buhusi M., Schlatter M.C., Demyanenko G.P., Thresher R., and Maness P.F. L1 interaction with ankyrin regulates mediolateral topography in the retinocollicular projection. *The Journal of Neuroscience (2008)*, 28(1):177–188.

[22] Saugier-Veber P., Martin C., Le Meur N., Lyonnet S., Munnich A., and David A. et al. Identification of novel

L1CAM mutations using fluorescence-assisted mismatch analysis. *Human mutation (1998)*, 12(4):259–266.

[23] Kamiguchi H. and Lemmon V. A neuronal form of the cell adhesion molecule L1 contains a tyrosine-based signal required for sorting to the axonal growth cone. *The Journal of Neuroscience (1998)*, 18(10):3749–3756.

[24] Wei C.H. and Ryu S.E. Homophilic interaction of the l1 family of cell adhesion molecules. *Experimental and Molecular Medicine (2012)*, 44(7).

[25] Lutz D., Wolters-Eisfeld G., Schachner M., and Kleene R. Cathepsin E generates a sumoylated intracellular fragment of the cell adhesion molecule L1 to promote neuronal and Schwann cell migration as well as myelination. *Journal of Neurochemistry (2014)*, 128(5):713–724.

[26] Lutz D., Wolters-Eisfeld G., Joshi G., Djogo N., Jakovcevski I., Schachner M., and Kleene R. Generation and nuclear translocation of sumoylated transmembrane fragment of cell adhesion molecule L1. *The Journal of Biological Chemistry (2012)*, 287(21):17161–17175.

[27] Schäfer M.K.E., Schmitz B., and Diestel S. L1CAM ubiquitination facilitates its lysosomal degradation. *FEBS Letters (2010)*, 584(21):4475–4480.

[28] Schaefer A.W., Kamei Y., Kamiguchi H., Wong E.V., Rapoport I., Kirchhausen T., Beach C.M., Landreth G., Lemmon S.K., and Lemmon V. L1 endocytosis is controlled by a phosphorylation-dephosphorylation cycle stimulated by outside-in signaling by L1. *The Journal of Cell Biology (2002)*, 157(7):1223–1232.

[29] Whittard J.D., Sakurai T., Cassella M.R., Gazdoiu M., and Felsenfeld D.P. MAP kinase pathway–dependent phosphorylation of the L1-CAM ankyrin binding site

regulates neu ronal growth. *Molecular Biology of the Cell (2006)*, 17(6):2696– 2706.

[30] Kallunki P., Edelman G.M., and Jones F.S. Tissue-specific expression of the L1 cell adhesion molecule is modulated by the neural restrictive silencer element. *The Journal of Cell Biology (1997)*, 138(6):1343–1354.

[31] Schneegans T., Borgmeyer U., Hentschke M., Gronostajski R.M., Schachner M., and Tilling. T. Nuclear factor I-A represses expression of the cell adhesion molecule L1. *BMC Molecular Biology (2009)*, 10(107).

[32] Geismann C., Arlt A., Bauer I., Pfeifer M., Schirmer U., Altevogt P., Müerköster S.S., and Schäfer H. Binding of the transcription factor slug to the L1CAM promoter is essential for transforming growth factor-β1 (TGF-β)-induced L1CAM expression in human pancreatic ductal adenocarcinoma cells. *International Journal Oncology (2011)*, 38(1):257–266.

[33] Mikulak J. et al. Dual REST-dependence of L1CAM: from gene expression to alternative splicing governed by Nova2 in neural cells. *Journal of Neurochemistry (2012)*, 120(5):699–709.

[34] Kenwrick S., Watkins A., and De Angelis E. Neural cell recognition molecule L1: relating biological complexity to human disease mutations. *Human Molecular Genetics (2000)*, 9(6):879–886.

[35] Arevalo E., Shanmugasundararaj S., Wilkemeyer M.F., Chen S. Dou X., Charness M.E., and Miller K.W. An alcohol binding site on the neural cell adhesion molecule L1. *PNAS (2008)*, 105(1):371–375.

[36] Kurumaji A., Nomoto H., Okano T., and Toru M. An association study between polymorphism of L1CAM gene and schizophrenia in a Japanese sample. *American Journal of Medical Genetics (2001)*, 105(1):99–104.

[37] Loers G., Appel D., Lutz D., Congiu L., Kleene R., Hermans-Borgmeyer I., Schäfer M.K.E, and Schachner M. Amelioration of the abnormal phenotype of a new L1 syndrome mouse mutation with L1 mimetics. *FASEB Journal (2021)*, 35(2): e21329.

[38] Itoh K., Cheng L., Kamei Y., Fushiki S., Kamiguchi H., Gutwein P., Stoeck A., Arnold B., Altevogt P., and Lemmon V. Brain development in mice lacking L1–L1 homophilic adhesion. *The Journal of Cell Biology (2004)*, 165(1):145–154.

[39] Rolf B., Kutsche M., and Bartsch U. Severe hydrocephalus in L1-deficient mice. *Brain Research (2001)*.

[40] Kraus K, Kleene R., Henis M., Braren I., Kataria H., Sharaf A., Loers G., Schachner M., and Lutz D. A fragment of adhesion molecule L1 binds to nuclear receptors to regulate synaptic plasticity and motor coordination. *Molecular Neurobiology (2018)*, 55(9):7164–7178.

[41] Altevogt P., Doberstein K., and Fogel M. L1CAM in human cancer. *International Journal of Cancer (2016)*, 138(7):1565–1576.

[42] Schäfer M.K.E. and Altevogt P. L1CAM malfunction in the nervous system and human carcinomas. *Cellular and Molecular Life Sciences (2010)*, 67(14):2425–2437.

[43] Kiefel H., Bondong S., Hazin J., Ridinger J., Schirmer U., Riedle S., and Altevogt P. L1CAM. a major driver for tumor cell invasion and motility. *Cell Adhesion and Migration (2012)*, 6(4):374–384.

[44] Wachowiak R., Fiegel H.C., and Kaifi J.T. et al. L1 is associated with favorable outcome in neuroblastomas in contrast to adult tumors. *Annals of Surgical Oncology (2007)*, 14(12):3575–3580.

[45] Kleene R., Lutz D., Loers G., Bork U., Borgmeyer U., Hermans-Borgmeyer I., and Schachner M. Revisiting the proteolytic processing of cell adhesion molecule L1. *Journal of Neurochemistry (2020)*, 157(4):1102–1117.

[46] Kalus I., Schnegelsberg B., Seidah N.B., Kleene R., and Schachner M. The proprotein convertase PC5A and a metalloprotease are involved in the proteolytic processing of the neural adhesion molecule L1. *The Journal of Biological Chemistry (2002)*, 278(12):10381–10388.

[47] Nayeem N., Silletti S., Yang X., Lemmon V.P., Reisfeld R.A., Stallcup W.B., and Montgomery A.M. Potential role for the plasmin(ogen) system in the posttranslational cleavage of the neural cell adhesion molecule L1. *Journal of Cell Science (1999)*, 112(Pt 24):4739–4749.

[48] Silletti S., Mei F., Sheppard D., and Montgomery A.M. Plasmin-sensitive dibasic sequences in the third fibronectin-like domain of L1-cell adhesion molecule (CAM) facilitate homomultimerization and concomitant integrin recruitment. *The Journal of Cell Biology (2000)*, 149(7):1485–1502.

[49] Mechtersheimer S., Gutwein P., Agmon-Levin N., Stoeck A., Oleszewski M., Riedle S., Postina R., Fahrenholz F., Fogel M., Lemmon V., and Altevogt P. Ectodomain shedding of l1 adhesion molecule promotes cell migration by autocrine binding to integrins. *The Journal of Cell Biology (2001)*, 155(4):661–674.

[50] Sadoul K., Sadoul R., Faissner A., and Schachner M. Biochemical characterization of different molecular forms of the neural cell adhesion molecule L1. *Journal of Neurochemistry (1988)*, 50(2):510–521.

[51] Faissner A., Teplow D.B., Kübler D., Keilhauer G., Kinzel V., and Schachner M. Biosynthesis and membrane topography of the neural cell adhesion molecule L1. *The EMBO Journal (1985)*, 4(12):3105–3113.

[52] Lutz D., Sharaf A., Drexler D., Kataria H., Wolters-Eisfeld G., Brunne B., Kleene R., Loers G., Frotscher M., and Melitta Schachner. Proteolytic cleavage of transmembrane cell adhesion molecule L1 by extracellular matrix molecule Reelin is important for mouse brain development. *Scientific Reports (2017)*, 7(1):15628.

[53] Maretzky T., Schulte M., Ludwig A., Rose-John S., Blobel C., Hartmann D., Altevogt P., Saftig P., and Reiss K. L1 is sequentially processed by two differently activated metalloproteases and presenilin/γ-secretase and regulates neural cell adhesion, cell migration, and neurite outgrowth. *Molecular and cellular biology (2005)*, 25(20):9040–9053.

[54] K. Matsumoto-Miyai, Ninomiya A., Yamasaki H., Tamura H., Nakamura Y., and Shiosaka S. NMDA-dependent proteolysis of presynaptic adhesion molecule L1 in the hippocampus by neuropsin. *The Journal of Neuroscience (2003)*, 23(21):7727–7736.

[55] Riedle S., Kiefel H., Gast D., Bondong S., Wolterink S., Gutwein P., and Altevogt P. Nuclear translocation and signalling of L1-CAM in human carcinoma cells requires ADAM10 and presenilin/γ-secretase activity. *Biochemical Journal (2009)*, 420(Pt 3):391–402.

[56] Gutwein P., Mechtersheimer S., Riedle S., Stoeck A., Gast D., Joumaa S., Zentgraf H., Fogel M., and Altevogt D.P. ADAM10-mediated cleavage of L1 adhesion molecule at the cell surface and in released membrane vesicles. *FASEB Journal (2003)*, 17(2):292–294.

[57] Lutz D., Loers G., and Oezen I. Kleene R., Kataria H., Katagi-hallimath N., Braren I., Harauz G., and Schachner M. Myelin basic protein cleaves cell adhesion molecule L1 and promotes neuritogenesis and cell survival. *The Journal of Biological Chemistry (2014)*, 289(19):13503–13518.

[58] Kraus K., Kleene R., Braren I, Loers G., Lutz D., and Schachner M. A fragment of adhesion molecule L1 is imported into mitochondria, and regulates mitochondrial metabolism and trafficking. *Journal of Cell Science (2018)*, 131(9): jcs210500.

[59] Tilokani L., Nagashima S., Paupe V., and Prudent J. Mitochondrial dynamics: overview of molecular mechanisms. *Essays in Biochemistry (2018)*, 62(3):341–360.

[60] Bratic I. and Trifunovic A. Mitochondrial energy metabolism and ageing. *Biochimica et Biophysica Acta (BBA) - Bioenergetics (2010)*, 1797(6):961–967.

[61] Rizzuto R., De Stefani D., Raffaello A., and Mammucari C. Mitochondria as sensors and regulators of calcium signalling. *Nature Reviews Molecular Cell Biology (2012)*, 13(9):566–578.

[62] Nikoletopoulou V., Markaki M., Palikaras K., and Tavernarakis N. Crosstalk between apoptosis, necrosis and autophagy. *Biochimica et Biophysica Acta (2013)*, 1833(12):23448–3459.

[63] Bukowiecki R., Adjaye J., and Prigione A. Mitochondrial function in pluripotent stem cells and cellular reprogramming. *Gerontology (2014)*, 60.

[64] Rambold A.S and Pearce E.L. Mitochondrial dynamics at the interface of immune cell metabolism and function. *Trends in immunology (2018)*, 39(1):6–18.

[65] Spinelli J.B. and Haigis M.C. The multifaceted contributions of mitochondria to cellular metabolism. *Nature Cell Biology (2018)*, 20(7):745–754.

[66] Kang I., Chu C.T., and Kaufman B.A. The mitochondrial transcription factor TFAM in neurodegeneration: Emerging evidence and mechanisms. *FEBS Letters (2018)*, 592(5):793–811.

[67] St John J. C., Facucho-Oliveira J., Jiang Y., Kelly R., and Salah R. Mitochondrial DNA transmission, replication and inheritance: a journey from the gamete through the embryo and into offspring and embryonic stem cells. *Human Reproduction Update (2010)*, 16(5):488–509.

[68] Kühlbrandt W. Structure and function of mitochondrial membrane protein complexes. *BMC Biology (2015)*, 13(1):89.

[69] Bayrhuber M., Meins T., Habeck M., Becker S., Villinger S. Giller K., and et al. Structure of the human voltage-dependent anion channel. *Proceedings of the National Academy of Sciences of the United States of America (2008)*, 105(40):15370–15375.

[70] Chacinska A., Koehler C.M, Milenkovic D., Lithgow T., and Pfanner N. Importing mitochondrial proteins: Machineries and mechanisms. *Cell (2009)*, 138(4):628–644.

[71] Vogtle F.N., Wortelkamp S., Zahedi R.P., Becker D., Leidhold C., Gevaert K., and et al. Global analysis of the mitochondrial N-proteome identifies a processing peptidase critical for protein stability. *Cell (2009)*, 139(2):428–439.

[72] Zhao F. and Zou M.H. Role of the mitochondrial protein import machinery and protein processing in heart disease. *Frontiers in Cardiovascular Medicine (2021)*, 8:749756.

[73] Saitoh T., Igura M., Obita T., Ose T., Kojima R., Maenaka K., Endo T., and Kohda D. Tom20 recognizes mitochondrial presequences through dynamic equilibrium among multiple bound states. *The EMBO Journal (2007)*, 26(22):4777–4787.

[74] Meinecke M., Wagner R., Kovermann P., Guiard B., Mick D.U., Hutu D.P., Voos W., Truscott K.N., Chacinska A., Pfanner N., and Rehling P. Tim50 maintains the permeability barrier of the mitochondrial inner membrane. *Science (2006)*.

[75] Truscott K.N., Kovermann P., Geissler A., Merlin A., Meijer M., Driessen A.J., Rassow J., Pfanner N., and Wagner R. A presequence-and voltage-sensitive channel of the mitochondrial preprotein translocase formed by Tim23. *Nature Structural Biology (2011)*, 8(12):1074–1082.

[76] Turakhiya U., von der Malsburg K., Gold V., Guiard B., Chacinska A., van der Laan M., and Ieva R. Protein import by the mitochondrial presequence translocase in the absence of a membrane potential. *Journal of Molecular Biology (2016)*, 428(6):1041–1052.

[77] Kang P.J., Ostermannt J., Shilling J., Neupertt W., Craig E.A., and Pfannert N. Requirement for hsp70 in the mitochondrial matrix for translocation and folding of precursor proteins. *Nature (1990)*, 348(6279):137–143.

[78] Stiller S.B., Höpker J., Oeljeklaus S., Schütze C., Schrempp SG., Vent-Schmidt J., Horvath S.E., Frazier A.E., Gebert N., van der Laan M., Bohnert M., Warscheid B., Pfanner N., and Wiedemann N. Mitochondrial OXA translocase plays a major role in biogenesis of inner-membrane proteins. *Cell Metabolism (2016)*, 23(5):901–908.

[79] Wiedemann N. and Pfanner N. Mitochondrial machineries for protein import and assembly. *Annual Review of Biochemistry (2017)*, 86(1):685–714.

[80] Durigon R., Wang Q., Ceh Pavia E., Grant C.M., and Lu H. Cytosolic thioredoxin system facilitates the import of mitochondrial small Tim proteins. *EMBO Reports (2012)*, 13(10):916–322.

[81] Gornicka A., Bragoszewski P., Chroscicki P., Wenz L.S., Schulz C., Rehling P., and et al. A discrete pathway for the transfer of intermembrane space proteins across the outer membrane of mitochondria. *Molecular Biology of the Cell (2004)*, 25(25):3999–4009.

[82] Terziyska N., Grumbt B., Kozany C., and Hell K. Structural and functional roles of the conserved cysteine residues of the redox-regulated import receptor Mia40 in the intermembrane space of mitochondria. *Journal of Biological Chemistry (2009)*, 284(3):1353–1363.

[83] Nolfi-Donegan D., Braganza A., and Shiva S. Mitochondrial electron transport chain: Oxidative phosphorylation, oxidant production, and methods of measurement. *Redox Biology (2020)*, 37:101674.

[84] Zhao R.Z., Jiang S., Zhang L., and Yu Z.B. Mitochondrial electron transport chain, ROS generation and uncoupling (Review). *International Journal of Molecular Medicine (2019)*, 44(1):3–15.

[85] Vogel R.O., Smeitink J.A., and Nijtmans L.G. Human mitochondrial complex I assembly: a dynamic and versatile process. *Biochimica et biophysica acta, (2007)*, 1767(10):1215–1227.

[86] Ghezzi D. and Zeviani M. Assembly factors of human mitochondrial respiratory chain complexes: Physiology and pathophysiology. *Advances in experimental medicine and biology (2012)*, 748(65):65–106, 2001.

[87] Schagger H., Link T.A., Engel W.D., and von Jagow G. Isolation of the eleven protein subunits of the bc1 complex from beef heart. *Methods in enzymology (1986)*, 126:224–237.

[88] Rich P.R. and Maréchal A. The mitochondrial respiratory chain. *Essays in Biochemistry (2010)*, 47:1–23.

[89] Watt I.N., Montgomery M.G., Runswick M.J., Leslie A.G., and Walker J.E. Bioenergetic cost of making an adenosine triphosphate molecule in animal mitochondria. *Proceedings of the National Academy of Sciences (2010)*, 107(39):16823–16827.

[90] Jonckheere A.I., Smeitink J.A., and Rodenburg R.J. Mitochondrial ATP synthase: Architecture, function and pathology. *Journal of Inherited Metabolic Disease (2012)*, 35(2):211–225.

[91] Meyer J.N., T.C. Leuthner, and A. L. Luz. Mitochondrial fusion, fission, and mitochondrial toxicity. *Toxicology (2017)*, 391:42–53.

[92] Tilokani L., Nagashima S., Paupe V., and Prudent J. Mitochondrial dynamics: overview of molecular mechanisms. *Essays in Biochemistry (2018)*, 62(3):341–360.

[93] Schwarz T.L. Mitochondrial trafficking in neurons. *Cold Spring Harbor Perspectives in Biology (2013)*, 5(6): a011304.

[94] Hollenbeck P.J. and Saxton W.M. The axonal transport of mitochondria. *Journal of Cell Science (2005)*, 118(Pt 23):5411–5419.

[95] Milone M. and Benarroch E.E. Mitochondrial dynamics: general concepts and clinical implications. *Neurology (2012)*, 78(20):1612–1619.

[96] Drerup C.M., Herbert A.M., Monk K.R., and Nechiporuk A.V. Regulation of mitochondria-dynactin interaction and mitochondrial retrograde transport in axons. *eLife (2017)*, 6: e22234.

[97] Ni H.M, Williams J.A, and Ding W.X. Mitochondrial dynamics and mitochondrial quality control. *Redox Biology (2014)*, 4:6–13.

[98] van der Bliek A. M., Shen Q., and Kawajiri S. Mechanisms of mitochondrial fission and fusion. *Cold Spring Harbor perspectives in biology (2013)*, 5(6): a011072.

[99] Pernas L. and Scorrano L. Mito-morphosis: Mitochondrial fusion, fission, and cristae remodeling as key mediators of cellular function. *Annual Review of Physiology (2016)*, 78(1):505– 531.

[100] Eura Y., Ishihara N., S. Yokota, and Mihara K. Two mitofusin proteins, mammalian homologues of FZO, with distinct functions are both required for mitochondrial fusion. *Journal of biochemistry (2003)*, 164(3):333–344.

[101] Chen H., Detmer S.A., Ewald A.J., Griffin E.E., S.E. Frase, and Chan D.C. Mitofusins Mfn1 and Mfn2 coordinately regulate mitochondrial fusion and are essential for embryonic development. *The Journal of Cell Biology (2003)*, 160(2):189– 200.

[102] de Brito O.M. and Scorrano L. Mitofusin 2 tethers endoplasmic reticulum to mitochondria. *Nature (2008)*, 456(7222):605– 610.

[103] Zhan M., Brooks C., Liu F., Sun L., and Dong Z. Mitochondrial dynamics: regulatory mechanisms and emerging role in renal pathophysiology. *Kidney international (2013)*, 83(4):568– 581.

[104] Rojo M., Legros F., Chateau D., and Lombès A. Membrane topology and mitochondrial targeting of mitofusins, ubiquitous mammalian homologs of the transmembrane GTPase Fzo. *Journal of Cell Sciencel (2002)*, 115(8):1663– 1674.

[105] Song Z., Ghochani M., McCaffery J.M., Frey T.G., and Chan D.C. Mitofusins and OPA1 mediate sequential steps in mitochondrial membrane fusion. *Molecular Biology of the Cell (2009)*, 20(15):3525–3532.

[106] Cipolat S., de Brito O.M., Dal Zilio B., and Scorrano L. OPA1 requires mitofusin 1 to promote mitochondrial fusion. *Proceedings of the National Academy of Sciences of the United States of America (2004)*, 101(45):15927–15932.

[107] Song Z., Chen H., Fiket M., Alexander C., and Chan D.C. OPA1 processing controls mitochondrial fusion and is regulated by mRNA splicing, membrane potential and Yme1L. *The Journal of Cell Biology (2007)*, 178(5):749–755.

[108] Otera H., Wang C., Cleland M.M., Setoguchi K., Yokota S., Youle R.J., and Mihara K. Mff is an essential factor for mitochondrial recruitment of Drp1 during mitochondrial fission in mammalian cells. *The Journal of Cell Biology (2010)*, 191(6):1141–1158.

[109] Ashrafi G. and Schwarz T.L. The pathways of mitophagy for quality control and clearance of mitochondria. *Cell Death and Differentiation (2013)*, 20(1):31–42.

[110] Liu L., Sakakibara K., Chen Q., and Okamoto K. Receptor-mediated mitophagy in yeast and mammalian systems. *Cell research (2014)*, 24(7):787–795.

[111] Durcan T.M. and Fon E.A. The three 'P's of mitophagy: PARKIN, PINK1, and post-translational modifications. *Genes and development (2015)*, 29(10):989–999.

[112] Ding W.X. and Yin X.M. Mitophagy: mechanisms, pathophysiological roles, and analysis. *Biological chemistry (2012)*, 393(7):547–564.

[113] Greene A.W., Grenier K., Aguileta M.A., Muise S., Farazifard R., Haque M.E., McBride H.M., Park D.S., and Fon E.A. Mitochondrial processing peptidase regulates PINK1 processing, import and Parkin recruitment. *EMBO Reports (2012)*, 13(4):378–385.

[114] Youle R.J. and Narendra D.P. Mechanisms of mitophagy. *Nature Reviews Molecular Cell Biology (2011)*, 12(1):9–14.

[115] Narendra D.P., Jin S.M., Tanaka A., Suen D.F., Gautier C.A., Shen J., and Youle R.J Cookson M.R. PINK1 is selectively stabilized on impaired mitochondria to activate Parkin. *PLoS Biology (2010)*, 8(1): e1000298.

[116] Narendra D., Tanaka A., Suen D.F., and Youle R.J. Parkin is recruited selectively to impaired mitochondria and promotes

their autophagy. *The Journal of Cell Biology (2008)*, 183(5):795–803.

[117] Aerts L., Craessaerts K., De Strooper B., and Morais V.A. PINK1 kinase catalytic activity is regulated by phosphorylation on serines 228 and 402. *Journal of Biological Chemistry (2015)*, 290(5):2798–2811.

[118] Kondapalli C., Kazlauskaite A., Zhang N., Woodroof H.I., Campbell D.G., Gourlay R., Burchell L., Walden H., Macartney T.J., Deak M., Knebel A., Alessi D.R., and Muqit M.M. PINK1 is activated by mitochondrial membrane potential depolarization and stimulates Parkin E3 ligase activity by phosphorylating Serine 65. *Open biology (2012)*, 2(5):120080.

[119] Tanaka A., Cleland M.M., Xu S., Narendra D.P., Suen D.F., Karbowski M., and Youle R.J. Proteasome and p97 mediate mitophagy and degradation of mitofusins induced by Parkin. *The Journal of Cell Biology (2010)*, 191(7):1367–1380.

[120] Koukourakis M.I., Kalamida D., Giatromanolaki A., Zois C.E., Sivridis E., Pouliliou S., Mitrakas A., Gatter K.C., and Harris A.L. Autophagosome proteins LC3A, LC3B, and LC3C have distinct subcellular distribution kinetics and expression in cancer cell lines. *PLoS One (2015)*, 10(9): e0137675.

[121] Tanida I., Ueno T., and Kominami E. LC3 and autophagy. *Methods in molecular biology (2008)*, 445:77–88.

[122] Xie Z. and Klionsky D. Autophagosome formation: core machinery and adaptations. *Nature Cell Biology (2007)*, 9(10):1102–1109.

[123] Kabeya Y., Mizushima N., Ueno T., Yamamoto A., Kirisako T., Noda T., and et al. LC3, a mammalian homologue of yeast Apg8p, is localized in autophagosome membranes after processing. *The EMBO Journal (2000)*, 19(21):5720–5728.

[124] Lee Y.K. and Lee J.A. Role of the mammalian ATG8/LC3 family in autophagy: differential and compensatory roles in the spatiotemporal regulation of autophagy. *BMB Reports (2016)*, 49(8):424–430.

[125] Birgisdottir A.B., Lamark T., and Johansen T. The LIR motif-crucial for selective autophagy. *Journal of Cell Science (2013)*, 126(15):3237–3247.

[126] Moyzis A.G., Sadoshima J., and Gustafsson Å.B. Mending a broken heart: the role of mitophagy in cardioprotection. *American journal of physiology. Heart and circulatory physiology (2015)*, 303(3):H183–H192.

[127] Lutz D., Loers G., Kleene R., Oezen I., Kataria H., Katagihallimath N., Braren I., Harauz G., and Schachner M. Myelin basic protein cleaves cell adhesion molecule L1 and promotes neuritogenesis and cell survival. *The journal of biological chemistry (2014)*, 289(19):13503–13518.

[128] Shiotsuki H., Yoshimi K., Shimo Y., Funayama M., Takamatsu Y., Ikeda K., Takahashi R., Kitazawa S., and Hattori N. A rotarod test for evaluation of motor skill learning. *Journal of Neuroscience Methods (2010)*, 189(2):180–185.

[129] Makhina T., Loers G., Schulze C., Ueberle B., Schachner M., and Kleene R. Extracellular GAPDH binds to L1 and enhances neurite outgrowth. *Molecular and Cellular Neuroscience (2009)*, 41(2):206–218.

[130] Loers G., Makhina T., Bork U., Dörner A., Schachner M., and Kleene R. The interaction between cell adhesion molecule L1, matrix metalloproteinase 14, and adenine nucleotide translocator at the plasma membrane regulates L1-mediated neurite outgrowth of murine cerebellar neurons. *The Journal of Neuroscience (2012)*, 32(11):3917–3930.

[131] Guseva D., Angelov D.N., Irintchev A., and Schachner M. Ablation of adhesion molecule L1 in mice favours Schwann

cell proliferation and functional recovery after peripheral nerve injury. *Brain (2009)*, 132(8):2180–2195.

[132] Kilkenny C., Browne W.J., Cuthill I.C., Emerson M., and Altman D.G. The ARRIVE guidelines for reporting animal research. *PLOS Biology (2010)*.

[133] Wilfinger et al. Effect of pH and ionic strength on the spectrophotometric assessment of nucleic acid purity. *BioTechniques (1997).*, 22(3):478–481.

[134] Rietdorf J. and Seitz A. Kymograph analysis handout. (`https://www.embl.de/eamnet/html/body_kymograph.html`). *Heidelberg: Homepage of European Advanced Light Microscopy Network (2008).*

[135] Marra M.H., Tobias Z.J.C, Cohen H.R., Glover G., and Weissman T.A. In vivo time-lapse imaging in the zebrafish lateral line: A flexible, open-ended research project for an undergraduate neurobiology laboratory course. *The Journal of Undergraduate Neuroscience Education (2015.*, 13(3): A215–A224.

[136] Seibenhener M.L. and Wooten M.C. Use of the open field maze to measure locomotor and anxiety-like behavior in mice. *Journal of visualized experiments (2015)*, (96): e52434.

[137] Walf A.A. and Frye C.A. The use of the elevated plus maze as an assay of anxiety-related behavior in rodents. *Nature (2007)*, 2(2):322–328.

[138] Rodgers R.J and Johnson N.J.T. Factor analysis of spatiotemporal and ethological measures in the murine elevated plus- maze test of anxiety. *Pharmacology Biochemistry and Behavior (1995)*, 52(2):297–303.

[139] Angoa-Pérez M., Kane M.J., Briggs D.I., Francescutti D.M., and Kuhn D.M. Marble burying and nestlet shredding as tests of repetitive, compulsive-like behaviors in mice. *Journal of visualized experiments (2013)*, (82):50978.

[140] Freitag S., Schachner M., and Morellini F. Behavioral alterations in mice deficient for the extracellular matrix glycoprotein tenascin- R. *Behavioural Brain Research (2003)*, 145(1):189– 207.

[141] Kucharczyk R., Zick M., Bietenhader M., Rak M., Couplan E., Blondel M., Caubet S.D., and di Rago J:P. Mitochondrial ATP synthase disorders: Molecular mechanisms and the quest for curative therapeutic approaches. *Biochimica et Biophysica Acta (2009)*, 1793(1):186–199.

[142] Ramzan R., Weber P., Linne U., and Vogt S. GAPDH: the missing link between glycolysis and mitochondrial oxidative phosphorylation? *Biochemical Society Transactions (2013)*, 41(5):1294–1297.

[143] Oliveira J.M.A. Mitochondrial membrane potential and dynamics. *Mitochondrial Dysfunction in Neurodegenerative Disorders (2011)*, 3(Chapter 8):127–139.

[144] Henriques-Alves A.M. and Queiroz C.M. Ethological evaluation of the effects of social defeat stress in mice: Beyond the social interaction ratio. *Frontiers in Behavioral Neuroscience (2016)*, 9:364.

[145] Fey A., Schachner M., and Irintchev A. A novel motion analysis approach reveals late recovery in C57BL/6 mice and deficits in NCAM-deficient mice after sciatic nerve crush. *Journal of neurotrauma (2010)*, 27(5):815–828.

[146] Irintchev A., Simova O., Eberhardt K.A., Morellini F., and Schachner M. Impacts of lesion severity and tyrosine kinase receptor B deficiency on functional outcome of femoral nerve injury assessed by a novel single-frame motion analysis in mice. *European Journal of Neuroscience (2006)*, 22(4):802–808.

[147] Kraus K. Doctoral dissertation: The functional role of the cell adhesion molecule L1 in mitochondrial metabolism and dynamics and the functional consequences of L1's

interaction with nuclear receptors in the murine central nervous system. *Faculty of Mathematics, Informatics and Natural Sciences Department of Biology of Universität Hamburg (2017)*.

[148] Johansen T. and Lamark T. Selective autophagy: ATG8 family proteins, LIR motifs and cargo receptors. *Journal of Molecular Biology (2020)*, 432(1):80–103.

[149] Noda N.N., Kumeta H., Nakatogawa H., Satoo K., Adachi W., Ishii J., Fujioka Y., Ohsumi Y., and Inagaki F. Structural basis of target recognition by Atg8/LC3 during selective autophagy. *Genes to Cells (2008)*, 13(12):1211–1218.

[150] Zhang J., Loyd M.R., Randall M.S., Waddell M.B., Kriwacki R.W., and Ney P.A. A short linear motif in BNIP3L (NIX) mediates mitochondrial clearance in reticulocytes. *Autophagy (2012)*, 8(9):1325–1332.

[151] Zhang L., Li L., Liu H., Borowitz J.L., and Isom G.E. BNIP3 mediates cell death by different pathways following localization to endoplasmic reticulum and mitochondrion. *FASEB Journal (2009)*, 23(10):3405–3414.

[152] Gao A., Jiang J., Xie F., and Chen L. Bnip3 in mitophagy: novel insights and potential therapeutic target for diseases of secondary mitochondrial dysfunction. *Clinica Chimica Acta (2020)*, 506:72–83.

[153] Kilbride S.M., Telford J.E., and Davey GP. Complex I controls mitochondrial and plasma membrane potentials in nerve terminals. *Neurochemical Research (2021)*, 46(1):100–107.

[154] Rikka S., Quinsay M.N., Thomas R.L., Kubli D.A., Zhang X., Murphy A.N., and Gustafsson Å.B. Bnip3 impairs mitochondrial bioenergetics and stimulates mitochondrial turnover. *Cell Death and Differentiation (2011)*, 18(4):721–731.

[155] Lee S., Zhang C., and Liu X. Role of glucose metabolism and ATP in maintaining PINK1 levels during Parkin-mediated

mitochondrial damage responses. *Journal of Biological Chemistry (2015)*, 290(2):904–917.

[156] Navarro A., Gomez C., López-Cepero J.M., and Boveris A. Beneficial effects of moderate exercise on mice aging: survival, behavior, oxidative stress, and mitochondrial electron transfer. *American Journal of Physiology-Regulatory, Integrative and Comparative Physiology (2004)*, 286(3): R505–R511.

[157] Yan Z., Lira V.A., and Greene N.P. Exercise training-induced regulation of mitochondrial quality. *Exercise and Sport Sciences Reviews (2012)*, 40(3):159–164.

[158] Gusdon A.M., Callio J., O'Doherty R.M. Distefano G., Goodpaster B.H., Coen P.M., and Chu C.T. Exercise increases mitochondrial complex I activity and DRP1 expression in the brains of aged mice. *Experimental Gerontology (2017)*, 90:1–13.

[159] Schapira A.H. et al. Mitochondrial complex I deficiency in Parkinson's disease. *Journal of Neurochemistry (1990)*, 54(3):823–827.

[160] Parker W.D. Jr, Parks J.K., and Swerdlow R.H. Complex I deficiency in Parkinson's disease frontal cortex. *Brain research (2008)*, 1189:215–218.

[161] Rollins B.L., Morgan L., Hjelm B.E., Sequeira A., Schatzberg A.F., Barchas J.D., Lee F.S., Myers R.M., Watson S.J., Akil H., Potkin S.G., Bunney W.E., and Vawter M.P. Mitochondrial complex I deficiency in schizophrenia and bipolar disorder and medication influence. *Complex Psychiatry (2018)*, 3(3):157–169.

[162] Chen T., Wu Q., Zhang Y., and Zhang D. NDUFV2 regulates neuronal migration in the developing cerebral cortex through modulation of the multipolar–bipolar transition. *Brain Research (2015)*, 1625:102–110.

[163] Congiu L., Granato V., Loers G., Kleene R., and Schachner M. Mitochondrial and neuronal dysfunctions in L1 mutant mice. *International Journal of Molecular Sciences (2022)*, 23(8):4337.

[164] Pravdic D., Hirata N., Barber L., Sedlic F., Bosnjak Z.J., and Bienengraeber M. Complex i and ATP synthase mediate membrane depolarization and matrix acidification by isoflurane in mitochondria. *European journal of pharmacology (2012)*, 690(1-3):149–157.

[165] Huang J., Hao L., Xiong N., Cao X., Liang Z., Sun S., and Wang T. Involvement of glyceraldehyde-3-phosphate dehydrogenase in rotenone-induced cell apoptosis: Relevance to protein misfolding and aggregation. *Brain Research (2009)*, 1279:1–8.

[166] Bolaños J.P., Almeida A., and Moncada S. Glycolysis: a bioenergetic or a survival pathway? *Trends in Biochemical Sciences (2010)*, 35(3):145–149.

[167] Li Y., D'Aurelio M., Deng J.H., Park J.S., Manfredi G., Hu P., Lu J., and Bai Y. An assembled complex IV maintains the stability and activity of complex I in mammalian mitochondria. *Journal of Biological Chemistry (2007)*, 282(24):17557–17562.

[168] Lin M.Y. and Sheng Z.H. Regulation of mitochondrial transport in neurons. *Experimental Cell Research (2015)*, 334(1):35–44.

[169] Watters O., Connolly N.M.C., König H.G., Düssmann H., and Prehn J.H.M. AMPK preferentially depresses retrograde transport of axonal mitochondria during localized nutrient deprivation. *The Journal of Neuroscience (2020)*, 40(25):4798–4812.

[170] Bressan C., Pecora A., Gagnon D., Snapyan M., Labrecque S., De Koninck P., Parent M., and Saghatelyan A. The dynamic interplay between ATP/ADP levels and autophagy sustain neuronal migration in vivo. *Elife. (2020)*, 9: e56006.

[171] Seabright A.P., Fine N.H.F., Barlow J.P., Lord S.O., Musa I., Gray A., Bryant J.A., Banzhaf M., Lavery G.G., Hardie D.G., Hodson D.J., Philp A., and Lai YC. AMPK activation induces mitophagy and promotes mitochondrial fission while activating TBK1 in a PINK1-Parkin independent manner. *FASEB Journal (2020)*, 34(5):6284–6301.

[172] Kleene R., Loers G., Castillo G., and Schachner M. Cell adhesion molecule l1 interacts with the chromo shadow domain of heterochromatin protein 1 isoforms *α, β, and γ* via its intra- cellular domain. *The FASEB Journal (2021)*, 36(1): e22074.

[173] Demyanenko G.P., Shibata Y., and Maness P.F. Altered distribution of dopaminergic neurons in the brain of L1 null mice. *Developmental Brain Research (2001)*, 126(1):21–30.

[174] Groń ska-Pȩ ski M., Schachner M., and Hébert J.M. L1cam curbs the differentiation of adult-born hippocampal neurons. *Stem cell research, (2020)*, 48:101999.

[175] Saré R.M., Lemons A., and Smith C.B. Behavior testing in rodents: Highlighting potential confounds affecting variability and reproducibility. *Brain Sciences (2021)*, 11(4):522.

[176] Crusio W.E. Genetic dissection of mouse exploratory be- haviour. *Behavioural brain research (2001)*, 125(1-2):127–132.

[177] Rodgers R.J. and Dalvi A. Anxiety, defence and the elevated plus-maze. *Neuroscience and biobehavioral reviews (1997)*, 21(6):801–810.

[178] Tang X., Orchard S.M., and Sanford L.D. Home cage activity and behavioral performance inbred and hybrid mice. *Behavioural Brain Research (2002)*, 136(555-569).

[179] Tucker L.B. and McCabe J.T. Measuring anxiety-like behaviors in rodent models of traumatic brain injury. *Frontiers in Behavioral Neuroscience (2021)*, 15:682935.

[180] Sestakova N., Puzserova A., Kluknavsky M., and Bernatova I. Determination of motor activity and anxiety-related behaviour in rodents: methodological aspects and role of nitric oxide. *Interdisciplinary Toxicology (2013)*, 6(3):126–135.

[181] Montarolo F., Martire S., Perga S., Spadaro M., Brescia I., Allegra S., De Francia S., and Bertolotto A. NURR1 deficiency is associated to ADHD-like phenotypes in mice. *Translational Psychiatry (2019)*, 9(1):207.

[182] Zhuang X., Oosting R.S., Jones S.R., Gainetdinov R.R., Miller G.W., Caron M.G., and Hen R. Hyperactivity and impaired response habituation in hyperdopaminergic mice. *Proceedings of the National Academy of Sciences of the United States of America (2001)*, 98(4):1982–1987.

[183] Leo D. and Gainetdinov R.R. Transgenic mouse models for ADHD. *Cell and Tissue Research (2013)*, 354(1):259–271.

[184] Kaidanovich-Beilin O., Lipina T., Vukobradovic I., Roder J., and Woodgett J.R. Assessment of social interaction behaviors. *Journal of Visualized Experiments (2011)*, (48):2473.

[185] Moy S.S., Nadler J.J., Perez A., Barbaro R.P., Johns J.M., Magnuson, T.R., Piven J., and Crawley J.N. Sociability and preference for social novelty in five inbred strains: an approach to assess autistic-like behavior in mice. *Genes, brain, and behavior (2004)*, 3(5):287–302.

[186] Morellini F., Lepsveridze E., Kähler B., Dityatev A., and Schachner M. Reduced reactivity to novelty, impaired social behavior, and enhanced basal synaptic excitatory activity in perforant path projections to the dentate gyrus in young adult mice deficient in the neural cell adhesion molecule CHL1. *Molecular and cellular neurosciences (2007)*, 34(2):121–136.

[187] Gireco F. and et al. Measuring behavior in the home cage: Study design, applications, challenges, and perspectives. *Frontiers in Behavioral Neuroscience (2021)*, 15:735387.

[188] Rosenfeld C.S. Sex-dependent differences in voluntary physical activity. *Journal of neuroscience research (2017)*, 95(1-2):279– 290.

[189] Djogo N., Jakovcevski I., Müller C., Lee H.J., Xu J.C., Jakovcevski M., Kügler S., Loers G., and Schachner M. Adhesion molecule L1 binds to amyloid beta and reduces Alzheimer's disease pathology in mice. *Neurobiology of disease (2013)*, 56:104–115.

[190] Strekalova H., Buhmann C., Kleene R., Eggers C., Saffell J., Hemperly J., Weiller C., Müller-Thomsen T., and Schachner M. Elevated levels of neural recognition molecule L1 in the cerebrospinal fluid of patients with Alzheimer disease and other dementia syndromes. *Neurobiology of Aging (2006)*, 27(1):1-9

ACKNOWLEDGEMENTS

CURRICULUM VITAE

Name: Viviana Granato
Birthday: 26.05.1991
Place of birth: Avellino, Italy

Education and Experience

March 2018-
August 2022:
-PhD Student
Senior Group 'Biosynthesis of Neural Structures'
Center for Molecular Neurobiology Hamburg
(ZMNH)

June 2017-
July 2017:
-Qualifying examination for the
profession of biologist
University of Campania, Luigi Vanvitelli

October
2014-
January 2017:
-Master's degree in Neurobiology
Master's thesis: *Enriched environment induces changes in the epigenetic modification that are able to reduce the growth and development of glioma: role of EZH2*
University of Rome "La Sapienza"

October
2010-
October 2014:
-Bachelor´s Degree in Applied and
General Biology
University of Naples "Federico II"

July 2010:
-High School Diploma
Liceo Socio-Psico Pedagogico "C.
Colombo" Marigliano, Italy

EIDESSTATTLICH ERKLÄRUNG

Ich versichere ausdrücklich, dass ich die Arbeit selbständig und ohne fremde Hilfe verfasst, andere als die von mir angegebenen Quellen und Hilfsmittel nicht benutzt und die aus den benutzten Werken wörtlich oder inhaltlich entnommenen Stellen einzeln nach Ausgabe (Auflage und Jahr des Erscheinens), Band und Seite des benutzten Werkes kenntlich gemacht habe.

Ferner versichere ich, dass ich die Dissertation bisher nicht einem Fachvertreter an einer anderen Hochschule zur Überprüfung vorgelegt oder mich anderweitig um Zulassung zur Promotion beworben habe.

Ich erkläre mich einverstanden, dass meine Dissertation vom Dekanat der Medizinischen Fakultät mit einer gängigen Software zur Erkennung von Plagiaten überprüft werden kann.

Unterschrift Viviana Granato